



EEEE3001

Final Year Individual Project Thesis

Hands-free “dead reckoner” for stable navigation in sailing or orienteering

AUTHOR: Mr Tianchen YU

ID NUMBER: 20124989

SUPERVISOR: Dr. Kevin Webb

MODERATOR: Dr. Rikesh Patel

DATE: May 1, 2022

Third year project report is submitted in part fulfilment of the requirements of the
degree of Bachelor of Engineering.

Abstract

This report describes a complete development process consisting of research, design, implementation, and validation of a glasses frame prototype for stable navigation in orienteering. The report begins with an introduction to the current navigation dilemma in orienteering and a literature review is conducted to investigate the forms of wearable electronic devices that are suitable for the problem. Various methodologies used to accomplish the electronic system design, glasses frame modelling, code development and post signal processing are explained. The achieved results of each of these four stages are discussed and reflected separately following the realistic progression of the project. An overall reflection section is presented to illustrate the attainment of the objectives and propose future enhancements of the project. Finally, a conclusion is drawn to summarise technical discoveries and valuable lessons for potential investors.

Keywords: orienteering, hands-free navigation, smart glasses, inertial navigation, visual and auditory feedback, 3D printing

Table of Contents

1. Introduction.....	1
2. Literature Review and Market Research	2
2.1 Wearable Electronic Device and Product Form Choice.....	2
2.2 Human Machine Interface.....	3
2.2.1 Visual Signal.....	3
2.2.2 Auditory Signal.....	5
2.2.3 Haptic Signal.....	6
2.3 Enabling Technologies and Their Comparison	6
2.4 Inertial Navigation versus Satellite Navigation	8
2.5 Market Analysis and Available Commercial Products	9
3. Aims, Objectives, Deliverables and Milestones	11
3.1 Aims	11
3.2 Objectives.....	11
3.2.1 Preparation Stage	11
3.2.2 Design and Construction Stage.....	12
3.2.3 Validation Stage.....	12
3.3 Justifications for Aim and Objectives	12
3.3.1 Aim Elaboration.....	12
3.3.2 Objective Elaboration and Justification	12
3.4 Deliverables.....	13
3.5 Milestones	13
3.6 Risk Management & Elaboration for Deliverable and Milestones	13
3.7 Time Plan (Gantt Chart).....	14
4. Methodology	14
4.1 High-level Project Architecture	14
4.1.1 Detailed Technical Specifications of the Glasses Frame	14
4.1.2 Signal Flowchart	16
4.2 Electronic Components Choice	16
4.2.1 Processing Unit	16

4.2.2	Sensors and Micro SD	17
4.2.3	Human Machine Interface.....	18
4.2.4	Glasses Power System and Voltage Translator	19
4.3	PCB Design.....	21
4.4	Glasses Frame 3D Modelling and Printing	22
4.5	Glasses Programming.....	23
4.6	Post Signal Processing	24
5.	Results, Discussions and Reflections	27
5.1	PCB Design.....	27
5.1.1	PCB Results and Discussions	27
5.1.1.1	PCB1: Left Leg.....	27
5.1.1.2	PCB2: Frontal Frame.....	29
5.1.1.3	PCB3: Right Leg	29
5.1.2	PCB Reflection	31
5.1.2.1	Via Size and Silkscreen	31
5.1.2.2	Location and Orientation of Components on Board.....	31
5.1.2.3	PCB Assembly.....	32
5.1.2.4	Future Possibility of Flexible Circuit	32
5.2	Glasses Frame 3D Modelling and Printing	32
5.2.1	3D Modelling Results and Discussions	32
5.2.1.1	Overview and Dimensions.....	33
5.2.1.2	Connections with PCBs and Reserved Slots	33
5.2.1.3	“Teeth-Slot” Structure	34
5.2.1.4	Hinge System.....	35
5.2.1.5	Slots in Tails	36
5.2.2	3D Printing Results and Discussions	36
5.2.2.1	Different Printing Options	36
5.2.2.2	Printing Results and Tests on Face.....	38
5.2.3	Modelling and Printing Reflections	38
5.2.3.1	Ergonomic Concerns	38
5.2.3.2	Aesthetic Concerns	39
5.2.3.3	Waterproof and Shock-resistant	39

5.3	Glasses Programming.....	39
5.3.1	Glasses Programming Results and Discussions.....	39
5.3.1.1	Main Program Flowchart and Time Sequence	39
5.3.1.2	The Derivation of Magnetic North and Current Bearing	42
5.3.1.3	Glasses Frame Validation 1: LED and Buzzer Indication.....	42
5.3.1.4	Glasses Frame Validation 2: Guiding the Wearer on a Straight Line	43
5.3.2	Glasses Programming Reflection.....	44
5.3.2.1	Potential Improvements of HMI.....	44
5.3.2.2	Algorithm Efficiency and Robustness.....	45
5.3.2.3	Battery Life.....	45
5.4	Post Signal Processing on PC.....	46
5.4.1	Post Signal Processing Results and Discussions	46
5.4.1.1	Flowchart of Three Algorithms	46
5.4.1.2	Basic “Back and Forth (BAF)” Test of Three Algorithms	47
5.4.1.3	Field Validation 1: Trajectory around a Building	49
5.4.1.4	Field Validation 2: Trajectory around a Grassland in Open Field	51
5.4.2	Post Signal Processing Reflection	52
5.4.2.1	Legitimacy of Inertial Navigation	52
5.4.2.2	Trajectory Reconstruction Algorithms and a Reference to Sailing	53
5.4.2.3	Development of Software Package for Customers.....	53
6.	Overall Project Reflection.....	53
6.1	Attainment of Objectives and Deliverables	53
6.2	Future Hardware Variations and Upgrades.....	54
6.3	Supply Chain Management (SCM).....	54
6.4	Ethical Concerns	54
6.5	Intellectual Property (IP).....	55
6.6	Device’s Accordance with IOF Foot Orienteering Rules	55
6.7	Revision on Time Plan	55
7.	Conclusion	56
8.	Reference	58

9. Appendices.....	61
9.1 Appendix A Time Plan.....	61
9.2 Appendix B PCB Schematics and 2D Layout Designs.....	62
9.2.1 PCB1 in Left Leg	62
9.2.2 PCB2 in Frontal Frame	64
9.2.3 PCB3 in Right Leg.....	64
9.3 Appendix C PCB BOM List	66
9.4 Appendix D Public Human Head Model Dataset	67

List of Tables

Table 2-1. The sound pressure level of 6 practical scenarios [10]	5
Table 2-2. Enabling technologies comparison of five wearable navigation devices in [5], [6], [14]-[16]	7
Table 4-1. Maximum current of major components of glasses frame [27] -[31], [34]	19
Table 5-1. Number of times that Buzzer 1 and Buzzer 2 were triggered in each test	44
Table 5-2. Journey duration (s), distance (m) and average speed(m/s) estimation from GPS data and three inertial algorithms in the building test	50
Table 5-3. Journey duration (s), distance (m) and average speed (m/s) estimation from GPS data and three inertial algorithms in the grassland test.....	52
Table 9-1. BOM List of three PCBs of the glasses frame	66
Table 9-2. Explanations of head dimensions and relevant measurement methods [40]..	67
Table 9-3. Statistics of head dimensions [40].....	68

List of Figures

Figure 1-1. An example of orienteering map and control points [2]	1
Figure 2-1. LED indicator based smart glasses frame for navigation in [6]	3
Figure 2-2. The dynamic range of rod and cone system in human eyes [8]	4
Figure 2-3. Relative sensitivity of human eyes versus wavelength in scotopic (low lighting) and photopic (high lighting) condition [8]	4
Figure 2-4. Equal loudness level contours for a human hearing system [10]	5
Figure 2-5. Diagrams of Kinesthetic feedback and Tactile feedback.	6
Figure 2-6. Number of participants in the events held by BOF from 2012 to 2020 [20] ...	9
Figure 2-7. First mode of Google Glass (left) and Glass Enterprise Edition 2 (right) [22]	10
Figure 2-8. Ray-Ban smart sunglasses [25]	11
Figure 2-9. Echo Frames developed by Amazon [26]	11
Figure 4-1. Blueprint of the glasses frame	15
Figure 4-2. High-level signal flowchart of the project	16
Figure 4-3. Appearance and dimension of the selected red LED and buzzer [30], [31] ..	18
Figure 4-4. Frequency response of the selected buzzer [31]	18
Figure 4-5. The choice of slide switch (left) and push button (right) [32], [33]	19
Figure 4-6. Power system flowchart of glasses frame	20
Figure 4-7. PCB architecture of the glasses frame	21
Figure 4-8. Specifications of the selected FFC [38]	22
Figure 4-9. FT232RL based USB debugger from SparkFun [44]	24
Figure 4-10. Simplified diagram of the trajectory reconstruction problem	24
Figure 5-1. Top side (top) and bottom side (bottom) view of PCB1 3D rendered design with notations of major components	27
Figure 5-2. Top side of the soldered PCB1 with missing IMU and magnetic chip	27
Figure 5-3. IMU and magnetic meter modules attached to the frame with the notation of directions of 3-axis acceleration, rotational speed and magnetic field intensity.	28
Figure 5-4. Optimised IIC configuration method of one IO	29
Figure 5-5. Top side (top) and bottom side (bottom) view of PCB2 3D rendered design 29	29
Figure 5-6. Top side of the soldered PCB2 with full functionalities	29
Figure 5-7. The symmetrical design of left leg and right leg components	30
Figure 5-8. Top side (left) and bottom side (right) view of PCB3 3D rendered design with the notations of major components	30
Figure 5-9. Top side of the soldered PCB3 with full functionalities	30
Figure 5-10. 3.3V and 5V power sources measured oscilloscope	31
Figure 5-11. An example of flexible circuit [49]	32
Figure 5-12. Exploded view (left) and assembled view (right) of the modelled glasses frame	33
Figure 5-13. Front (bottom right), top (left) and right (top right) view of the glasses frame with notations of major dimensions	33

Figure 5-14. Installed PCBs on cylinders in frontal frame (top), left leg (bottom left), right leg (bottom right)	34
Figure 5-15. Reserved slots for HMI components and micro SD card on left leg (bottom left), right leg (bottom right), frontal frame (top)	34
Figure 5-16. “Teeth-Slot” structure implementation in left leg (top left), right leg (top right), frontal frame (bottom)	35
Figure 5-17. Exploded view (top left and right) and assembled view (bottom) of the hinge system in left leg	35
Figure 5-18. Regular (left) and maximum folding condition (right) of the glasses frame	36
Figure 5-19. The slots in tails of the glasses frame for secure mounting	36
Figure 5-20. Printing directions of left leg (top left), right leg (middle left), left lid (top right), right lid (middle right), frontal frame (bottom left), nose support (bottom right)	37
Figure 5-21. Some sacrificed and improved features between the abandoned method and the current method	37
Figure 5-22. Fully integrated glasses frame from top (left), left (top right) and right (bottom right) view	38
Figure 5-23. Four different perspectives of the glasses frame on human’s face	38
Figure 5-24. Program flowchart of glasses frame	40
Figure 5-25. Time sequence of the 250 Hz ISR and 50 Hz LED PWM	40
Figure 5-26. An example section of stored data to micro SD card	40
Figure 5-27. An example of relative positions of head direction, vector of earth magnetic field and the magnetic coordinates of the magnetic meter	42
Figure 5-28. Total seven different states of LED and buzzer indication	43
Figure 5-29. Ideal straight trajectory (top left, red line) and the recorded trajectory (orange line) from Strava for Test 1 (bottom left), Test 2 (top right) and Test 3 (bottom right)	44
Figure 5-30. Flowchart of three processing algorithms	46
Figure 5-31. Magnitude response of the 70th order low pass filter	47
Figure 5-32. Acceleration of X axis, compass bearing and integrated velocity for three processing algorithms in a basic BAF test	48
Figure 5-33. The actual trajectory (Subplot 1) and reconstructed trajectories of basic method (Subplot 2), digital filter (Subplot 3) and Kalman filter (Subplot 4)	48
Figure 5-34. Theoretical trajectory (Subplot 1, red line) and result from GPS receiver (Subplot 2, orange line)	49
Figure 5-35. Acceleration of X axis, compass bearing and integrated velocity for three processing algorithms in the building test	49
Figure 5-36. The reconstructed trajectories of basic method (Subplot 1), digital filter (Subplot 2) and Kalman filter (Subplot 3) of the building test	50

Figure 5-37. Theoretical trajectory (Subplot 1, red line) and result from GPS receiver (Subplot 2, orange line), and reconstructed trajectories of basic method (Subplot 3), digital filter (Subplot 4) and Kalman filter (Subplot 5) of the grassland test	51
Figure 5-38. Acceleration of X axis, compass bearing and integrated velocity for three processing algorithms in the grassland test	51
Figure 6-1. Revised time plan based on the actual project development progress	56
Figure 9-1. Original project time plan	61
Figure 9-2. Schematic of PCB1 in the left leg of the glasses frame	62
Figure 9-3. Top layer (top), middle layer of 5V (second top), middle layer of 3.3V (second bottom), bottom layer (bottom) of 2D PCB layout design of PCB1	63
Figure 9-4. Schematic of PCB2 in the frontal frame	64
Figure 9-5. Top layer (top) and bottom layer (bottom) of 2D PCB layout design of PCB2	64
Figure 9-6. Schematic of PCB3 in the right leg	64
Figure 9-7. Top layer (top) and bottom layer (bottom) of 2D PCB layout design of PCB3	65
Figure 9-8. Head dimensions marked by numbers [40]	67

1. Introduction

Many interesting forms of physical activities have emerged in the modernisation progress of human society. Navigational sport is a unique category that not only requires physical strength to achieve a faster speed, but also involves continuous decision-making according to multiple information sources to accomplish the intermediate or final goals. Orienteering is a typical example.

Originally designed as a form of military training, Orienteering was first introduced in Scandinavia (Sweden) in the late 19th century. [1] There are totally four different orienteering sports, namely Foot Orienteering, Mountain Bike Orienteering, Ski Orienteering and Trail Orienteering. Their forms vary but the essence is the same, hence the following description will focus on Foot Orienteering due to its prevalence and straightforwardness. The target of the players is to identify and reach the so called “control points” that are pre-determined by the game organiser with limited resources, usually a specially customised map and a normal compass. The control points are marked on the map and the player who manages to cover all of them (on foot, obviously) in shortest time will be the champion of the game. **Figure 1-1** is an example of an orienteering map and the control points are shown as pink circles. Typically most useful information apart from elevation, terrain types and buildings are removed from the tailored orienteering map to emulate the situation of arriving in an enemy territory with minimal prior knowledge, which actually adheres to the inherent military purpose of this sport.

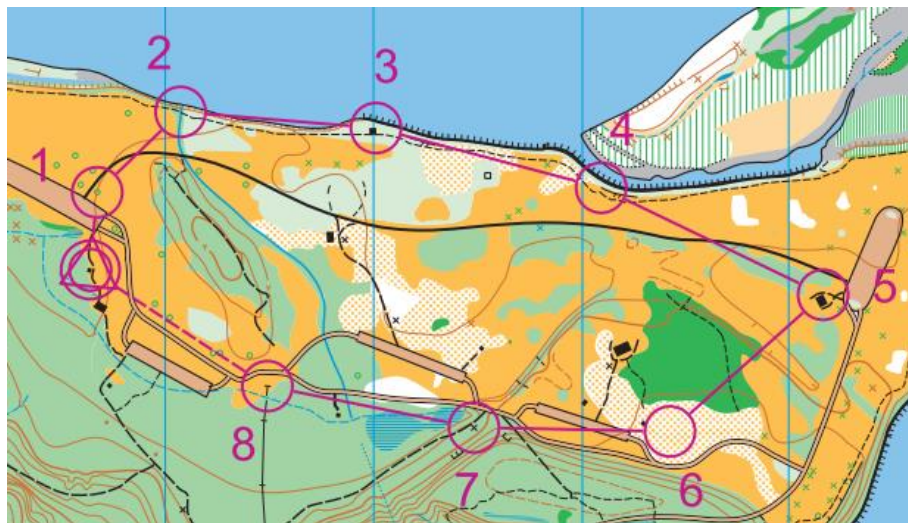


Figure 1-1. An example of orienteering map and control points [2]

As shown in **Figure 1-1** above, although there is no legend, it should be clear that this typical orienteering field is consisting of many different terrains, and this is common for any orienteering game. Various terrains including mountains, forests, bushes, lakes or man-made buildings add to the complexity and diversity of the game, giving players landmark-based clues and allowing them to make different navigational decisions to travel from point to point. This makes orienteering very exciting, though also complicated and demanding, since the players must constantly divide their attention between confirming the current location on map, calibrating their heading directions and worrying about the difficult terrains. The players must strike a balance between looking at the map and ensuring their safe traverse across unpredictable terrains, in other words, they have to take some risks if they want to be faster.

This is where the idea of this project originates from, which attempts to generate a solution to resolve, or at least mitigate, the safety risks brought by the unique features of orienteering. The project also aims to reduce the situations during which the player has to tackle different tasks

simultaneously, so that the player can solely concentrate on overcoming difficult terrains and the average speed could be faster. Due to the essence of this sport, it is meaningless to implement any form of “powerful” guiding device that is capable of explicitly computing what the user is supposed to do next (the accordance of such device to the rules of the game is covered in *6.6 Device’s Accordance with IOF Foot Orienteering Rules*). Hence, the project is looking for a device that can provide adequate assistance to the player to alleviate safety concerns and achieve a faster speed but will not spoil the sport itself.

2. Literature Review and Market Research

It is worth noting that this section is beyond the traditional “literature review” but close to a bridging section between the orienteering problem mentioned in the above *Introduction* and the detailed product specifications of this project. This section defines and justifies how the idea of a “smart glasses frame” is chosen based on the uniqueness of the problem and the available technologies, also specifies which technologies are potentially applicable for the glasses frame. Different examples proposed by other research papers, various component choices and algorithms will be tabulated and compared to provide a comprehensive analysis. Eventually the glasses frame is discussed in a marketing context and compared with other commercial products to justify for its competitiveness.

2.1 Wearable Electronic Device and Product Form Choice

The requirement of the project is to prevent the player from being overwhelmed by the multi-tasking during orienteering and accelerate player’s movement. The key point in this objective is to somehow inform the player whether he/she is moving toward a correct direction, or how much he/she deviates from the correction direction, without the necessity to check the compass bearing and the map repetitively. The player needs certain kinds of feedback that will not distract his/her attention significantly but can still be reliably perceived. As mentioned in the *Introduction* section, these feedbacks do not need to include explicit instructions guiding the player what to do next, but rather some information about the current bearing like what the player is supposed to know in an orienteering game. Based on such requirements and characteristics, small wearable electronic device can be a legitimate choice for this circumstance. These devices are usually highly-portable, easy to mount on the body and can provide assistance that is just enough to replicate the function of a compass without great distraction. From a very general perspective, the wearable device in this project should allow the player to set and lock onto a bearing, and communicate the selected bearing to the player during orienteering with minimal interface until the player opts to set another target. This will be the core function to realise for the project.

For a reference to prior examples, there are countless existing commercial or research-based wearable electronic devices. Specifically for this project, wearable devices related to personal navigation are most relevant. Different technological examples are designed to be worn on different body parts. For example, a foot-mounted wearable device that was capable of estimating step length and foot orientation using an extended Kalman filter algorithm was introduced in [3]. A multi-sensor approach was implemented on this device to provide Pedestrian Dead Reckoning (PDR) navigation and it reached an error less than 1% by only manipulating data from inertial measurement units (IMUs). [3] (The details description of PDR with IMUs will be covered in *2.4 Inertial Navigation versus Satellite Navigation*) Similarly, another waist-worn device developed in [4] was also pure IMU-based, but it focused on utilising a 3D PDR model to detect the wearer attitudes such as standing, walking or sitting, to classify the current activity and apply corresponding algorithms to improve the accuracy of step length estimation. Other examples may choose GPS (Global Positioning System)

technology or a combination of both GPS and IMUs, such as the hand-held device called ULISS proposed in [5], which implemented a data fusion algorithm to integrate the on-board GPS and IMU data to performance a navigation that was applicable for both interior and exterior environment. The error of travelled distance was controlled below 6% and the error value of walking direction was below 15° as the final results of ULISS.

A final example in [6] described a LED (Light Emitting Diode) indicator based glasses frame that can provide turn-by-turn navigation at each intersection during a bicycle trip. A series of LEDs were mounted on the glasses frame and some of them would be lit up corresponding to the computed direction from GPS signal. For example, LEDs located at the right section of the frame would be lit up when user should turn right as shown in **Figure 2-1**.

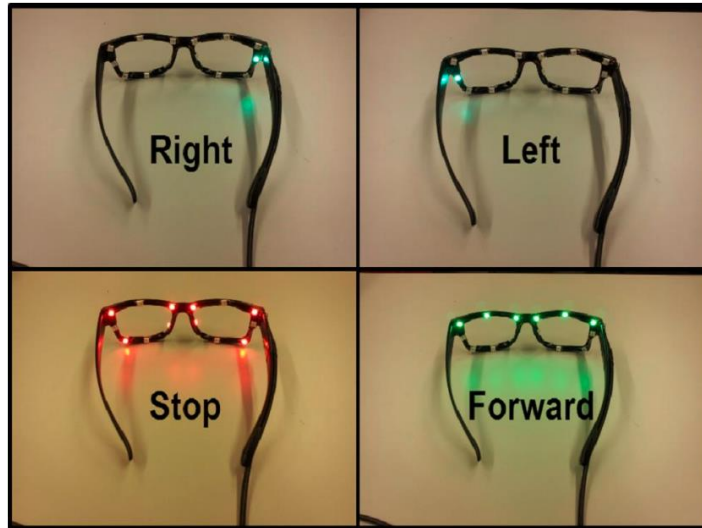


Figure 2-1. LED indicator based smart glasses frame for navigation in [6]

Referring back to the requirements of the orienteering problem, the above idea of a “smart glasses frame” is an applicable and feasible solution with the turn-by-turn navigation function removed, since it is similar to offering explicit instructions. The form of glasses frame makes it easy to convey visual, acoustic, vibrational or haptic feedback to the wearer effectively because the glasses frame will be close to many sensitive sensory organs like eyes or ears. Another advantage is that the glasses frame always aligns with the current heading of the wearer’s face, and it usually also aligns with the moving direction (assuming the player moves forward for most of the time). This makes it intuitive for the wearer to understand the information from the glasses frame and the frame itself can also capture a relatively stable bearing reading from wearer compared to the devices attached to other body parts such as wrist or foot. Hence, the product form of this project is selected as a smart glasses frame with LEDs as basic indication.

2.2 Human Machine Interface

Besides the visual indication described above, there are other feedback forms such as auditory or haptic feedback that can be implemented as complementary sources to establish the complete human machines interface (HMI) of the glasses frame. This section is used to illustrate relevant biological parameters of human for detecting these signals, and also the appropriate technical specifications of these signal (wavelength, loudness etc.) that are detectable and tolerable by average humans.

2.2.1 Visual Signal

Two most distinguishable parameters of light are light intensity and light colour (wavelength). They are discussed together here as there is some correlation between them when detected by human eyes. Two types of photoreceptor cells called rod system and cone system exist in human eyes, responsible for detecting light intensity and distinguish colours under different circumstances. [7] The rod system is highly sensitive to light and it only works in a relatively low light environment, while the cone system is less sensitive to light and contribute to the visual perception at bright conditions. [7] Based on the relative activity of rod and cone system, it is possible to classify a light level as photopic, mesopic and scotopic, representing the scenarios that only cone system works, both cone and rod systems are active, and only rod system works. [7] The following **Figure 2-2** could describe this characterisation process.

Visual environments	Starlight	Moonlight	Indoor lighting	Sunlight				
Photopic luminance ($\log \text{cd/m}^2$)	-6	-4	-2	0	2	4	6	8
Light category	Scotopic	Mesopic	Photopic					
Photoreceptors	Rods only	Rods and cones	Cones only					
Visual function	Rod absolute threshold	Cone absolute threshold	Rod saturation begins	Damage possible				
	No or poor color vision			Good color vision				

Figure 2-2. The dynamic range of rod and cone system in human eyes [8]

The cone cells are consisting of three different photo pigments that are sensitive to different light wavelengths (red, green and blue specifically), thus enabling human eyes to distinguish millions of colours. [9] The rod cells, however, are only composed of a single photo pigment, indicating that they cannot recognise colour but are only able to perceive black, white and grey. [9] This means that human eyes will be less sensitive to colours in low light condition as only rods cells, which are only consisting of a single photo pigment, are working.

When the overall sensitivity to light of human eyes is measured under normal lighting condition, it had been found that eyes are most sensitive to the light wavelength near 555 nm [8], which corresponds to a yellow-green colour. This sensitivity peak will change in low lighting condition. The entire sensitivity versus wavelength spectrum will shift to shorter wavelength and the new peak occurs at 507 nm as shown in the **Figure 2-3** below. This means that human eyes become more sensitive to blue/violet colours in low lighting conditions.

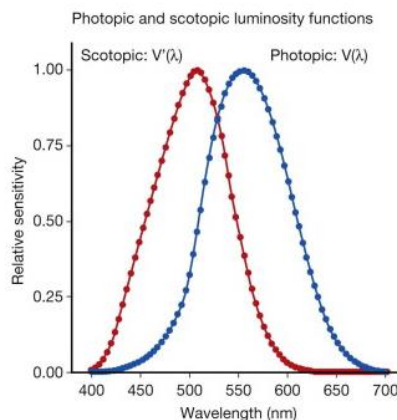


Figure 2-3. Relative sensitivity of human eyes versus wavelength in scotopic (low lighting) and photopic (high lighting) condition [8]

Besides the light sensitivity of rod and cone systems, the pupils in human eyes will also behave differently in low and high lighting conditions. The pupil will dilate to allow more light to pass

through the eyes in low lighting condition so that eyes can capture more information and provide a clearer vision. [8] On the contrary, the pupil will contract to reduce the light emitted inside to protect the retina from being damaged in high lighting condition. [8] Meanwhile, the pupil will also respond differently to different light wavelengths. For example, red light (wavelength \approx 630 nm) tends to trigger less pupil contraction in low lighting condition compared to other colours [8], as human eyes are not sensitive to red colour especially when surrounding environment is dark as shown in **Figure 2-3**. This means red light is a good choice for illumination (or indication) in the dark to prevent repetitive pupil dilations or contractions, leading to the preservation of night vision.

2.2.2 Auditory Signal

The audible sound range for human ears is usually treated as 20 Hz \sim 20 kHz [10]. This range may differ for various groups of people with different age, gender or race [10]. The human hearing system, however, is not equally sensitive to the entire audible frequency range. This means two auditory signals with a same Sound Pressure Level (SPL) may be perceived by human ears as different loudness levels (phons). This characteristic can be described by the following equal loudness level contour in **Figure 2-4**, where each contour describes the variation of SPL in the frequency domain with respect to a fixed loudness level.

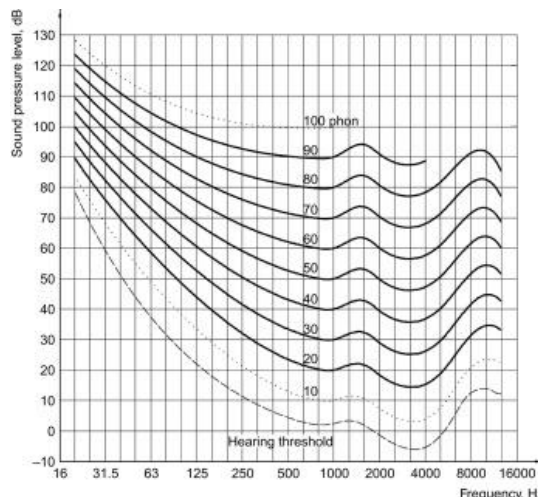


Figure 2-4. Equal loudness level contours for a human hearing system [10]

It could be seen from **Figure 2-4** that human ears are most sensitive to the sound frequency between 3-4 kHz as a minimum SPL is required to reach same loudness level as other frequencies.

Regarding the reference of different SPLs to realistic scenarios, the following **Table 2-1** contains some typical examples:

Table 2-1. The sound pressure level of 6 practical scenarios [10]

Type of Sound	Sound Pressure Level (dB)
Perception threshold	0
Sound of falling leaves	20
Normal Speech	60
Motor Vehicle	60-100
Jet plane during take-off	120
Pain threshold	120-140

2.2.3 Haptic Signal

Haptic feedback is closely related to the sense of touch. The haptic feedback usually means the device is communicating to user via different feelings of touch. This feedback can be divided into two categories, the kinesthetic feedback and tactile feedback. [11] The kinesthetic feedback refers the feelings of force and torque from bending, rotating or stretching joints and muscles, while the tactile feedback refers to feelings of vibration, surface texture or temperature perceived from the mechanoreceptors in the skin. [12] These two haptic categories are described by the diagrams in **Figure 2-5** below.

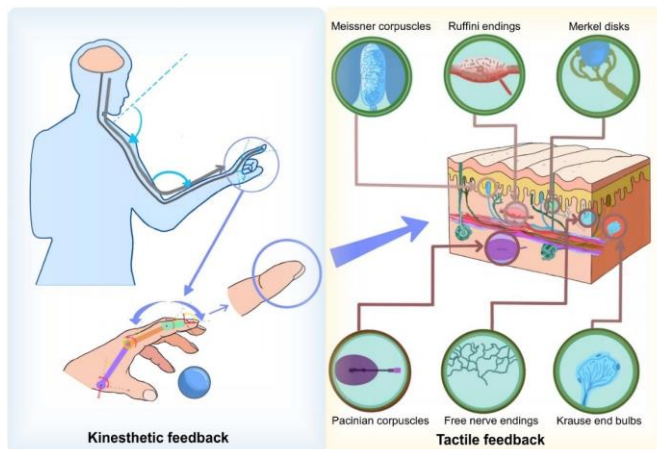


Figure 2-5. Diagrams of Kinesthetic feedback and Tactile feedback [12]

The tactile feedback is more relevant to this project as it mainly focuses on small wearable electronic devices. It is possible for the wearable device to trigger tactile feedback and communicate with the wearer through vibrations generated from motor or piezoelectric actuator. The tactile sensation itself results from different types of mechanoreceptors under the skin, such as Merkel disks, Ruffini endings, Meissner corpuscles and Pacinian corpuscles. [12] Each type of mechanoreceptor is sensitive to different stimulus. For example the Merkel disks and Ruffini endings are good at capturing low frequency vibrations that are below 10 Hz, while Meissner and Pacinian corpuscles are more sensitive to the high frequency vibrations from tens of Hz up to hundreds of Hz. [12] These mechanoreceptors will be able to detect the tactile sensation when it is above certain threshold value. Sensitive mechanoreceptors on human fingertips are able to recognise the force at the level of 10-100 mN with the displacements of 0.01 to 0.1 mm.

However, some studies have found that the human perception of haptic feedback is different in moving and static condition. [13] The perception of vibration could be degraded in the moving condition, even if the subjects are just walking normally. [13] Different body parts will also respond differently to the sensitivity degradation brought by the moving condition. The ankle and waist will be significantly affected while the foot and hand will mostly preserve their sensitivities. [13]

(How the mentioned visual, auditory and haptic signals are implemented in the project and their relevant engineering decisions will be covered in later sections. Specifically, the implementations of visual and auditory signal are discussed in *4.2 Electronic Components Choice* and the decision about haptic signal is covered in *4.1 High-level Project Architecture*)

2.3 Enabling Technologies and Their Comparison

Four wearable navigation devices of [3]-[6] discussed in *2.1 Wearable Electronic Device and Product Form Choice* section are enabled by certain modern technologies that are potentially

applicable to the smart glasses frame in this project. The enabling technologies of these devices are mainly related to power source, processing unit, inertial units, magnetic measurement unit and positioning unit. Totally five wearable navigation devices are discussed and compared below based on these aspects. Two of them are [5] (a hand-held device called ULISS that uses data fusion to perform navigation) and [6] (a glasses frame for turn-by-turn navigation), which have already been described in previous section. Three additional examples of [14] (a foot-mounted inertial PDR device), [15] (a torso-attached complex system for assisting blind people) and [16] (a back-mounted device for tracking movement of football players) are included for a more comprehensive analysis. The technical specifications of these five examples are tabulated in the **Table 2-2** below, where the information that is not available in the paper is denoted as N/A.

Table 2-2. Enabling technologies comparison of five wearable navigation devices in [5], [6], [14]-[16]

	ULISS [5]	Glasses Frame [6]	Foot PDR [14]	Torso Device [15]	Back Device [16]
Power Source	850 mAh LiPo Battery	LiPo Battley	LiPo Battery	Main Power: 2650 mAh LiPo Battery Auxiliary: 1000 mAh LiPo Battery	Two AAA-sized alkaline battery
IMUs	VN-300 3-axis Accel 3-axis Gyro (MEMS)	None	LSM303DLH 3-axis Accel (MEMS) L3G4200D 3-axis Gyro (MEMS)	None	LSM9DS1 3-axis Accel 3-axis Gyro (MEMS)
Magnetic	3-axis Mag (MEMS)	None	LSM303DLH 3-axis Mag (MEMS)	None	LSM9DS1 3-axis Mag (MEMS)
Positioning Unit (GNSS)	GPS (Chip-based)	GPS (Chip-based)	None	None	GPS GLONASS (Chip-based)
Processing Unit	N/A	ATMega48V (microprocessor)	STM32F217IGH6 (microprocessor)	Arduino Nano ATMega328P (microprocessor) Jetson TX2 (GPU accelerator)	ARM Cortex-M4 (microprocessor)
Additional Features	Pressure Sensor SD Storage	Bluetooth Web server	Bluetooth	Bluetooth Stereo camera Vibration Motor Haptic Feedback	Bluetooth On-board GNSS antenna

Where accelerometer, gyroscope and magnetic meter are abbreviated as Accel, Gyro, Mag in **Table 2-2**. LiPo stands for Lithium Polymer. The term MEMS stands for Microelectromechanical system. GNSS is for Global Navigation Satellite System and GLONASS stands for Global Navigation Satellite System.

It can be seen from **Table 2-2** that most examples have chosen LiPo battery as their portable power source. LiPo battery is a modern battery form that can provide high energy capacity in a

very compact form with reasonable cost. Typically the energy density of LiPo could reach 200 Wh/L [17]. This high energy density is critical to extend the lifetime per charge of wearable electronic device, particularly when volume and weight of the device is very limited.

Regarding the IMUs and magnetic meter, all devices in **Table 2-2** equipped with these units have chosen MEMS-based sensors. MEMS sensors integrate micro electrical components and mechanical system into a single integrated circuit package, which could provide extraordinary versatility and sensing performance in a very compact form. [18] This type of sensors is an excellent choice for wearable devices with limited power and space and also a key enabling technology to capture motions and detect bearing.

For the devices installed with positioning units in **Table 2-2**, all examples have chosen chip-based GNSS receiver that utilises the signal from one GNSS system (e.g., GPS) or multiple GNSS systems (e.g., GPS and GLONASS). One device ([16]) has designed additional on-board GNSS antenna to strengthen the captured positioning signals. Similar to the MEMS sensors, the chip-based GNSS receiver module is a compact solution to obtain real-time longitude and latitude with a relatively low cost. The power consumption of chip-based GNSS receiver, relatively low as it is (typically 200~300 mW), but usually the value is much higher than the power of MEMS accelerometer or gyroscope (typically 3~5 mW).

The choice of processing unit for the devices in **Table 2-2** is generally a certain model of microprocessor. The modern advanced 32-bit microprocessors can handle very complex tasks such as real-time signal processing from multiple signal sources or the control of various actuators to perform human-like tasks. Even the 8-bit microprocessors like the ATMega48V used by [6] and ATMega328P used by [15] can easily handle the basic sensor data capturing, processing and storing sequence. For some more demanding tasks such as real-time image analysis, more powerful processing units such as the Nvidia Jetson TX2 GPU accelerator used by [15] is required, but its power consumption will be much larger judging from the battery capacity (3650 mAh) of the device in [15]. A balance needs to be reached between the processing power and the size of the battery package.

(The specific engineering choices of these technologies for this project will be covered in 4.2 *Electronic Components Choice*)

2.4 Inertial Navigation versus Satellite Navigation

Beside the core function of guiding the wearer on a selected bearing using a series of feedbacks, other functions could also be added to the smart glasses frame in this project to enhance its performance, which will potentially broaden the product market and attract different customer groups. Since the inherent feature of the device is “guiding and navigating”, it is reasonable to add navigation-related functionalities that may not necessarily be implemented to provide additional assistance during orienteering (may spoil the game), but could be used to generate post-orienteering statistics such as travelled trajectory or average speed as activity summary to user for reviewing or coaching purposes. To produce such statistical results, motional information or the real-time location of the player need to be continuously recorded during the activity. Two mainstream methods to realise this are using motion sensors such as accelerometer, gyroscope and magnetic meter to capture human body dynamics, or using GNSS receiver to record the longitude and latitude constantly. These two methods correspond to the so called inertial navigation and satellite navigation.

The principle of satellite navigation is more intuitive. The GNSS receiver captures the transmitted signals from multiple dedicated satellites in the constellation so that the geolocation and time information of the receiver could be decoded and obtained. [4] The

trajectory of the receiver could then be derived based on the geolocation samples taken during the activity, as long as the sampling frequency is not too low. The advantages of satellite navigation are that it is a mature technology and a well-established solution that can typically reach an accuracy of 5 meters [4] for outdoor circumstances. A modern miniature GNSS receiver has a size similar to a coin and can be acquired at a relatively low cost.

The inertial navigation has a reverse logic compared to satellite navigation. The real-time acceleration, rotational speed and the heading could be obtained by the system rather than the actual geolocation in the form of longitude and latitude. The current wearer's location is estimated according to the previous location and the data from multiple sensors during this period. [19] This process is iterated to establish the travelled trajectory. Because the actual geolocation is never known, the error tends to accumulate as time gone by and the estimated trajectory is likely to drift away from the reality. [19] However, the advantage of inertial navigation is that the entire inertial system is independent of any satellite or infrastructure, which means the system will not be affected by the surrounding environment such as tall buildings, indoor scenarios or tunnels, where the GNSS signal could be significantly degraded or completely blocked. Also, the MEMS inertial sensors are usually smaller than a GNSS receiver and can be updated at a high frequency (a few hundred Hz up to 1000 Hz) with a lower power consumption. This enables them to capture more details within a certain period of time and a better accuracy could possibly be achieved.

(The decision about which navigation method to implement is covered in *4.1 High-level Project Architecture*)

2.5 Market Analysis and Available Commercial Products

The primary target group of the smart glasses frame is the people interested in the orienteering activity, or people who want to improve their record and speed by the assistance of technology. The number of people participated in the orienteering matches organised by the International Orienteering Federation (IOF) and British Orienteering Federation (BOF) could be used to estimate the potential market size of this product. The relevant statistics are not available from IOF but could be found in BOF annual report, which described the number of people participated in their orienteering matches from 2012 to 2020. These numbers are shown in the **Figure 2-6** below.

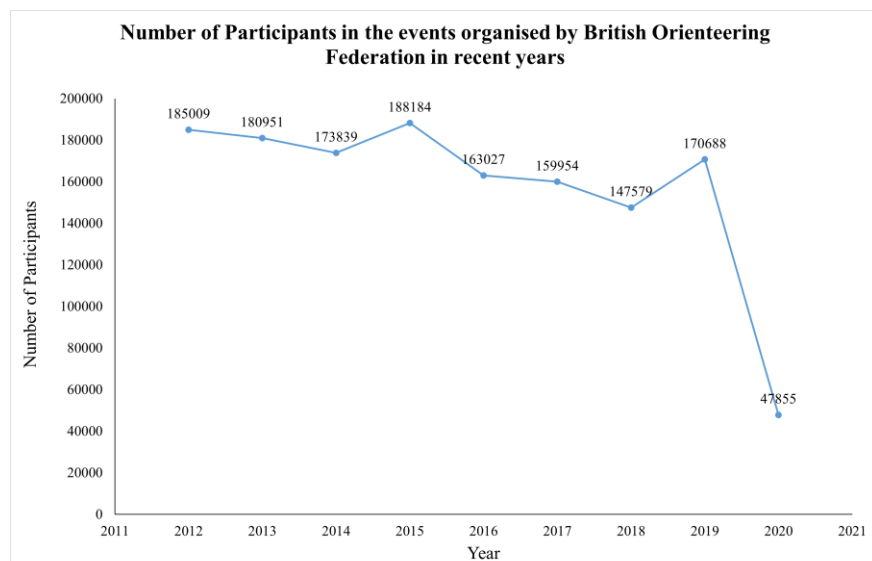


Figure 2-6. Number of participants in the events held by BOF from 2012 to 2020 [20]

It could be seen from **Figure 2-6** that the number of participants in the year of 2012 to 2019 was relatively stable. There was a dramatic decrease in 2020, which mainly resulted from the domestic travel and public event restrictions set by the government to cope with the spread of COVID 19 pandemic. The average number of participants was 171153 from 2012 to 2019, which was a relatively large number considering this was only the result of UK. The orienteering sport is more popular in countries located in northern Europe like Norway and Finland [21] thus the entire European market is considerable.

For the people who are interested in orienteering, there is no identical product (a LED indicator based smart glasses frame that can guide the wearer on a stable bearing) existing in the market but many commercial smart glasses that can realise similar functions do exist. These are alternative options for the same target group thus can be treated as competitors. Three commercial products from Google, Ray-Ban and Amazon are used as examples to demonstrate the features and technical specifications of mainstream smart glasses.

Google Glass is one of the well-known smart glasses projects launched in 2013 [22]. It is a glasses frame integrated with a head-mounted optical display with a human machine interface and a camera [22] as shown in the **Figure 2-7**. The glasses frame can undertake some functions that are originally provided by mobile phone such as calls, messages, video recording and notifications etc. via its own hardware or the Bluetooth connection to a smart phone. [22] For its implementation in orienteering, it is possible to utilise the optical head display as a window to display the real-time bearing measured by itself or the connected mobile phone to fulfil the guiding requirement. The camera could be used record the first-person footage during orienteering for analytic or collection purposes. However, the Google Glass has been controversial since its first prototype was launched as the head-wore camera is very likely to infringe others' privacy and expose safety risks. [23] The latest generation of Google Glass on sale is called Glass Enterprise Edition 2 and it costs around 881 [24] pounds.



Figure 2-7. First mode of Google Glass (left) and Glass Enterprise Edition 2 (right) [22]

The smart sunglasses developed by Ray-Ban has a dual-camera system, stereo speakers and 3 built-in microphones [25] as shown in **Figure 2-8**. The product positioning of this sunglasses is similar to Google Glass which acts as a complementary device to mobile phone and provides usual calling, messaging, music or video recording experience in the form of glasses. There is no visual interface in Ray-Ban glasses and the wearer can interact with the device using a touch panel and audio feedback via speakers. Such glasses, again, could possibly be implemented in orienteering to realise the required guiding functions by receiving the compass bearing or GPS location from the connected mobile phone and communicate this information to wearer via auditory signals. The dual-camera system can be utilised to capture stereoscopic photos or videos during orienteering. The Ray-Ban glasses is available in many different styles and costs 299 pounds each. [25]



Figure 2-8. Ray-Ban smart sunglasses [25]

The final example is from Amazon called Echo Frames [26] as shown in **Figure 2-9**. This device has minimised the product complexity and used audio feedback via speakers as the only method to communicate with the wearer. Similar to the previous two examples, Echo Frames can be connected to user's mobile phone for calls, messages, music and notifications. The visual assistant Alexa developed by Amazon is integrated into the glasses to provide voice control and AI (Artificial Intelligence) recognition. [26] As for the implementation in orienteering, it is possible for Echo Frames to receive real-time bearing or GPS location from the mobile phone and output them to the wearer, but the signal form is limited to audios only. Each Echo Frames costs 120 [26] pounds.



Figure 2-9. Echo Frames developed by Amazon [26]

(The difference between these commercial examples and the glasses frame developed in this project will be covered in *4.1 High-level Project Architecture*. The competitiveness of the proposed glasses frame will also be covered in the same section)

3. Aims, Objectives, Deliverables and Milestones

3.1 Aims

The aim of this project is to design, implement and validate a smart glasses frame that can guide the wearer on a stable compass heading and record data from sensors for subsequent analysis.

3.2 Objectives

3.2.1 Preparation Stage

- O1. Extensive literature review in the state-of-the-art wearable technologies for sports purpose and navigation purpose, meanwhile also covering the marketing needs and the driver for the technology.
- O2. Research about miniature IMUs, compass and other ICs required for the project and complete a list of components for order placement.

O3. Design an overall architecture of the entire system and confirm the functions to realise.
(The specific functions are described in *4.1 High-level Project Architecture*)

3.2.2 Design and Construction Stage

- O4. Design three PCBs that will be installed in the left leg, right leg and frontal frame of the glasses, and order the PCBs from the manufacturer.
- O5. Design and 3D print the glasses frame and test its compatibility with PCBs (if available).
- O6. Solder the PCBs and verify every sensor is working properly while applying necessary debugging procedure.
- O7. Programme the MCU to add basic navigation function first, then focus on logging system and signal processing.
- O8. Develop PC scripts to read the data from glasses and manipulate them to output required results of trajectory, distance and average speed.

3.2.3 Validation Stage

- O9. Assemble the entire system to validate all desiring functions and exhaust possible tests to assess the performance by recording experimental data. (All tests are covered in *5 Results, Discussions and Reflections*)
- O10. Optimise the system from both hardware and software perspectives to improve user experience
- O11. Complete the thesis to summarise the entire project development and include relevant analysis as well as potential improvements.

3.3 Justifications for Aim and Objectives

3.3.1 Aim Elaboration

The main aim of the project corresponds to the required core function of the glasses frame, that is, to use various sensors for collecting information to guide the wearer on a stable compass heading. The user should be able to select and lock onto an arbitrary heading, and the glasses frame should effectively communicate this information back to user through certain feedbacks, allowing the user to correct his/her moving direction with a hands-free operation.

The secondary aim is related to advanced navigation features mentioned in *2.4 Inertial Navigation versus Satellite Navigation* section. Positioning or motional information should be measured, recorded and stored by the glasses frame to enable the subsequent reconstruction of the travelled trajectory and the calculation of relevant statistics. The data should be processed on PC as post signal processing to obtain the desired results.

(The specific choices of sensors, the forms of feedback and the navigation method are covered in *4.1 High-level Project Architecture* and *4.2 Electronic Components Choice*)

3.3.2 Objective Elaboration and Justification

- O2: Because the UK is still under the impact of COVID-19, logistic and supply chain problems do exist. Confirming the component list and placing the order at an early stage is to cope with this uncertainty, thus there will be enough time to choose an alternative if the first choice is not available.

O3: An overall product architecture is planned at an early stage to ensure the conformability of shapes, slots, and weights between the PCBs and the glasses frame's mechanical structure design. The statistical parameters to realise during O8 will also be confirmed in O3.

O4: The PCBs are designed before the 3D model of the glasses frame because they will take a longer period to fabricate, and there is a 3D printing workshop in the university dedicated for the final year projects, thus the frame is more flexible to adjust and it can be iterated for multiple generations. The risks related to PCB are discussed in the *3.6 Risk Management & Elaboration for Deliverable and Milestones*.

O10: Since the glass frame is designed for sports like orienteering and sailing, the operating environment may have great humidity or vibration. It is necessary to ensure that the frame is firmly attached to wearer's face and is light, comfortable, waterproof and shock-resistant to some extent, to guarantee the durability of the device.

3.4 Deliverables

- D1. A completed literature review covering the project area and field, including the marketing needs, technology driver and potential ethical, social problems.
- D2. A list of all components required for this project, including their alternatives, manufacturers and the websites to order.
- D3. Three completed schematics and PCB designs
- D4. 3D printed glasses frame
- D5. Fully soldered and debugged PCBs
- D6. C program that can realise the basic navigation function
- D7. C program that can log all data successfully into a SD card during activity and the data can be exported for analysis
- D8. PC scripts for post-processing the data from glasses to generate statistical results
- D9. Optimised human-machine interaction and greater comfortability and durability of glasses frame
- D10. Debugged and validated smart glasses with all functionalities

3.5 Milestones

- M1. Three PCBs are designed and fabricated
- M2. Glasses frame is designed and printed
- M3. The whole system is assembled and basic navigation functions are verified
- M4. The logging system is working properly and corresponding signal processing algorithms on PC are developed
- M5. Final project report is completed and submitted

3.6 Risk Management & Elaboration for Deliverable and Milestones

*It should be noted that the content in this section is based on the detailed technical specifications covered in *4.1 High-level Project Architecture* and *4.2 Electronic Components Choice* sections, in order to propose feasible measures to very specific risks. This section is written before its basis contents in *4.1* and *4.2* to maintain a rigorous report structure.

The risks in this project majorly originate from PCB fabrication and debugging, since the success of this integrated glasses frame is heavily dependent on well-designed and functional PCBs. Most subsequent deliverables cannot be realised without the hardware from D3, D5 and M1. However it is possible that PCBs cannot be fabricated due to the closed factories and shipping delays caused by COVID-19 pandemic, or the assembled system can never be debugged successfully, thus a backup plan is proposed as follows.

The compactness of the system will be abandoned in Plan B and the revised version will be based on an existing Arduino Nano board. Commercially available IMUs and compass modules that can be directly connected to Arduino via Dupont wires will be implemented. Veroboard will be used to connect other components and an additional 3D printed box that can be mounted on the backside of wearer's head will be designed to contain all "magnified" components. These auxiliary components will be selected and purchased together with other components in D2, and will not be wasted if the PCBs work as anticipated, since they form a platform to familiarise with sensors and test the programs at an early stage. The algorithms for signal processing on PC will remain the same, and the programs in the embedded system and the 3D frame structure only need to be modified minorly, thus the progress will not be delayed and only the compactness will be sacrificed. The arrangement of this backup plan is covered in the Gantt Chart in *9.1 Appendix A Time Plan*.

Another risk, which is not as severe as the previous one, is related to the signal processing algorithms in D8 and M4. It is predictable that using raw data from IMUs to extract trajectory information and reconstruct it on PC will be difficult to realise, though other parameters like average speed or distance will be easier. If the algorithm for trajectory reconstruction cannot be developed, or the calculated result is far from reality, it will be discussed in the thesis and the difficulties encountered will be analysed as well. Complementarily, the existing algorithms proposed in research papers will be studied and discussed in the thesis to demonstrate the feasibility of inertial navigation and its merits and drawbacks compared to traditional satellite navigation.

3.7 Time Plan (Gantt Chart)

To maintain the proper text flow in the body of the thesis, the complete Gantt Chart of the project is included in *9.1 Appendix A Time Plan*. Relevant interpretation of the time plan is also included in the same appendix.

4. Methodology

4.1 High-level Project Architecture

4.1.1 Detailed Technical Specifications of the Glasses Frame

This section is used to describe the chosen human machine interface, navigation method, design ethos of the glasses frame in the form of a blueprint. The appearance of the proposed glasses frame and user experience will be fully clarified in this section.

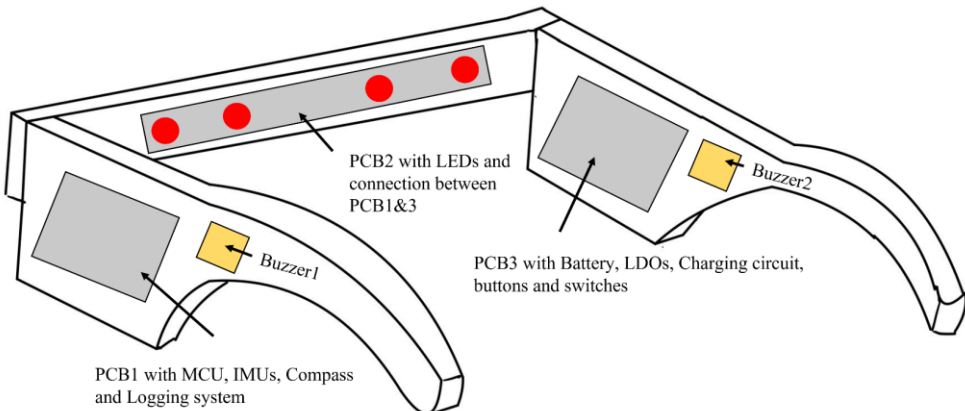


Figure 4-1. Blueprint of the glasses frame

The general idea of the above blueprint is to guide the wearer on a stable compass heading using the feedback signals of LEDs and buzzers. The user will be able to set a heading target by pressing a button on the glasses frame. Four LEDs will be used to indicate how much the current heading deviates from the selected target and the wearer will be alerted by the corresponding buzzer if the deviation to a certain direction becomes significant (the specific threshold values are covered in *5.3 Glasses Programming*). The user can press the button again to reset the heading target and the feedback system will respond to the updated heading accordingly.

As shown in the **Figure 4-1** above, red LEDs and piezoelectric buzzers are chosen to provide visual and auditory feedbacks to the wearer. The red LEDs are selected to maximally preserve wearer's night vision when the surrounding environment is dark during orienteering. This choice is made in consideration of safety risks and user comfort in the night. Relevant principles have been explained in the *2.2.1 Visual Signal* section. The piezoelectric buzzers are selected (instead of speaker) for their compact size and low power consumption. The alerting signal to the user does not need to be high-quality but distinctive and recognisable, which can be fulfilled by the energy-saving buzzers with no problem. The haptic feedback will not be implemented in the project due to its uncertain human perception during an intensive activity as mentioned in *2.2.3 Haptic Signal*.

Meanwhile, three PCBs (Printed Circuit Boards) together with other components will all be integrated into the legs and frontal frame of the device. The idea is to design and implement a very compact glasses frame with minimal weight and volume, since the purpose of the device is to accelerate wearer's movement during an intensive orienteering. A device with a heavy weight and a large size could cause additional burden to the player and may even diminish the performance. This design ethos means no existing boards or modules will be implemented in the design (except in the circumstances mentioned in *3.6 Risk Management & Elaboration for Deliverable and Milestones*) otherwise they cannot be fully integrated into the glasses frame. That is why the solution of fully customised PCBs with soldered chips is opted in this project.

It could also be seen from the blueprint that IMUs (Inertial Measurement Units) are included but not the GNSS receiver, indicating that the project opts to use inertial navigation to realise advanced features. The main reason is that the LiPo battery that can be installed in such a compact glasses frame will not be able to power the miniature chip-based GNSS receiver for even half an hour (more quantitative evidences and calculations in *4.2 Electronic Components Choice*). This duration is not acceptable as the normal battery life of a wearable device is at least one to two hours. The project also attempts to validate the performance of inertial navigation to see its feasibility and effectiveness in such a sport scenario.

(Other components, such as microprocessor and digital compass, that are included in the blueprint but will not affect the understanding of the whole picture of the project are covered in *4.2 Electronic Components Choice*.)

The entire glasses frame does not involve an optical displaying system or communication with other devices such as mobile phone and satellite, enabling it to be highly portable and fully independent. These two characteristics make it very suitable for the orienteering scenario in which the player can have a device with minimum weight and its working condition will not be affected by the surrounding environment. Not involving complex or expensive technologies also means the unit price of the product will be rather low after mass production. It is estimated that the unit price of the glasses frame could be controlled within 30 pounds, which clearly differentiates itself from the mentioned commercial examples of [24], [25] and [26] that are worth hundreds of pounds.

4.1.2 Signal Flowchart

A high-level signal flowchart of the project is shown in **Figure 4-2** below. The flowchart describes two different signal paths existing in the project. One of them originates from the real-time compass heading derived from the digital compass, flows into the microprocessor and followed by the output interface of LEDs and buzzers, finally flows towards the wearer of the device, indicating that the wearer receives the guiding information from the compass thus the core function of the glasses frame is realised. Another path starts from both the compass heading and the data from IMUs, then flows into the microprocessor. The IMU raw data and the compass heading are then stored into a micro SD card for the export into a PC. Post signal processing algorithms will be applied to the imported data and eventually the navigational results could be displayed to the user. This signal path corresponds to the advanced inertial navigation features that are related to the secondary aim of the project.

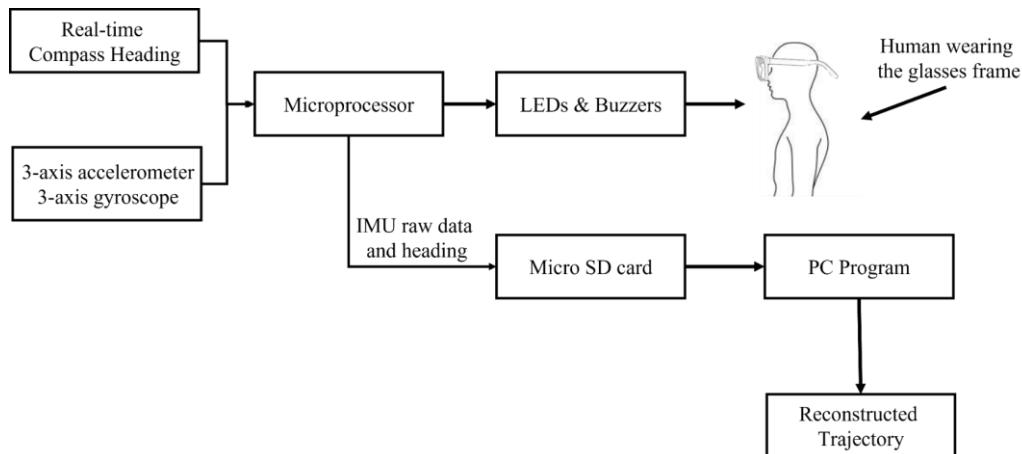


Figure 4-2. High-level signal flowchart of the project

4.2 Electronic Components Choice

This section is used to explain and justify for the component choices of the glasses frame. These choices are made based on the theoretical principles and comparisons covered in the *2 Literature Review and Market Research* section and they eventually lead to the PCB schematic designs in *5.1 PCB Design*.

4.2.1 Processing Unit

As compared in *2.3 Enabling Technologies and Their Comparison*, most examples of the wearable devices have chosen a microprocessor as its processing unit, which is a cheap,

compact and energy-saving solution. The tasks to be executed by the microprocessor in this project are mainly related to serial communications with sensors, LED and buzzer driving, data storage. These are not very demanding tasks for modern microcontrollers thus a mid-performance microprocessor will be able to fulfil all the requirements, and the resources and IO (Input and Output) pins could be maximally exploited.

An 8-bit low-power microprocessor called ATMega328P is selected for the glasses frame. The microprocessor has 32 KB of programmable flash memory and 2 KB of internal SRAM (Static Random Access Memory), 3 timers and 1 ADC (Analogue to Digital Converter) module, various built-in communication interfaces such as UART (Universal Asynchronous Receiver-Transmitter), IIC (Inter-Integrated Circuit) and SPI (Serial Peripheral Interface). [27] These peripheral and IO resources will be enough to handle the tasks required by the glasses frame.

Meanwhile, the microprocessor of Arduino Nano board is also ATMega328P, which means this model is available in the market and can be easily bought. Another advantage is that the ATMega328P will be able to seamlessly accept the open source Arduino Nano bootloader, allowing the developer to use Arduino IDE (Integrated Development Environment) to easily control and manipulate the hardware resources. This will accelerate the development progress thus more tests could be conducted in a time-limited one year FYP (Final Year Project).

4.2.2 Sensors and Micro SD

As inertial navigation is opted for the glasses frame, accelerometer, gyroscope together with magnetic meter are necessary sensors to be installed. It has been analysed in the *2.1 Wearable Electronic Device and Product Form Choice* section that MEMS sensors were adopted by many wearable device examples and their compactness, ultra-low current and cheap price are desirable for the current project. Thus all sensors implemented in the glasses frame are selected as MEMS chips.

MPU6050 in a QFN (Quad Flat No-lead) package containing both a 3-axis accelerometer and a 3-axis gyroscope based on IIC interface is selected for realise all inertial functions. The chip dimension is $4\text{mm} \times 4\text{mm} \times 0.9\text{mm}$. [28] There are six built-in 16-bit ADCs dedicated for digitising the 6-axis outputs from accelerometer and gyroscope, and the accelerometer supports the scale range of $\pm 2\text{g}$, $\pm 4\text{g}$, $\pm 8\text{g}$ and $\pm 16\text{g}$, while the gyroscope supports the scale range of ± 250 , ± 500 , ± 1000 , ± 2000 degrees/second. [28] These acceleration and rotational speed sensitivities should be enough to accurately capture the movement of the player during orienteering, and the chip size is small enough to be integrated into the compact glasses frame. Moreover, the MPU6050 is a very common inertial module in worldwide electronic developer communities thus there are countless useful libraries, program examples and debugging experience to refer to, which somehow reduces the development risks of this glasses frame.

For 3-axis magnetic meter, HMC5883L in a 16-pin LPCC (Leadless Plastic Chip Carrier) package is selected for the project. The chip dimension is $3\text{mm} \times 3\text{mm} \times 0.9\text{mm}$ and it can provide a heading accuracy of 1° to 2° . [29] The built-in 12-bit ADC will digitise the output data and the host device could read the 3-axis magnetic intensity information based on IIC interface. [29] Similar to MPU6050, the size, communication interface and measurement accuracy of HMC5883L are appropriate for the glasses frame. It is also a widely studied and used magnetic chip in user community thus open source libraries and examples are readily available.

As shown in the high level signal flowchart **Figure 4-2**, the output data from IMUs and magnetic sensors will be stored into a Micro SD card for subsequent analysis. The storage

room of the SD card should be big enough to contain the continuous samples from all sensors for 2 hours (the duration of desired battery life). Assuming the length of each number is 4 Byte (double precision) and 10 numbers (9-axis IMU and magnetic data plus the calculated bearing) are considered as one sample, 50 samples are required for one second if the sampling frequency is 50 Hz. The totally storage room for 10 different trips (each with a duration of 2 hours) is:

$$\text{Required Minimum Storage} = \frac{4 \times 10 \times 50 \times 3600 \times 2 \times 10}{1024 \times 1024} = 137 \text{ MB} \quad \text{Eqn. 4-1}$$

This is a relatively easy requirement for modern micro SD cards, as their storages usually reach 4 GB or higher. An 8 GB micro SD card from SanDisk is chosen for this project because the cards with smaller storage are becoming obsolete and their prices are even higher than the 8 GB model.

4.2.3 Human Machine Interface

As described in *4.1.1 Detailed Technical Specifications of the Glasses Frame*, red LEDs and piezoelectric buzzers will constitute the output feedbacks in the glasses HMI. The red LEDs are chosen to be 5mm through-hole tinted diffused LEDs as shown in the **Figure 4-3** below. The diameter is relatively large so that the visible light area is large for the wearer to easily recognise the light indication. The diffused package is selected to improve user comfort as the emitted light will not be too glaring. The buzzer is selected to be a thin, square, surface-mounted buzzer than can be easily integrated onto the PCB as shown in **Figure 4-3**. The frequency response of the buzzer (provide by the manufacturer) is shown in **Figure 4-4** and it could be seen from the figure that there is a waveform peak located at the frequency range of 3 kHz to 4 kHz, which is just the range in which the human hearing is most sensitive, as mentioned in the *2.2.2 Auditory Signal*. The loudness of the buzzer also reaches over 80 dB in that frequency range, which is louder than the normal human speech as noted in the *Table 2-1. The sound pressure level of 6 practical scenarios [10]*. This loudness is not very likely to be missed by the glasses frame wearer during the activity.

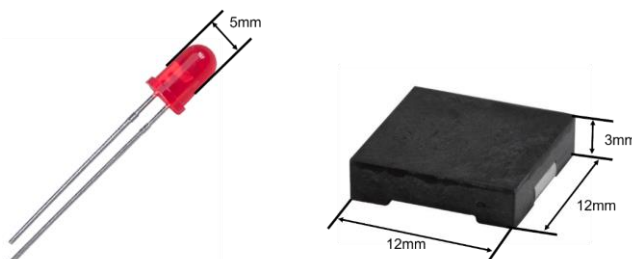


Figure 4-3. Appearance and dimension of the selected red LED and buzzer [30], [31]

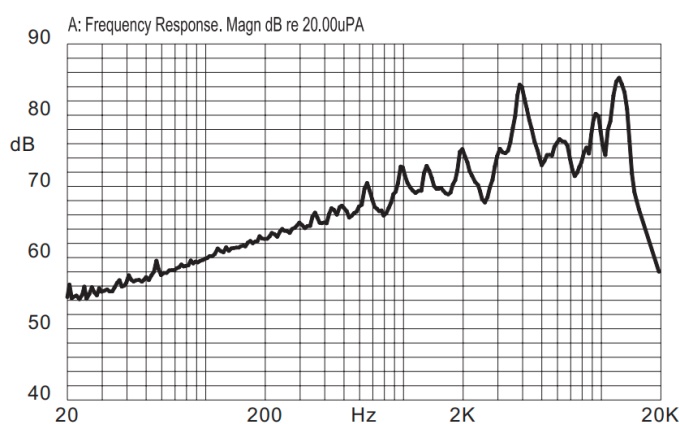


Figure 4-4. Frequency response of the selected buzzer [31]

Besides the red LEDs and buzzer in the device, additional HMI components such as switches and buttons are required to provide complete user interaction. One surface-mounted slide switch is selected to be the main power switch in the system. Two surface-mounted tactile buttons are chosen to provide customisable functions such as setting the target, changing the target or terminating the current activity. These components are all surface-mounted type because this form can be easily integrated with PCBs and occupies only small space.



Figure 4-5. The choice of slide switch (left) and push button (right) [32], [33]

4.2.4 Glasses Power System and Voltage Translator

The design of the glasses frame power system mainly focuses on the selection of battery capacity and the models of LDO (Low Dropout Regulator) and Boost chip. The maximum current in the system will be used as a criterion to determine the required current output from the LDO and Boost chips. This maximum current will also be used to determine the required battery capacity to reach a battery life of two hours per charge. Worst case estimation (assuming all components in the system are working at maximum power) is performed to obtain that maximum current value. Because the selected microprocessor is working at 5 V while other IMUs, digital compass and micro SD card are working at 3.3 V, two different voltage levels should be generated by different chips in the system. The current required by the 5 V components and 3.3 V components are calculated separately.

Before the worst case estimation of the current value, one additional component, the voltage translator, should be introduced to enable the communication between the 5V driven microprocessor and 3.3 V driven sensors and SD card. Both the IMU chip and compass chip communicate with host device using IIC protocol, thus requiring two channels of SCL and SDA. The micro SD card works under SPI protocol, hence four channels of CS, SCK, MISO, MOSI are required. Totally six channels require voltage level shifting thus an 8-channel (2^n) voltage level shifter is chosen to fulfil this task. The chosen model is called NXB0108, which is a dual supply voltage translator with auto direction sensing function and configurable voltage levels. [34] Two groups of ports could be powered by 5 V and 3.3 V respectively and the chip will complete the voltage translation automatically with an upper speed limit of 100 Mb/s [34], which is greatly beyond the required speed of IIC and SPI communication in this project.

(Certain characteristics of NXB0108 make it not an ideal choice for this project. This problem has been not considered during the designing stage but is discovered in the validation stage. Relevant discussions are covered in *5.1.2 PCB Reflection*)

With the voltage translator introduced, the current consumptions of all major components are summarised in the **Table 4-1** below. The power consumption of the peripheral decoupling capacitors and pull-up resistors are temporarily neglected.

Table 4-1. Maximum current of major components of glasses frame [27] -[31], [34]

Model Name	Model Type	Working Voltage (V)	Maximum Current Required (mA)
------------	------------	---------------------	-------------------------------

ATMega328P	Microprocessor	5	14
MPU6050	Accelerometer	3.3	3.9
HMC5883L	Magnetic Meter	3.3	0.1
NXB0108	Voltage Translator	5/3.3	0.07
/	8GB micro SD	3.3	70
TLHR640	Red LED	5	4×10
CPT-12123-81-SMT-TR	Buzzer	5	2×5

Based on **Table 4-1** above, the required current from the 5 V power supply is:

$$I_{5V} = 14 + 0.07 + 4 \times 10 + 2 \times 5 = 64.07 \text{ mA} \quad \text{Eqn. 4-2}$$

The required current from 3.3 V power supply is:

$$I_{3.3V} = 3.9 + 0.1 + 0.07 + 70 = 74.07 \text{ mA} \quad \text{Eqn. 4-3}$$

Since the typical voltage of a LiPo battery is 3.7 V, the 5 V in the system must be boosted from 3.7 V using boost chip, however the 3.3 V could be obtained by regulating 5 V or 3.7 V down to the desired voltage level. In this project, the 3.3 V is obtained from the boosted 5 V by connecting the LDO in cascade to the 5 V boost chip as shown in the **Figure 4-6** below. One reason for this cascade connection is that the entire system could still be properly powered during the debugging state, in which the battery will be replaced by the 5 V input from debugger. The 3.3 V will not be generated if the LDO input source is the battery. Another reason is that the 3.7 V from battery will not be stable when the device is working. It is possible that the battery voltage will drop below 3.3 V for a few milliseconds or longer, which may lead to the malfunction of LDO chip and the connected sensors and micro SD card may shut down. Using the regulated 5 V as LDO input source could avoid this problem.

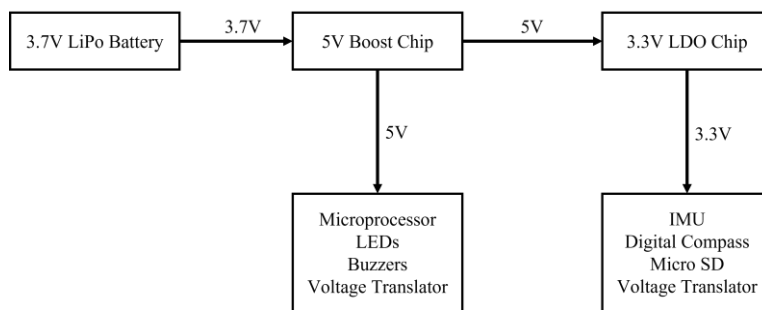


Figure 4-6. Power system flowchart of glasses frame

Following the power structure in **Figure 4-6**, the 5V Boost chip needs to supply both I_{5V} and $I_{3.3V}$, thus the minimum output capacity of the Boost chip is:

$$I_{Boost} = I_{5V} + I_{3.3V} = 64.07 + 74.07 = 138.14 \text{ mA} \quad \text{Eqn. 4-4}$$

(The Eqn.4-4 is not a rigorous current calculation but should be enough to estimate the required current for Boost chip)

The minimum output capacity of the LDO chip is:

$$I_{LDO} = I_{3.3V} = 74.07 \text{ mA} \quad \text{Eqn. 4-5}$$

Based on the current requirement calculated in Eqn.4-4, the Boost chip is selected to be MAX17223, which has a rated output current of 500 mA at 5 V with an accuracy of 1.5%. [35] The dimension of the chip is only 2mm by 2mm and the 500 mA output current has a huge

redundancy compared to the required 138.14 mA, ensuring the stable operation of the device. Similarly, for the current requirement in Eqn.4-5, the LDO chip is selected to be MIC5305, which has a rated output current of 150 mA at 3.3 V with an accuracy of 1%. [36] The dimension of the chip is also 2mm by 2mm, while the rated output current is doubled compared to the 3.3 V current requirement. These two Boost and LDO chip should be able to fulfil the power requirements of the system with a great stability.

Using the current values from Eqn.4-2 and 4-3, it is possible to calculate the energy required to keep the device running for an hour, and the result can be used to estimate the battery capacity. The maximum energy consumption of the device per hour is:

$$E_{max} = (5 \text{ V} \times 64.07 \text{ mA} + 3.3 \text{ V} \times 74.07 \text{ mA}) \times 1 \text{ h} = 0.56 \text{ Wh} \quad \text{Eqn. 4-6}$$

Ideally the battery should have $0.56 \times 2 = 1.12 \text{ Wh}$ to keep the device running continuously for two hours. Due to the physical size of the battery and its compatibility with the mechanical structure of the glasses frame, the redundancy of the battery capacity cannot be as large as the value for LDO and Boost chip. A 3.7 V LiPo battery in the dimension of 20mm \times 30mm \times 5mm is chosen for the system. The capacity of the battery is 0.925 Wh (250 mAh), which is slightly smaller than the ideal 1.12 Wh but should be enough to achieve a relatively satisfying battery life.

To easily recharge the battery in the device, an LiPo battery charging IC is also integrated into the electronic system. Since this chip is independent of other components, there is not much limitation on the selection criteria. The selected model is MCP73830/L, which is a dedicated single-cell LiPo battery management controller with a configurable maximum charging current and automatic control of “constant current” and “constant voltage” charging mode. [37] The chip dimension is 2mm by 2mm and the maximum constant charging current is 200 mA [37], indicating that the selected 250 mAh battery could be fully charged within 1.5 hours, which is a reasonable charging duration.

4.3 PCB Design

As proposed in the blueprint in **Figure 4-1**, three PCBs are required to complete the electronic system of the glasses frame and they will be installed in left leg, frontal frame and right leg of the glasses frame respectively. A more detailed overall PCB architecture is shown in **Figure 4-7** below.

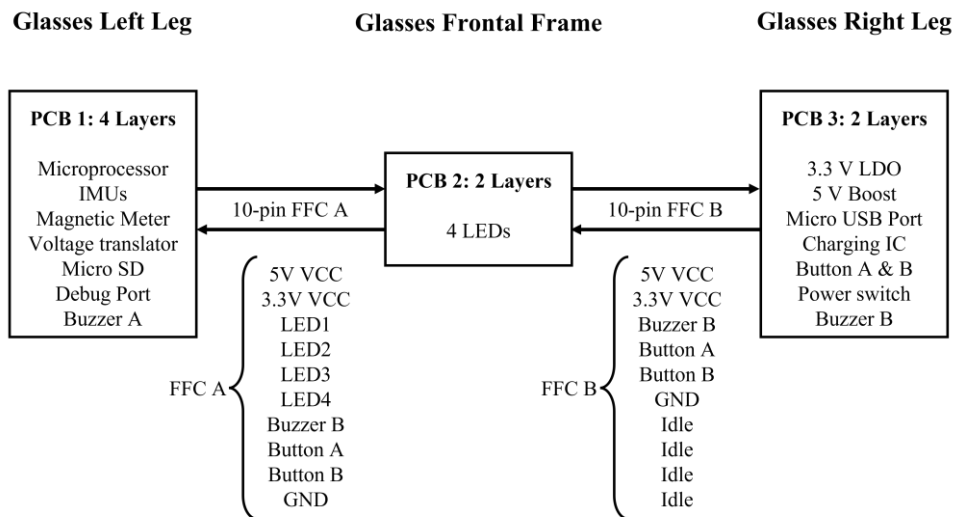


Figure 4-7. PCB architecture of the glasses frame

Four layers are required for the PCB in left leg since it contains the central processing unit and all sensors thus the routing density will be large, while two layers are enough for the less dense PCBs in the frontal frame and right leg. The connections between different PCBs are realised by 10-pin FFCs (Flat Flexible Cable) and the electrical assignment of each pin is specified in the **Figure 4-7**. 10 pins between PCB 1 and PCB 2 are fully utilised while only 6 six pins between PCB 2 and PCB 3 are used. The rest 4 pins are marked as idle and not electrically connected to any network in practice. The result in Eqn.4-3 has shown that the maximum possible current that will need to be supplied between boards on a single conductor is 74.04 mA, which means the pitch of the FFC (the width of each conductor) should be wide enough to reliably conduct this current. Also, the length of the FFC should be appropriate to bridge the gap between each PCB. To satisfy these two requirements, FFCs with a pitch of 0.5mm and a length of 51mm were selected as shown in **Figure 4-8**. [38] The 0.5mm wide conductor will be able to support 500 mA of current, which is well beyond the requirement of 74.04 mA.

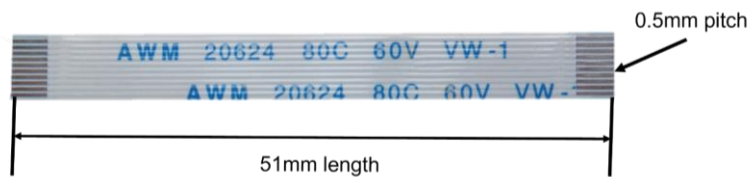


Figure 4-8. Specifications of the selected FFC [38]

The PCB schematics and layouts will be designed using Altium Designer in this project. This is a popular, powerful, and beginner-friendly CAD (Computer-Aided Design) tool. The company offers one year of student licence that is just enough to cover the development of the final year project. The schematic libraries and components footprints provided by manufacturers usually include the dedicated format for Altium Designer, which will simplify and accelerate the project development. Almost all footprints used in this project come from the official models from manufacturers and few exceptions are drawn manually due to the unavailability of relevant models on suppliers' websites.

4.4 Glasses Frame 3D Modelling and Printing

The mechanical structure of the glasses frame will be based on the blueprint in the **Figure 4-1**, which is consisting of a left leg, a frontal frame, and a right leg. The goal is to achieve a mechanical design that can be seamlessly integrated with three PCBs and rest firmly and comfortably on wearer's face. Both ergonomic factors such as lightweight, HMI accessibility and durability factors such as waterproof, shock-resistant will be considered in the designed process. Ergonomic factors are concerned to improve the human machines interaction and make operations of the device become intuitive and convenient for the user [39], while durability factors are improved to extend the lifetime of the device and make it more resilient to the external interference. In practice, the optimisation of the device on these factors is a complex and iterative process thus it is impossible to achieve a perfect design in a time limited FYP. The compatibility with PCBs and convenience for fast prototyping will be prioritised in the project and possible improvements for future generations are mentioned in *5.2.3 Modelling and Printing Reflections*. Because the device is a head-worn glasses frame, a dataset in [40] describing the average human head dimensions and shapes is used to determine the appropriate width and length of the legs, nose support etc. The dataset was included in *Appendix D Public Human Head Model Dataset*.

The 3D modelling process of the glasses frame will be completed by AutoCAD in this project. This CAD software from Autodesk is a very intuitive and beginner-friendly tool for 2D and 3D

modelling work. The company offers a student license to most of its CAD software to all engineering students in University of Nottingham and the license can be refreshed every year.

Regarding the prototyping method of the mechanical design, 3D printing technology is adopted in this project. There is a variety of different 3D printing methods existing in the market and the most common and widely used material extrusion-based method [41] is chosen for this project. The thermoplastic filament will be heated to a semi-liquid state and squeezed out from a very narrow nozzle along a certain path. [41] One layer of the component will be completed when the filament cools down. This process is repeated layer after layer thus finally the extrusion could be completed. The advantages of this technology are that its cost is very low and the printing speed is relatively fast, which means the design could be iterated and improved with a short duration and limited budget. 3D printers based on such technology are available in the EEE electronic workshop thus the printing service is still quite accessible even during the pandemic.

It should be noted that the 3D printing technology is a suitable method for quick prototyping and iterations but not for large-scale production. Its unit cost and manufacturing speed will quickly become unacceptable and disadvantageous when the number of products rises. In a realistic manufacturing process of a commercial product, assuming the product is still plastic-based, a plastic injection mould is required for fine precision and fast manufacturing speed. [42] The plastic particles will be heated and injected into the mould under a high temperature and pressure and the result workpiece will have very precise dimensions and low surface roughness. [42] Multiple workpieces may then be joined together using ultrasonic welding technology, which utilises a high frequency ultrasound vibration to slightly melt the contact surface of different components to realise a seamless and strong connection when cooled down. [43] These modern techniques are expensive though but should be able to achieve an overall lower unit price in a large-scale production.

4.5 Glasses Programming

Because the microprocessor of the glasses frame is selected to be the ATMega328P as mentioned in *4.2.1 Processing Unit*, which is the same choice as the Arduino Nano board thus the Arduino Nano Bootloader could be uploaded to the microprocessor to enable its compatibility with the Arduino IDE. This free IDE will be used to complete all embedded programming work of the glasses frame for its convenient code upload function and serial monitor. The serial monitor is particularly useful in calibrating the readings of IMUs and magnetic meter.

Another Arduino Nano board will be used as an ISP (In-system Programming) programmer to upload the bootloader to the microprocessor in the glasses frame via SPI protocol. The code required to set the Arduino Nano as an ISP programmer is provided by Arduino IDE as a code example ready to be implemented.

An additional debugger is required to convert the USB interface to serial UART communication to upload programs to the microprocessor (after the bootloader is installed). To mitigate the risk of incompatibility, a FT232RL based USB debugger as shown in the **Figure 4-9**, whose core translating chip is same the choice of Arduino Nano board, is chosen for this project. The original debugging through Mini USB port on the Arduino Nano board is replaced by 4 wires of TX, RX, 5V and GND connecting to the PCB located in the left leg of glasses frame. More details of the debugging related electrical connections will be covered in *5.1.1 PCB Results and Discussions*.

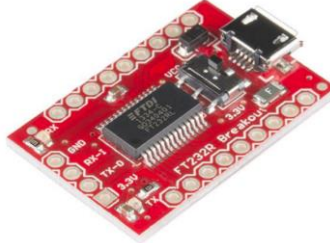


Figure 4-9. FT232RL based USB debugger from SparkFun [44]

All libraries and code examples used to program the glasses frame are either open source or under the MIT license, which specifies that the program can be used, copied and modified by anyone without restriction [45]. No infringement will be caused even if the developed glasses frame is for commercial purposes. A more detailed discussion about IP (Intellectual Property) problems will be covered in 6.5 *Intellectual Property*.

4.6 Post Signal Processing

The post signal processing will focus on reconstructing the trajectory based on the inertial and magnetic measurements. The calculation of other statistical results such as the travelled distance and average speed will become trivial if an accurate trajectory could be obtained. The recent methods proposed by other research papers to realise inertial navigation generally involve step length estimation and gait cycle analysis [3], [4], [14], which are mathematically complex and relatively difficult to accomplish within the limited time of FYP. A more basic method of double integration of acceleration in fusion with the estimated heading from magnetic meter is adopted in this project. The derivation of the heading from raw magnetic data is covered in 5.3.1 *Glasses Programming Results and Discussions* because it is related to the orientation of the chip HMC5883L on PCB. It is assumed that the current heading \hat{H} and the acceleration in parallel with the current travelling direction \vec{a} are known, thus the problem could be simplified as follows (2D discussion only):

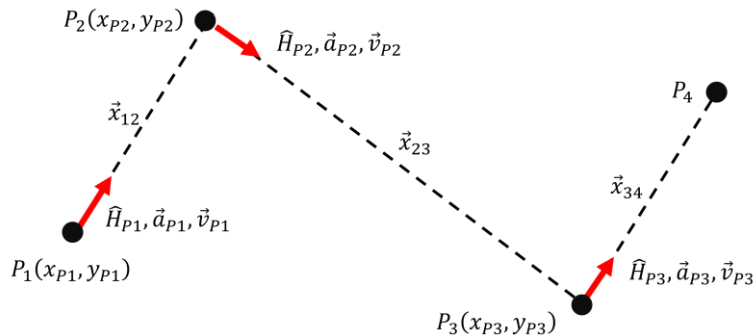


Figure 4-10. Simplified diagram of the trajectory reconstruction problem

Assuming the player traverses through point P_1, P_2, P_3, P_4 in turn and P_1 is the starting point thus its coordinates x_{P1}, y_{P1} and initial velocity \vec{v}_{P1} are known. The time duration between two adjacent points remains constant as Δt (constant sampling frequency). The accelerometer and magnetic meter can measure the instantaneous heading $\hat{H}_{P1}, \hat{H}_{P2}, \hat{H}_{P3}$ and instantaneous acceleration in parallel with the heading $\vec{a}_{P1}, \vec{a}_{P2}, \vec{a}_{P3}$. Taking the first two points P_1, P_2 as an example, assuming the \vec{a}_{P1} remains constant between P_1 and P_2 , the velocity at P_2 could be calculated as:

$$\vec{v}_{P2} = \hat{H}_{P2}(|\vec{v}_{P1}| + \vec{a}_{P1}\Delta t) \quad \text{Eqn. 4-7}$$

Thus the displacement between P_1 and P_2 is:

$$\begin{aligned}
\vec{x}_{12} &= \hat{H}_{P1} \left(\frac{|\vec{v}_{P1}| + |\vec{v}_{P2}|}{2} \right) \Delta t = \hat{H}_{P1} \left(\frac{|\vec{v}_{P1}| + |\vec{v}_{P1}| + \vec{a}_{P1} \Delta t}{2} \right) \Delta t \\
&= \hat{H}_{P1} \left(|\vec{v}_{P1}| \Delta t + \frac{1}{2} \vec{a}_{P1} \Delta t^2 \right)
\end{aligned}$$

Eqn. 4-8

The same derivation can be used again to calculate the displacement between P_2 and P_3 , P_3 and P_4 etc. thus not repeated. The coordinates of each point could also be obtained based on the coordinates of P_1 and the calculated displacements, the coordinates of P_2 are calculated as an example:

$$P_2(x_{P2}, y_{P2}) = \vec{x}_{12}(x, y) + P_1(x_{P1}, y_{P1}) \quad \text{Eqn. 4-9}$$

For general expressions of the velocity, displacement and coordinates of each point, they are derived as follows:

$$\vec{v}_{Pn} = \hat{H}_{Pn} (|\vec{v}_{P1}| + \vec{a}_{P1} \Delta t + \vec{a}_{P2} \Delta t + \vec{a}_{P3} \Delta t + \dots + \vec{a}_{Pn-1} \Delta t) = \hat{H}_{Pn} \left(|\vec{v}_{P1}| + \Delta t \sum_2^n \vec{a}_{Pn-1} \right)$$

Eqn. 4-10

$$\begin{aligned}
\vec{x}_{n-1|n} &= \hat{H}_{Pn-1} \left(\frac{|\vec{v}_{Pn-1}| + |\vec{v}_{Pn}|}{2} \right) \Delta t \\
&= \hat{H}_{Pn-1} \left(\frac{|\vec{v}_{P1}| + \Delta t \sum_2^{n-1} \vec{a}_{Pn-1} + |\vec{v}_{P1}| + \Delta t \sum_2^n \vec{a}_{Pn-1}}{2} \right) \\
&= \hat{H}_{Pn-1} \left(|\vec{v}_{P1}| + \Delta t \sum_2^{n-1} \vec{a}_{Pn-1} + \frac{1}{2} \vec{a}_{Pn-1} \Delta t \right)
\end{aligned}$$

Eqn. 4-11

$$\begin{aligned}
P_n(x_{Pn}, y_{Pn}) &= P_1(x_{P1}, y_{P1}) + \vec{x}_{12} + \vec{x}_{23} + \vec{x}_{34} + \dots + \vec{x}_{n-1|n} \\
&= P_1(x_{P1}, y_{P1}) + \sum_2^n \vec{x}_{n-1|n} \\
&= P_1(x_{P1}, y_{P1}) + \sum_2^n \hat{H}_{Pn-1} \left(|\vec{v}_{P1}| + \Delta t \sum_2^{n-1} \vec{a}_{Pn-1} + \frac{1}{2} \vec{a}_{Pn-1} \Delta t \right)
\end{aligned}$$

Eqn. 4-12

The translation of the above equations for inertial navigation into algorithms will be covered in *5.4.1 Post Signal Processing Results and Discussions*.

Before the implementation of the above reconstruction method, it is predictable that the samples from IMUs and magnetic meter are noisy and distorted, thus filters are required to perform pre-conditioning of the raw data to improve the integration accuracy. Because the data from IMUs and magnetic sensors are all discrete samples, software-based digital filters are applicable for this scenario. Two different digital filtering methods, impulse response with the correction of window function, and Kalman filter, are developed and implemented to reduce the noise and distortion of the raw sensor data.

The first method began with the impulse response is a common method to design FIR (Finite-Impulse Response) digital filter. The coefficients of the filter can be obtained if the

impulse response of the filter is determined. [46] Specifically for the glasses frame, it is the envelop of the sensor raw data that needs to be extracted thus a low pass filter with a cut-off frequency of ω_c is required. The ideal impulse response of a low pass filter is as follows, where n is the length of the filter:

$$h(n) = \frac{\omega_c}{\pi} \frac{\sin(n\omega_c)}{n\omega_c} \quad \text{Eqn. 4-13[47]}$$

Because the impulse response of a FIR filter is truncated to a finite length, unwanted ripples will be caused at the left and right side of the impulse peak. [46] To reduce such effects of FIR to the frequency spectrum, a window function could be selected to correct and compensate for the ripples caused. One common and useful choice is Hamming window, which has a low peak sidelobe amplitude and an appropriate width of the main lobe. The expression of the Hamming window is as follows, where M is the window width and n is the index of samples.

$$w(n) = \begin{cases} 0.54 - 0.46 \cos\left(\frac{2n\pi}{M}\right), & 0 \leq n \leq M \\ 0, & \text{otherwise} \end{cases} \quad \text{Eqn. 4-14[46]}$$

The corrected impulse response is $h'(n) = h(n)w(n)$ and can be used to derive the frequency response and coefficients of the filter.

The second method, Kalman Filter, is a digital filtering algorithm that can be used to estimate the unknown variables in the system based on a series of prior measurements and various types of noise and inaccuracies. [48] This filtering algorithm and its variants are widely implemented in dynamic motion analysis and control of aircrafts and robots, and has been proven effective for various scenarios. [48] The mathematically interpretation behind Kalman Filter is very complex thus not fully illustrated in this section. This project focuses on its application and its main equations are as follows:

$$x(k) = A \cdot x(k-1) + B \cdot u(k) + w(k) \quad \text{Eqn. 4-15[48]}$$

$$z(k) = H \cdot x(k) + y(k) \quad \text{Eqn. 4-16[48]}$$

$$x(k|k-1) = A \cdot x(k-1|k-1) + B \cdot u(k) \quad \text{Eqn. 4-17[48]}$$

$$P(k|k-1) = A \cdot P(k-1|k-1) \cdot A^T + Q \quad \text{Eqn. 4-18[48]}$$

$$K(k) = P(k|k-1) \cdot H^T \cdot (H \cdot P(k|k-1) \cdot H^T + R)^{-1} \quad \text{Eqn. 4-19[48]}$$

$$x(k|k) = x(k|k-1) + K(k) \cdot (z(k) - H \cdot x(k|k-1)) \quad \text{Eqn. 4-20[48]}$$

$$P(k|k) = (I - K(k) \cdot H) \cdot P(k|k-1) \quad \text{Eqn. 4-21[48]}$$

Where $x(k)$ is the status of the system at time k , $u(k)$ is the applied control at time k , $w(k)$ is the Gauss-distributed process noise at time k , $z(k)$ is the observed value of the system at time k , $y(k)$ is the Gauss-distributed measurement noise at time k , Q and R are the covariance of the noise $w(k)$ and $y(k)$, $P(k)$ is the covariance of the error, $K(k)$ is the Kalman gain. A, B, H are coefficients of the system.

To implement the above two filtering methods, MATLAB is selected as the post signal processing platform to accept the raw data and provide statistics/reconstructed trajectories. The main reason for this choice is that MATLAB has a wide variety of different signal processing tools and built-in functions that can be directly exploited to accelerate the development. Functions such as “designfilt()” can be used to easily design a low pass filter with certain orders and cut-off frequencies. The impulse response and Hamming window will be automatically processed by this function to generate the desired frequency response. Meanwhile, since MATLAB is optimised to cope with matrix operations, it is also an

appropriate choice for implementing the Kalman Filter algorithm which involves a great number of matrix manipulations.

5. Results, Discussions and Reflections

5.1 PCB Design

5.1.1 PCB Results and Discussions

In this section three PCBs of the glasses frame would be demonstrated one by one, covering their 3D rendered models and actual soldered boards. The schematics and 2D layout designs were included in *Appendix B PCB Schematics and 2D Layout Designs*. Relevant emphasis of major functions and components would be covered for each PCB respectively. Generally, the PCB design of the electronic system strictly followed the high-level system architecture proposed in *Figure 4-7. PCB architecture of the glasses frame*. A complete BOM (Bill of Material) list containing all the components for three PCBs was include in *Appendix C PCB BOM List*.

5.1.1.1 PCB1: Left Leg

The PCB1 in the left leg had a dimension of 20mm (width) by 70mm (length). The choices of width and length of this PCB were related to the PCB3 in the right leg thus they were all explained in *5.1.1.3 PCB3: Right Leg*. The design and implementation results of the PCB1 were shown below:

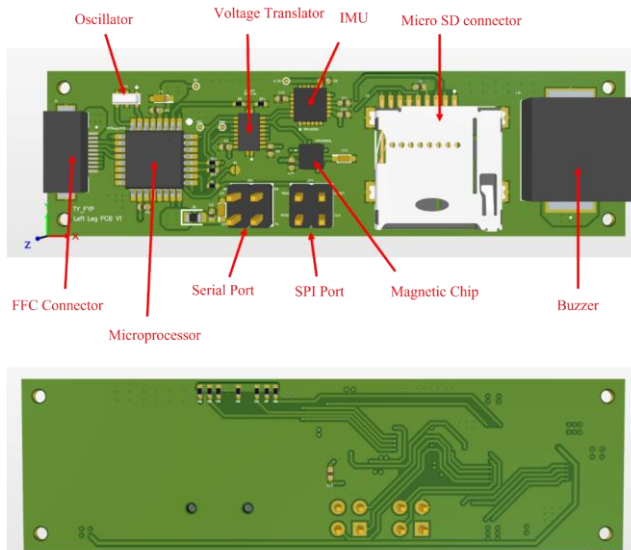


Figure 5-1. Top side (top) and bottom side (bottom) view of PCB1 3D rendered design with notations of major components

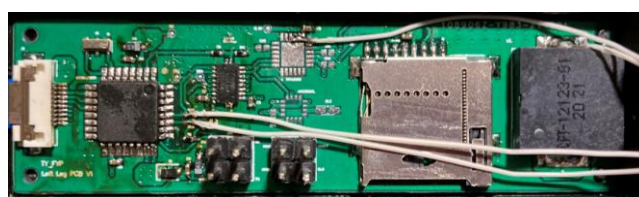


Figure 5-2. Top side of the soldered PCB1 with missing IMU and magnetic chip

It could be seen from **Figure 5-1** that the voltage translator was placed between the microprocessor and sensors to create an easy routing scheme. The opening slot of the Micro SD card connected was pointing downward so that water (rain drops) was less likely to enter the

device during the activity. The buzzer was placed closest to the right edge thus it was close to human ears and the perceived auditory signal will be loud and clear. It could also be seen that there were two ports on the PCB1, each was consisting of four header pins. The serial port was constituted of 5V, GND, TX and RX, and was used for regular program uploading and debugging process. The SPI port was constituted of MOSI, MISO, SCK and Reset, which was specifically used for uploading the bootloader of Arduino Nano to the microprocessor.

As mentioned in **Figure 4-7**, PCB1 was based on a 4-layer design. The top and bottom layers were used for signals and ground plane, while the middle two layers were used for power planes of 5V and 3.3V. This significantly reduced the number of tracks on the top and bottom planes as all power connections can be realised by depositing vias near the target components, thus components can be closer on the PCB and a more compact layout could be fulfilled. For all tracks responsible for conducting “signals” (with small current), the track width was set to 8 mils. For other tracks responsible for conducting “power” (large current) from vias to components, either a polygon copper region was introduced or the track width was selected based on the following Eqn.5-1, where w was the calculated width in mils and I was the required current in amperes. The criterion was followed for all three PCB designs.

$$w = 20I \quad \text{Eqn. 5-1}$$

It could be seen from **Figure 5-2** that the IMU and magnetic chips were missing on the actual soldered PCB1. This was because of an inappropriate choice of voltage translator in the electronic system designing stage, as mentioned in *4.2.4 Glasses Power System and Voltage Translator*. The chosen NXB0108 was a model specifically designed with low static drive strength, which was applicable for communications based on push-and-pull IOs such as SPI. [34] It would not be able to provide enough driving strength for open-drain applications such IIC. As all sensors were based on IIC communication but the micro SD was based on SPI communication, it had been validated practically that the micro SD card could be successfully read and written through the voltage translator but the IIC communication between the microprocessor and the sensors could never be established. To temporarily resolve this issue, the IMU chip and magnetic meter chip were removed from the PCB and two existing modules containing the identical chips were connected to the microprocessor directly via some wires as shown in **Figure 5-3**. They had the exact same functions as the chips on boards and this would make sure the prototype could still be demonstrated to the stakeholders within the time allowance (there was not enough time to manufacture another version of PCB).

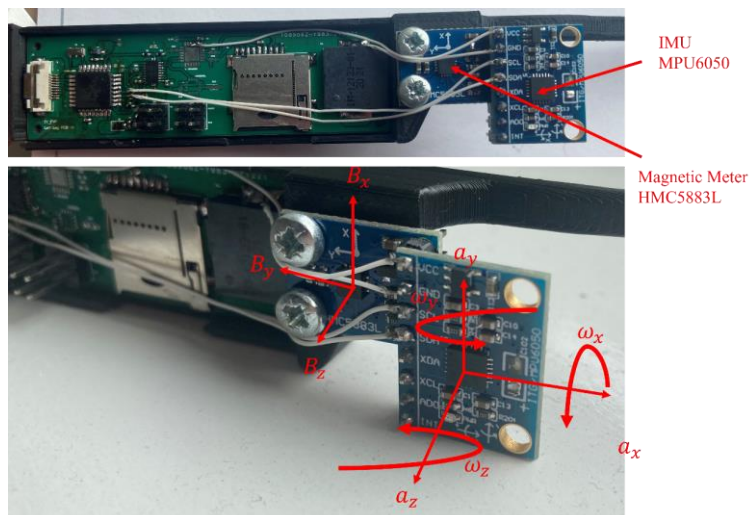


Figure 5-3. IMU and magnetic meter modules attached to the frame with the notation of directions of 3-axis acceleration, rotational speed and magnetic field intensity.

The best method to correct this mistake in future generation was to choose another 4-channel voltage translator designed for push-and-pull driving to ensure the operation of micro SD card, and establish the IIC communication only using the pull-up voltage of 3.3 V as shown in **Figure 5-4**. The 3.3 V voltage level would be recognised as a “logic high” in both 3.3V and 5 V system, and the chip running on 3.3 V would not be damaged by excessive voltage because the IO driving was realised by 3.3 V source via a pull-up resistor.

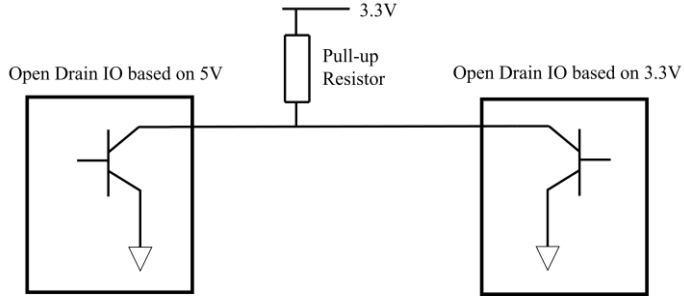


Figure 5-4. Optimised IIC configuration method of one IO

5.1.1.2 PCB2: Frontal Frame

The dimension of PCB2 in the frontal frame was 12mm (width) by 140mm (length). The width was selected to be a minimum value that was enough to incorporate the FFC connector on board. The length was selected to be slightly smaller than the mean value of human head breadth (145mm) proposed in [40] so that the distance between four LEDs could be maximised while the glasses frame could still be comfortably worn on user’s face. The design and implementation results of PCB2 were shown below:



Figure 5-5. Top side (top) and bottom side (bottom) view of PCB2 3D rendered design



Figure 5-6. Top side of the soldered PCB2 with full functionalities

The PCB2 was responsible for providing mechanical and electrical connections of four indicating LEDs and acting as wires to connect various signals and power supplies between the other two PCBs. The design and implementation results could be fully described by the figures above thus no more discussions were made.

5.1.1.3 PCB3: Right Leg

The dimension of PCB3 in the right leg was 20mm (width) by 30mm (length). The width of PCB3 (same as the width of PCB1) was selected to be same as the width of the battery as it was the minimum value for right leg to incorporate all the components. As stated before, the length of PCB1 was 70mm, which was selected to be smaller than the length between human eyes and ears thus the integrated PCB1 would not affect the wearing comfortability. The length of PCB3

was selected to realise a symmetrical design in right leg compared to left leg. The summation of the length of PCB3 (30mm), battery (30mm) and buzzer (10mm) just equalled to the length of PCB 1 in the left leg as shown in **Figure 5-7**.

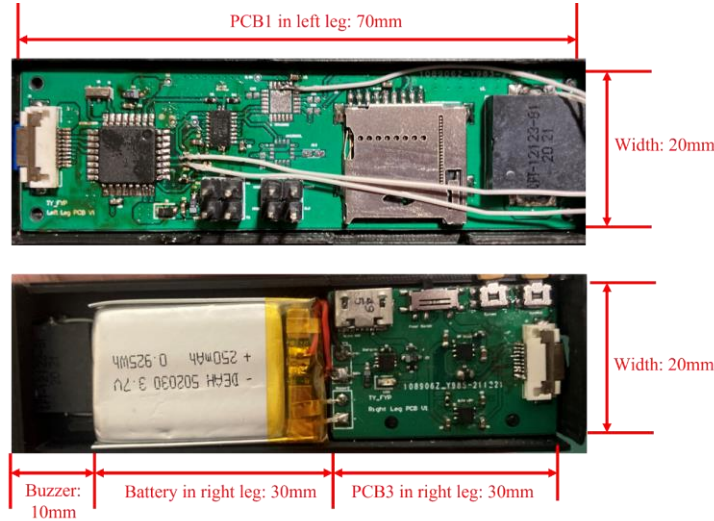


Figure 5-7. The symmetrical design of left leg and right leg components

The design and implementation results of PCB3 were shown below:

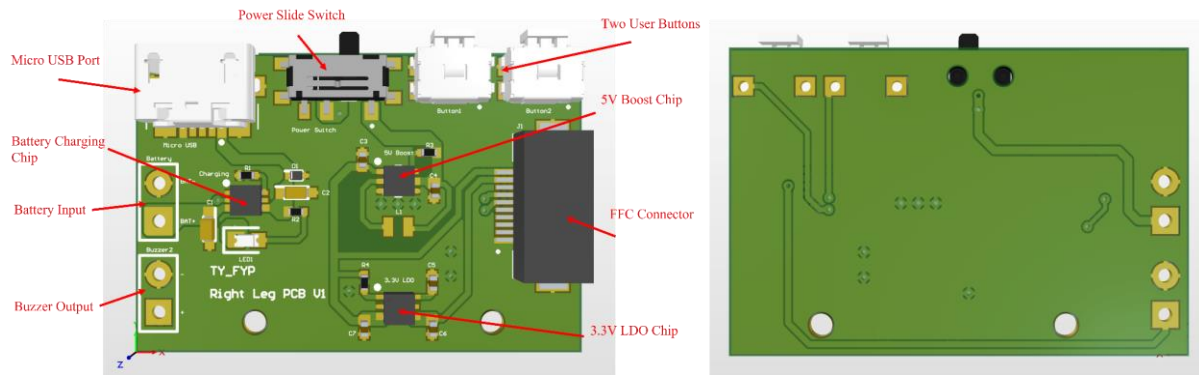


Figure 5-8. Top side (left) and bottom side (right) view of PCB3 3D rendered design with the notations of major components



Figure 5-9. Top side of the soldered PCB3 with full functionalities

The PCB3 was responsible for generating and controlling all the required power sources for the PCB1, charging the battery and providing interaction with the glasses frame via two buttons. The detailed functions of buttons were covered in *5.3 Glasses Programming*. It could be seen from **Figure 5-10** that the actual generated voltage levels were 3.30 V and 5.03 V, which were very close to the required values of 3.3 V and 5 V.



Figure 5-10. 3.3V and 5V power sources measured oscilloscope

(The rest validation of sensors, micro SD card, HMI and microcontroller were covered in *5.3.1 Glasses Programming Results and Discussions*)

5.1.2 PCB Reflection

5.1.2.1 Via Size and Silkscreen

Usually the minimum via size (diameter) used in a PCB design determined whether the manufacturer would charge additional fees for “small via cost”, since small vias would lead to a higher failure rate and the drill bits were more likely to break. The threshold value varied from manufacturer to manufacturer but generally it was close to 12 mils (0.3 mm), which was also the value adopted by the manufacturer chosen for this project’s PCBs. The reason for mentioning this was because smaller vias (10 mils, 0.25 mm) were used in the PCB1 due to the high density of tracks and IC pins. As PCB1 was also based on a 4-layer design, these two characteristics made its unit price four to five times more expensive than the other two PCBs, where 2-layer board and 12-mil via size were adopted. After a careful review of the layout design of PCB1, it was possible to redesign the board with the larger via size of 12 mil by re-allocating the positions of components and re-routing the PCB tracks. This might not be a major problem for prototyping purpose but would be able save a great amount of money in large-scale production thus the product could be more competitive.

It could be seen from the actual soldered boards in **Figure 5-2**, **Figure 5-6** and **Figure 5-9** that silkscreens on all boards were fuzzy and difficult to recognise. This was because the manufacturing precision of silkscreen characters were overestimated during the design stage and the font size and thickness were set to be too small, thus the actual printed annotations were not recognisable. This problem would not affect the electrical performance of the PCBs but would degrade the manual assembling efficiency because the value of resistance, capacitance etc. would need to be checked in the CAD software for soldering each component. Such problem could be easily corrected in future generations.

5.1.2.2 Location and Orientation of Components on Board

It could be observed from **Figure 5-9** that two user buttons were very close to each other (only few millimetres in between), which was likely to lead to the mis-press by the wearer. Four components of two buttons, one slide switch and one micro USB charging port in a row made it very difficult to adjust the locations of buttons due to the limited width of PCB3. One possible solution was to move the USB charging port to the bottom of PCB3 and flip its orientation to downward. The charging port would still be close to the battery and charging IC thus the no complex routing scheme was needed. Meanwhile, the charging point was pointing downward meant it was less likely to be affected by rain drops during the activity, hence the waterproof capability could be improved. One of the buttons could now be moved to the original location of USB charging port and the distance between two buttons would be much larger. Each button was just electrically connected to one pin of FFC connector and ground plane, which meant this movement would also not cause problematic routing issue.

5.1.2.3 PCB Assembly

All PCBs were assembled manually using a soldering iron and a hot air gun without any other specialist equipment. This was a difficult and risky process since most chips used in this project were very small (2mm by 2mm) and some MEMS sensors were also very sensitive to temperature variation and mechanical bump. Most chips were validated to be fully functional with two or three soldering attempts, during which some chips were permanently damaged due to inappropriate control of soldering temperature. The reliability of the soldering process could be greatly improved by introducing solder paste (rather than solder wire) and a reflow heating platform with precise temperature control. The soldering duration and temperature curve specified in the datasheets of ICs could be followed and the success rate and soldering quality would be much higher.

The manual assembly process also put limitations to the choice of minimum component size. The package of most standard components such as SMD (Surface-Mounted Device) resistors and capacitors on boards was 0402, as it was very difficult to manually solder smaller packages such as 0201. The PCB designs in this project were thus for prototype demonstration purpose but not suitable for large scale production, as the component package size was much larger than the size used in modern commercial products, particularly high-portable wearable electronic devices. The PCBs should be redesigned to resolve this issue if used for commercial purposes in the future.

5.1.2.4 Future Possibility of Flexible Circuit

The current design of PCB2 in the frontal frame was based on a standard piece of rectangle, unbendable FR-4 material (a type of fibreglass). Although the width of the PCB2 was relatively small, its long, rectangle shape still put many constraints on the mechanical structure of the frontal frame. The frontal frame had to be mostly straight and had a long rectangle slot to contain the current PCB2 design. One great solution to solve this issue was to implement the design using flexible circuits shown in **Figure 5-11** below, which would create a great number of possibilities to the mechanical structure of the glasses frame. Curvy designs could be used to improve user comfort and also aesthetic factors of the glasses frame. Meanwhile, metallic contact pads could be introduced to the terminals of the flexible circuit to provide electrical connections with other two PCBs instead of the current FFC solution. The stability of the entire electronic system could be enhanced and potentially the cost could also be reduced.



Figure 5-11. An example of flexible circuit [49]

5.2 Glasses Frame 3D Modelling and Printing

5.2.1 3D Modelling Results and Discussions

This section would first demonstrate the overall modelled structure of the glasses frame and then emphasise important sections and features such as the hinge system of the proposed model. The demonstration would be based on the screenshots of the constructed model in AutoCAD. The 3D models of the PCBs designed in the above section were exported from

Altium Designer as Step files to be integrated with the mechanical structure in AutoCAD, forming a complete preview of the eventual product.

5.2.1.1 Overview and Dimensions

Generally, the entire glasses frame was consisting of six major structures of left leg, left lid, right leg, right lid, frontal frame and nose support. These names would be referred to in subsequent discussions. An “fillet” operation with a radius of 1mm was conducted for most shape edges of the glasses frame to achieve round corners for user comfort. An exploded view and an assembled view of the glasses frame (including PCBs) were shown in the **Figure 5-12** below.

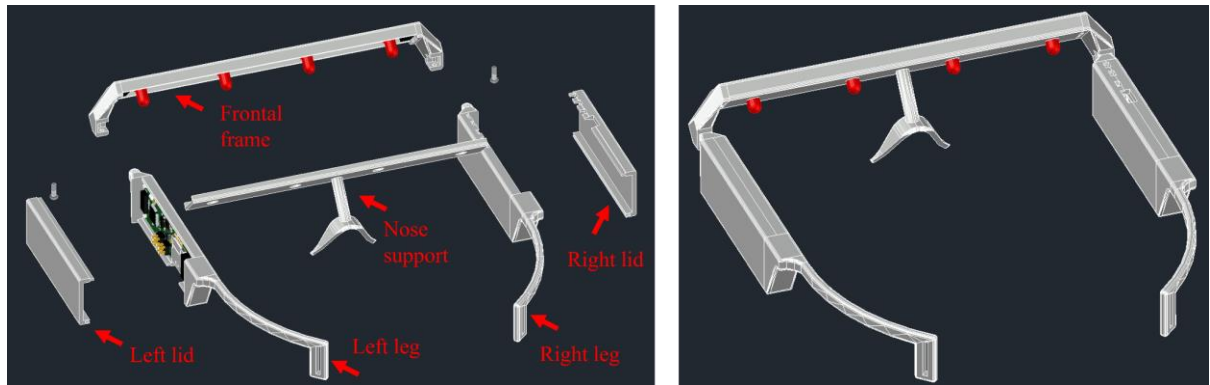


Figure 5-12. Exploded view (left) and assembled view (right) of the modelled glasses frame

The dimensions of the glasses frame were determined based on the dataset in [40] and developer’s own experience. These values had not been tested and validated for a large group of people thus were just primitive results for prototyping purpose. The following figures of the glasses frame from front, top and right perspective were used to describe major dimensions.

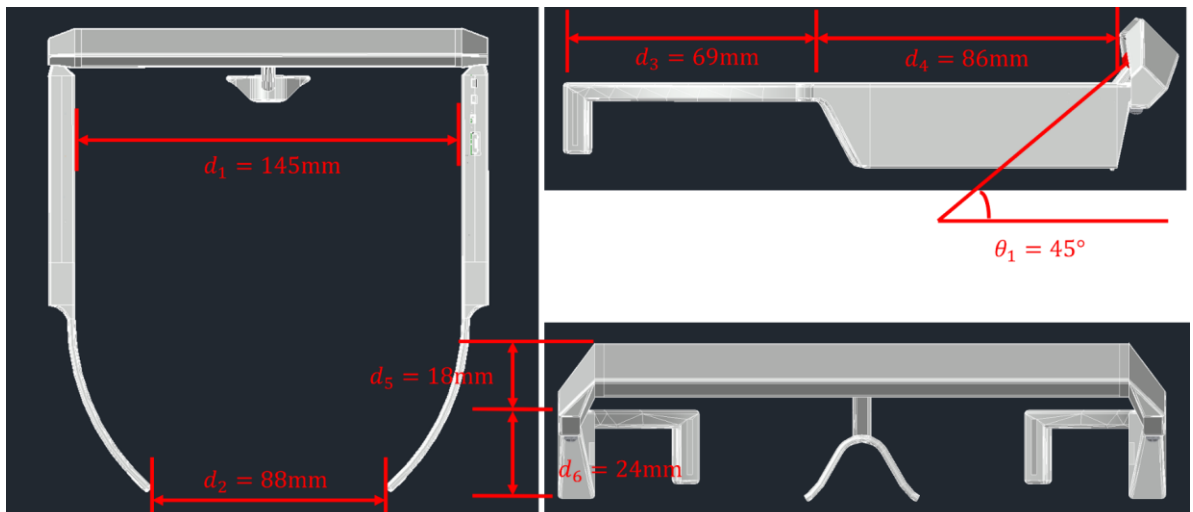


Figure 5-13. Front (bottom right), top (left) and right (top right) view of the glasses frame with notations of major dimensions

5.2.1.2 Connections with PCBs and Reserved Slots

The room inside the left leg, right leg and frontal frame of the glasses structure was designed to be just enough to contain the PCBs together battery and buzzer thus the PCBs in the glasses frame would not be able to move due to vibrations caused during orienteering. Besides this, a

“locking” mechanism was introduced to make the connections between PCBs and glasses frame even stronger, which was realised by dedicated cylinders that matched with positions and sizes of certain through-holes on the PCBs. The reserved through-holes on PCBs could be clearly seen from the 3D rendered models in **Figure 5-1**, **Figure 5-5**, **Figure 5-8**. The PCBs could be precisely installed onto these cylinders (marked by red squares) as shown below.

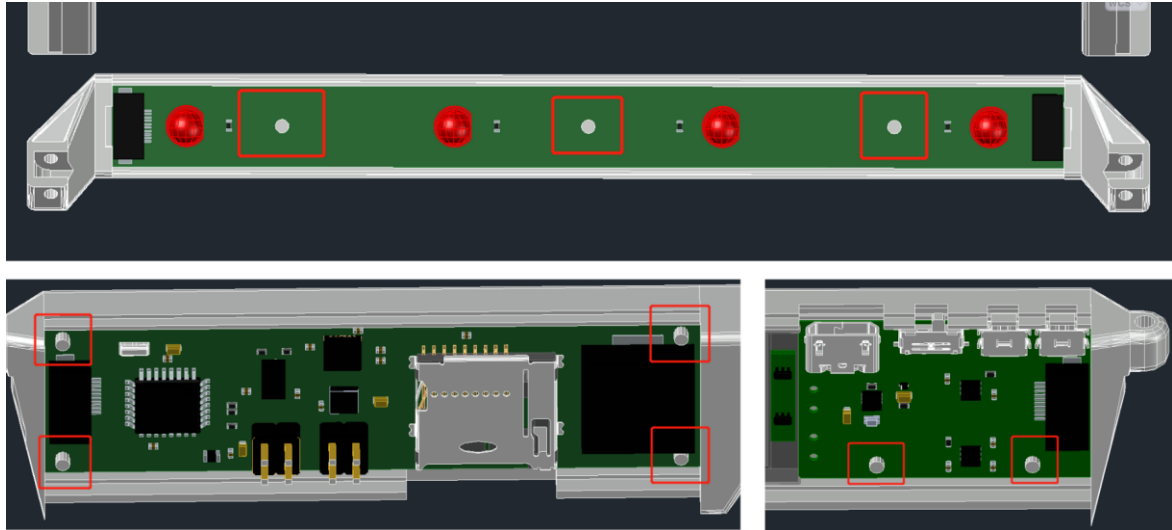


Figure 5-14. Installed PCBs on cylinders in frontal frame (top), left leg (bottom left), right leg (bottom right)

The design of each part of the glasses frame structure also reversed the slots for HMI components and micro SD card, ensuring these components were accessible to user during the activity. These slots were shown in the **Figure 5-15** below.

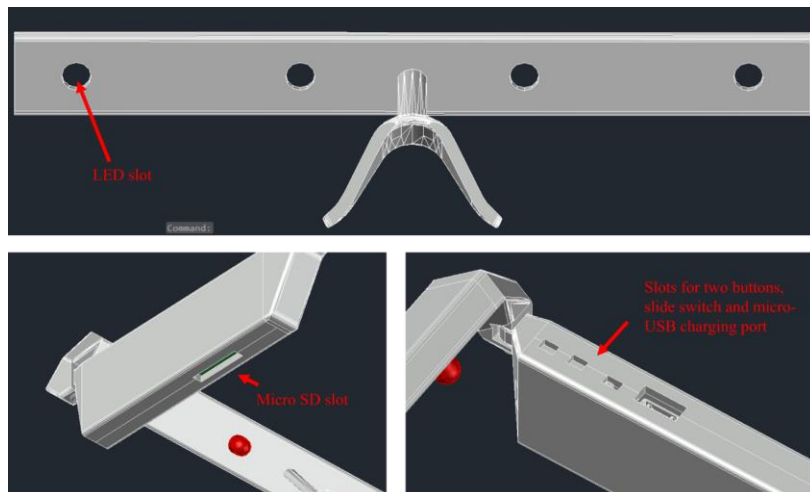


Figure 5-15. Reserved slots for HMI components and micro SD card on left leg (bottom left), right leg (bottom right), frontal frame (top)

5.2.1.3 “Teeth-Slot” Structure

To connect the left and right lid to the corresponding leg without glue or screws, a “Teeth-Slot” structure was developed as shown in **Figure 5-16** below.

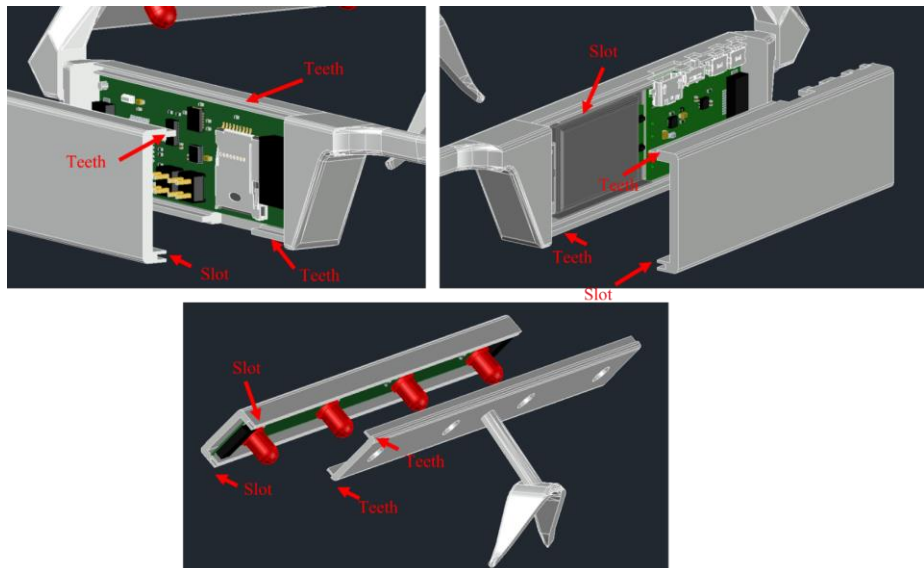


Figure 5-16. “Teeth-Slot” structure implementation in left leg (top left), right leg (top right), frontal frame (bottom)

The width of teeth was identical to the width of slot so that they could achieve a tight connection. It should be noted that this connection had been proven susceptible to the tolerance and other practical issues of 3D printing, and relevant discussion was covered in *5.2.2 3D Printing Results and Discussions*.

5.2.1.4 Hinge System

The hinge system was designed to enable adaptation of the glasses frame to wearer’ head shape and increase the portability. It was consisting of a cylindrical bulge part, a cylindrical slot on frontal frame and a M2 screw as its rotational axis. The exploded view and assembled view of the system was shown in the **Figure 5-17** below. The design of hinge system was identical in two legs thus only the structure of the left hinge was shown.

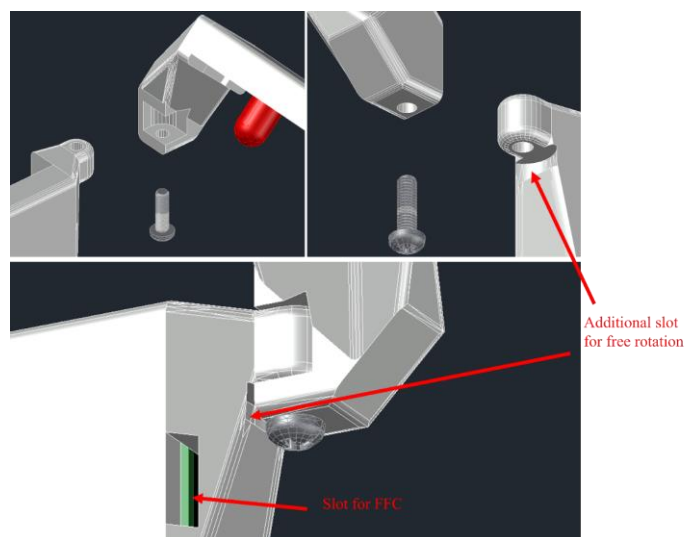


Figure 5-17. Exploded view (top left and right) and assembled view (bottom) of the hinge system in left leg

The holes of cylindrical slot had diameters (1.9mm) that were slightly smaller than the M2 screw (2mm) while diameter of the hole (2.1mm) in the bulge part was slightly larger than the M2 screw, so that the legs would be able to rotate freely along the screw and the screw would remain static with respect to the frontal frame. The cylindrical shape of both the bulge part and

the slot made the rotation smooth and easy for wearer to operate. This hinge system had been proven very effective in the subsequent 3D printing validation section. The **Figure 5-18** below showed the maximum folding angle of the glasses frame using the above hinge design.

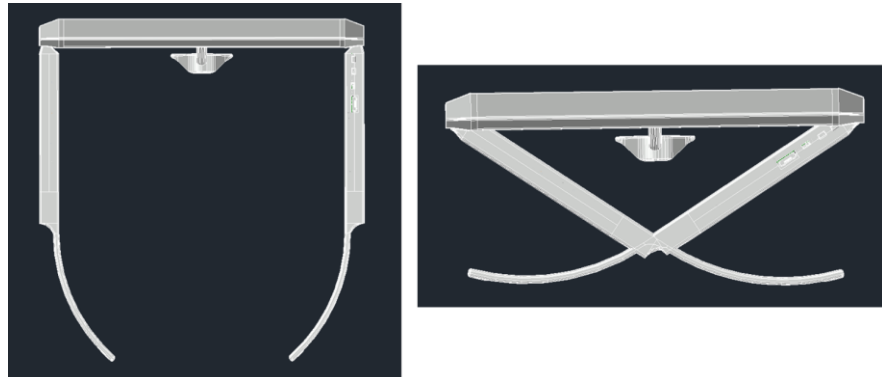


Figure 5-18. Regular (left) and maximum folding condition (right) of the glasses frame

5.2.1.5 Slots in Tails

To develop a mechanism to firmly attach the glasses frame to wearer's face during orienteering (as the activity was intensive), one slot had been created in each tail of the frame as shown in **Figure 5-19** below. A rubber band would be inserted into both slots to provide a contracting force to secure the glasses frame on wearer's face.

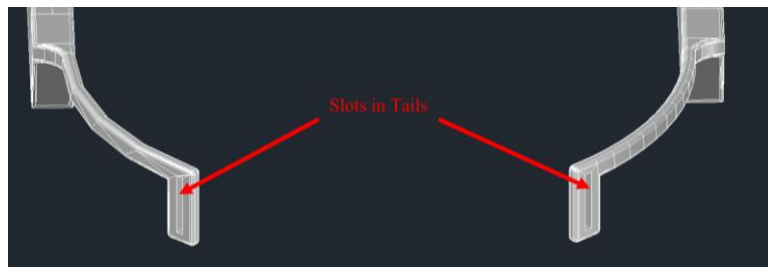


Figure 5-19. The slots in tails of the glasses frame for secure mounting

5.2.2 3D Printing Results and Discussions

This section was used to describe the printed results of the glasses frame and its integration with PCBs together with other components to form the complete system. Different printing directions and resultant qualities would be discussed in this section to analyse the limitation of 3D printing prototyping technology. All components were printed using black filaments with a layer thickness of 0.2mm.

5.2.2.1 Different Printing Options

Because the six major components of the glasses frame all had irregular shapes and curvy features, it was critical to select an appropriate printing direction for each of them to achieve reasonable accuracy and perverse the most important characteristics. The principle was that the printed components must be integrable and must be compatible with the PCBs, battery and FFCs, while the aesthetic factors or surface finish could be temporarily sacrificed in the first prototype. Since a component would be always printed from bottom to top, it was the orientation of the component that could be changed to adjust the focus on various features. Generally, cube-like sections without the need of supporting material would achieve maximum quality after printing. Both the curvy features and the introduction of supporting material would degrade the printing quality of certain surfaces, which typically led to a loss of surface fineness or distorted edges. Because the semi-liquid thermoplastic filament would not cool

down to solid state instantly after being squeezed out of the nozzle, it was usually difficult to decide whether to add supporting material to the structures that extended out of the main body, because the extended structure would either be negatively affected when removing the supporting material, or the non-instant filament cooling down process would lead to unwanted curves. This problem was particularly severe for some thin structures like the “Teeth-slot” structure of legs and lids, or the positioning cylinders for PCB installation. These, however, were critical structures for the integration of PCBs and the mechanical system thus could not be sacrificed, otherwise the PCBs would not fit in. Based on such considerations, the finalised printing directions of six major components of the glasses frame were shown below, where the directions were marked by red arrows and supporting material was marked by red squares:

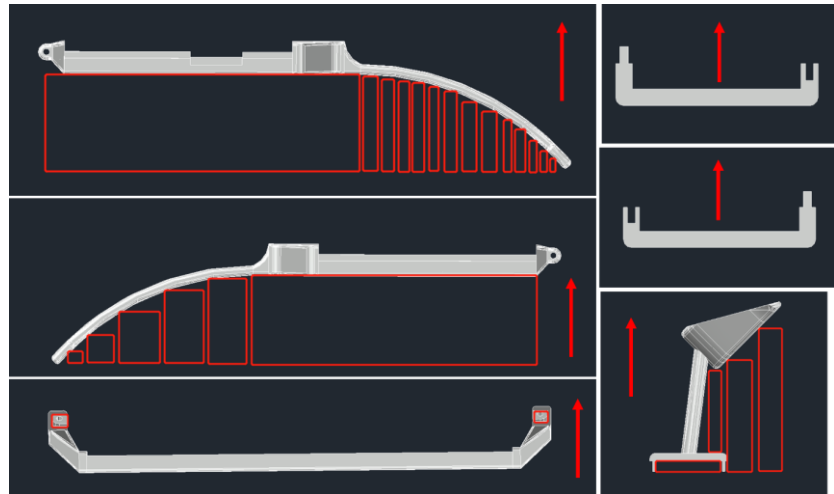


Figure 5-20. Printing directions of left leg (top left), right leg (middle left), left lid (top right), right lid (middle right), frontal frame (bottom left), nose support (bottom right)

Other printing directions had been attempted for left leg and right leg but were eventually abandoned for various reasons, mainly because of their failures to preserve the most important features mentioned above. A comparison was made in **Figure 5-21** to illustrate the superiority of current printing directions in preserving essential features of printed components. However, there must be a trade-off of such improvements, the current methodology also sacrificed the fineness of certain surfaces as shown in **Figure 5-21**, though they were not critical for the assembly of the glasses frame.

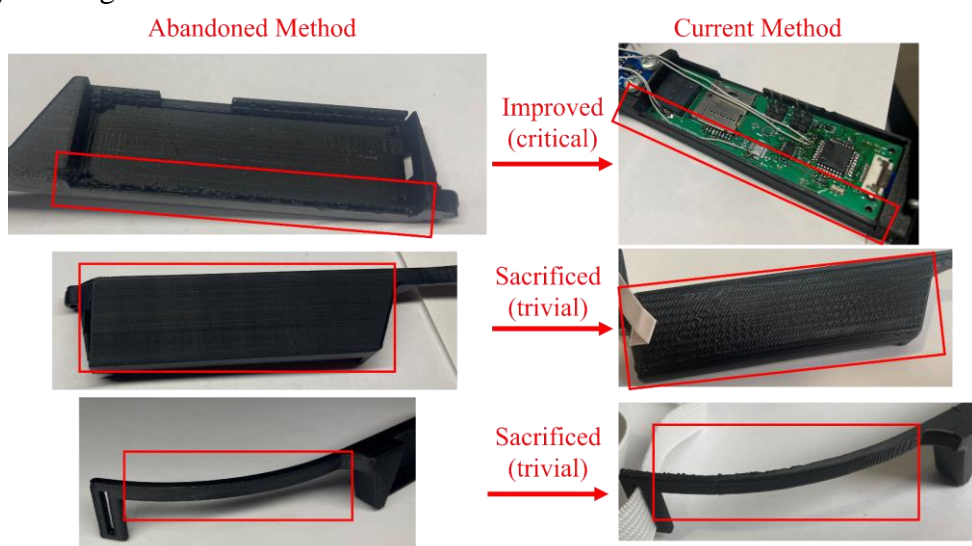


Figure 5-21. Some sacrificed and improved features between the abandoned method and the current method

5.2.2.2 Printing Results and Tests on Face

The fully integrated glasses frame was shown in the **Figure 5-22** below. The left lid and right lid were not installed to the legs so that the internal electronics could be seen. The validation of the functionalities of the glasses frame was covered in *5.3.1 Glasses Programming Results and Discussions*.



Figure 5-22. Fully integrated glasses frame from top (left), left (top right) and right (bottom right) view

Another figure below was used to prove that the glasses frame was compatible with human's face. It could be seen that the normal vision was not blocked by the additional glasses frame and the nose support and tails were effectively supporting the other parts on the face like a pair of regular glasses. The glasses frame was also firmly attached to wearer's face by the white rubber band.

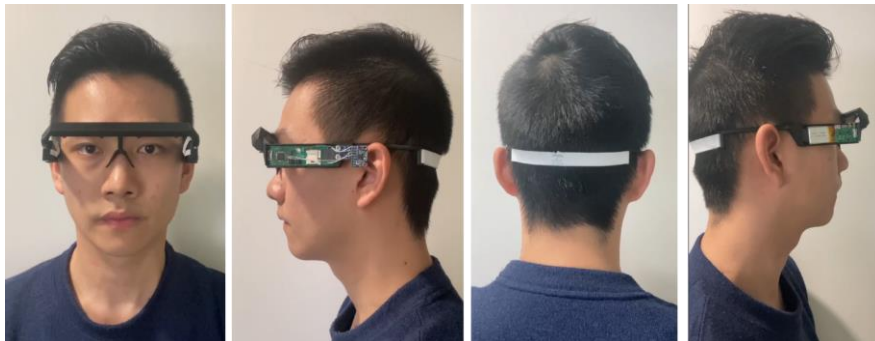


Figure 5-23. Four different perspectives of the glasses frame on human's face

5.2.3 Modelling and Printing Reflections

5.2.3.1 Ergonomic Concerns

The current ergonomic concerns of the mechanical system mainly focused the dimensions, that was, the basic compatibility of the glasses frame with human head. This, however, was still far from the commercial standard or a mature product. More ergonomic design factors such as the material used or the weight distribution should be considered to improve user experience. Like a regular pair of glasses, the glasses frame in this project could also be consisting of multiple types of material that had different textures and hardness. For example, pads made of silica gel could be attached to the contact surface between the nose support and human nose, to release the pressure and improve wearing comfort. Similar soft material could also be applied to the tails of the glasses frame since there was another contact surface with the head (specifically, ears). Regarding the weight distribution, it could be observed from the current design that most weight of the glasses frame came from the components in both legs and the frontal frame,

which led to a centre of gravity close to the frontal frame rather than the geometric centre of the glasses frame. In other words, the nose support would need to provide a much larger force than the tails, which would degrade the wearing comfort. If possible, some components could be moved to the rear section of the glasses frame to achieve a more balanced overall weight distribution. This, together with the consideration of multiple types of material, were beyond the prototyping purpose but could be used as guidance for future commercial purposes.

5.2.3.2 Aesthetic Concerns

The aesthetic consideration was not the top priority in this prototype design as it will not affect the performance of the glasses frame. Nevertheless, some concerns related to this factor had been incorporated into the 3D modelling and printing. The left leg and right leg were designed to be symmetrical and a considerable number of curves were added to the edge transitions on the legs. The black filament was used to print the entire mechanical structure and this was a common colour choice for other similar commercial products.

A real modern design usually involved a great number of irregular shapes and curves that needed to be accomplished using complex 3D modelling skills and operations. A thorough investigation of user preference with a summary of the aesthetic concerns from other similar products would be a good start to improve the appearance of the glasses frame for future generations.

5.2.3.3 Waterproof and Shock-resistant

As mentioned previously, waterproof and shock-resistant features were necessary to increase the durability of the device due to its application field. The current prototype was shock-resistant to some extent as the space in the glasses frame was designed to be just enough to incorporate all the components, thus electronic system would not move back and forth to cause short-circuit or similar problems (assuming the problem of voltage translator mentioned in *5.1.1.1 PCB1: Left Leg* is solved). The waterproof feature of current prototype, however, was almost negligible as it was very difficult to realise a seamless design with the 3D printing technology implemented in this project.

To improve the waterproof feature, one solution was to use a potting material such as epoxy to completely fill the gaps in the mechanical system thus all electronics would be immersed in this non-conductive liquid. [50] When the potting material hardened, the electronic system would be completely blocked from any liquid (even air) as long as the thermal dissipating requirement was fulfilled. This immersion process would also enhance the shock-resistant feature as the soldered components were less likely to be stripped off from PCBs by external force. The result of this solution was permanent, which meant the maintenance of the device would be difficult and the potting material also added additional weight to the device.

Another possible solution was to use the ultrasonic welding technology mentioned in *4.4 Glasses Frame 3D Modelling and Printing*, which was close a enhancement of current methodology used in prototyping. If the contact surface of two components could be slightly melted and joined together using this technology (in large-scale production), a good level of waterproof feature could also be reached.

5.3 Glasses Programming

5.3.1 Glasses Programming Results and Discussions

5.3.1.1 Main Program Flowchart and Time Sequence

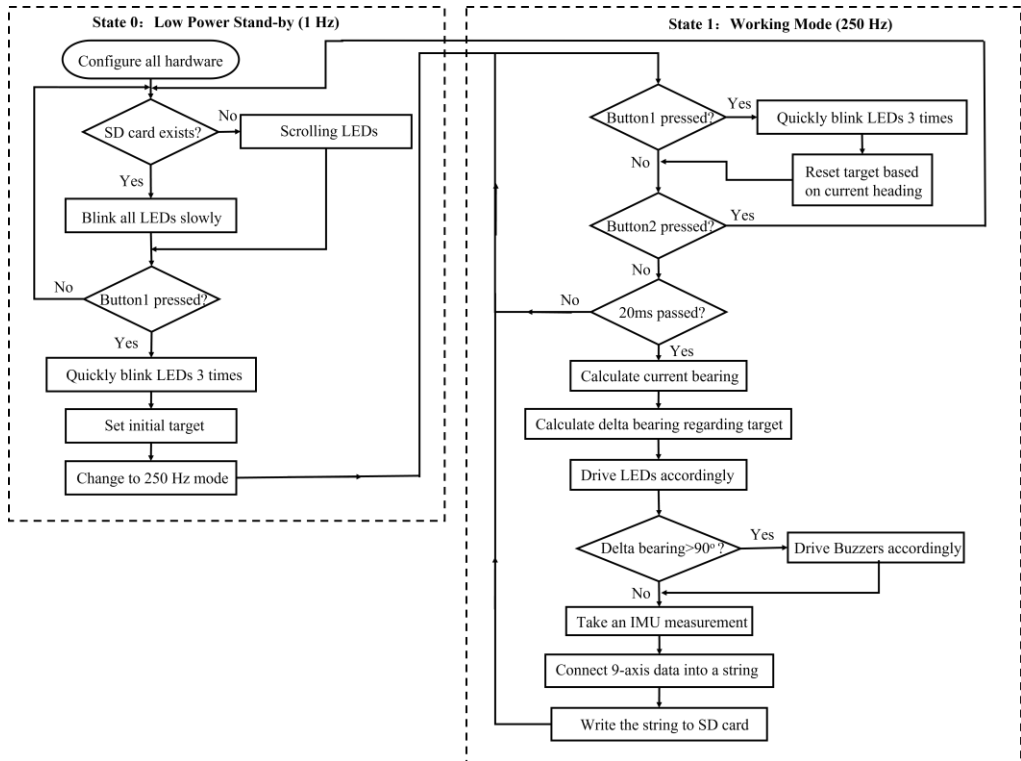


Figure 5-24. Program flowchart of glasses frame

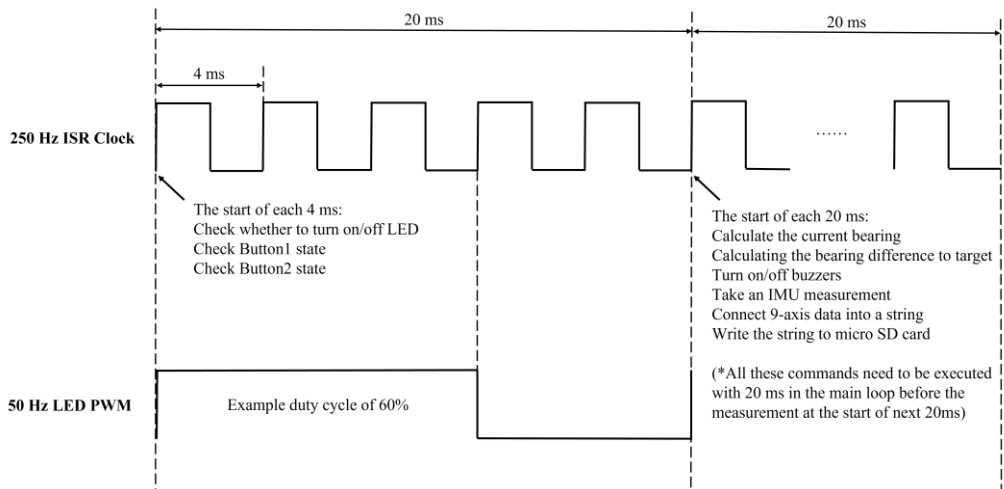


Figure 5-25. Time sequence of the 250 Hz ISR and 50 Hz LED PWM

The following is the data for Trip 1

Data Form: AcceleX AcceleY AcceleZ GyroX GyroY GyroZ MagX MagY MagZ
 1624 15496 1152 -354 91 132 -478.00 -107.87 3.00
 1948 15732 1132 -267 161 52 -480.00 -91.12 3.00
 2012 16132 984 -311 80 466 -480.00 -91.12 4.00
 1700 15764 956 -195 46 895 -483.00 -92.46 2.00

Figure 5-26. An example section of stored data to micro SD card

The program of glasses frame was mainly based on a state machine with various timers and ISR (Interrupt Service Routine) operations. As shown in the **Figure 5-24** above, it was consisting of State 0 and State 1. The State 0 was a stand-by mode, in which the glasses frame worked at a very low frequency (1 Hz) to maximally save power and kept waiting for user to press Button1 to start the journey. In this state the program also kept checking the existence of

micro SD card so that the user could insert the SD card any time before pressing the Button1 and the program would initialise the card. If the Button1 was pressed, all LEDs would quickly blink three times to indicate the start and the program would enter State 1.

The State 1 was a working routine to realise all guiding and data recording functions running at 250 Hz. This state was more complex than State 0 thus an additional **Figure 5-25** was included to illustrate the time sequence of different activities. Timing issue was critical in this project since the recorded data would be used for double integration in the subsequent signal processing.

The 250 Hz ISR in State 1 and the 1 Hz ISR in State 0 were realised by using Timer1 in the microcontroller as an interrupt trigger source. The 250 Hz ISR had two functions. One was to generate a bit-banging PWM (Pulse-Width Modulation) signal to drive 4 LEDs with a duty cycle resolution of 20%. The PWM method was a convenience way to achieve dimmable LEDs and this characteristic was important for orienteering as the players could be running in both bright and low-light conditions. It had been stated in [51] that the human eyes would not be able to perceive the flicker if the LED PWM frequency was higher than 24 Hz, while the brightness stability would be higher if the frequency was higher. 50 Hz was selected to be PWM frequency in this project since it was more than two times larger than the threshold value. The period of 50 Hz PWM was 20 ms and it was consisting of five period of the 250Hz ISR, hence there were five different possibilities of PWM duty cycles, leading to a resolution of 20%.

Another reason for choosing the 50 Hz PWM corresponded to the second function of 250 Hz ISR, that was, providing an accurate 50 Hz clock to take measurements and record the data into micro SD card. Because 50 Hz was also a good choice of sampling frequency of sensors in the glasses frame (not too low to miss the motional information, not too high to cause huge burden for the microcontroller), using the same 50 Hz for both sampling and LED PWM could save resources (fewer counter variables and simpler code structure) in the microcontroller. Assuming each 20 ms was a frame as shown in **Figure 5-25**, the 250 Hz ISR would keep checking the states of Button1 and Button2 (based on flags from external interrupt) and turn on/off the LEDs according to the pre-determined duty cycle option within each frame. At the end of each frame (which was also the start of the next frame), a flag that would enable the sensor measurements and data recording in the main loop was raised. The microcontroller would use the idle time (no interrupt was requested) in the next 20 ms (next frame) to complete the tasks of calculating current bearing, calculating the bearing difference to target, driving buzzers accordingly, taking IMU measurements and storing the data from current measurement into micro SD card. An example section of stored data was shown in **Figure 5-26**. The same process would repeat again at the end of next frame. It had been validated that the chosen microcontroller was able to fulfil the above requirement at the frequency of 50 Hz, though a higher frequency might be not feasible.

The bit-banging PWM was not an efficient choice for a microcontroller, but the ATMega328P lacked sufficient resources to realise hardware-based PWM output for all four LEDs without involving any dedicated LED driving chip. The software bit-banging was the only choice. The driving of buzzers, however, successfully exploited the hardware PWM output from Timer0 at 980 Hz. Timer0 was used to control the timing of many default functions in Arduino libraries such as `delay()`. Changing its frequency would lead to the malfunction of many built-in functions thus the default setting was preserved. According to the human earing response to sound frequency shown in **Figure 2-4**, human ears were relatively sensitive to the sound at 980 Hz thus this default frequency was adopted.

5.3.1.2 The Derivation of Magnetic North and Current Bearing

The calculation of current bearing was based on the direction of wearer's head but irrelevant to the moving direction of wearer, as the glasses frame remained static with respect to wearer's head and the head direction was independent of the moving direction. According to the installation of magnetic module in **Figure 5-3**, the direction of the axis B_y was always same as the direction of wear's head, thus the current bearing could be obtained if the angle between the axis B_y and magnetic north's project to the B_yB_z plane was calculated. The relative positions of these physical variable were shown in **Figure 5-27**.

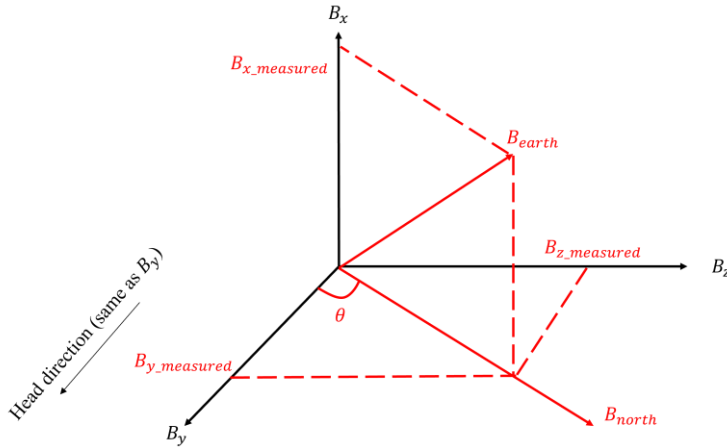


Figure 5-27. An example of relative positions of head direction, vector of earth magnetic field and the magnetic coordinates of the magnetic meter

The B_x, B_y, B_z were three determined axes of the magnetic meter and the head direction of the wearer was same as B_y . B_{earth} was the vector of earth magnetic field and B_{north} was the projection of B_{earth} to the B_yB_z plane. $B_{x_measured}, B_{y_measured}, B_{z_measured}$ were three measured intensities of magnetic field from magnetic meter. Assuming the B_yB_z plane was always in parallel with the ground plane, the angle θ could be used to represent the current bearing with respect to magnetic north and it could be calculated using the measured data from magnetic meter as shown in Eqn.5-2 below.

$$\theta = \left(\frac{B_{z_measured}}{B_{x_measured}} \right)^{-1} \quad \text{Eqn. 5-2}$$

Neglecting the difference between magnetic north and geographical north, the value of θ could be used as the required reference value to drive LEDs to provide guiding information. The program would also need to tackle some special circumstances such as when the value of $B_{x_measured}$ was zero, but they could be easily addressed using conditional statements thus not elaborated here.

5.3.1.3 Glasses Frame Validation 1: LED and Buzzer Indication

LEDs and buzzer were turned on according to the current deviation from the target to prompt the wearer to correct his/her direction. The design logic in this project was that the red light from LEDs and the high-frequency noise (≈ 1000 Hz) from buzzer were treated as warning signals for user, like the red colour in traffic light. The user should aim to eliminate all visual and auditory warnings during the activity and the elimination of them indicated that the wearer was on the correct track/direction. Based on such ideas, the human machine interface was programmed as follows:

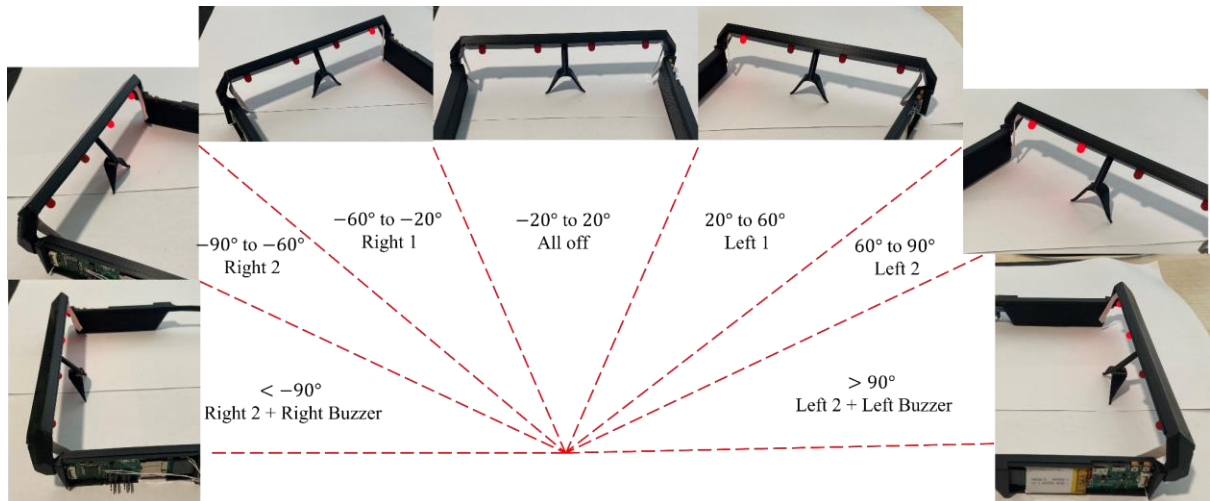


Figure 5-28. Total seven different states of LED and buzzer indication

All LEDs and buzzers would be turned off if the current deviation was smaller than 20 degrees, leaving a window for the wearer to focus on the activity without disruption when the deviation was small. One LED would be turned on when the deviation was between 20 degrees and 60 degrees on either side. For example, the leftmost LED will be turned on if the head deviation to the right side was bigger than 20 degrees, urging the wearer to eliminate the light on the left side by turning left. Two LEDs (on the same side) would be turned on when the deviation was between 60 degrees to 90 degrees, indicating that the deviation was more severe. The buzzer on the same side as the LEDs being turned on would begin to make noise if the deviation was larger than 90 degrees, which symbolised an ultimate warning to urge the wearer to correct the current moving direction otherwise the track would be completely wrong. (The threshold value of 20, 60 and 90 were selected as examples to demonstrate the idea. The optimal thresholds for the best interaction and guiding experience would need to be determined after a great number of tests to different groups of people)

5.3.1.4 Glasses Frame Validation 2: Guiding the Wearer on a Straight Line

To validate the effectiveness of the core guiding function of the glasses frame, a field test was designed and conducted in the Jubilee Campus, University of Nottingham. The field test aimed to investigate whether the wearer could walk in a straight line with the mere help from the glasses frame. The test was conducted in an open grassland in the midnight (thus no interference from other people) and the wearer was required to cross the grassland blindfolded in a straight line (approximately 145m), with the only guidance from the glasses frame. The blindfolded condition ensured that the wearer would not be able to use certain land reference (e.g., trees, buildings) to guide himself on a straight line. Because no visual signal could be perceived, the HMI of the glasses frame was modified to adapt to this test. All LEDs were disabled and two buzzers were used to provide auditory signal to guide the wearer. The sensitivity was set to be very high, the wearer would be notified by the buzzer if the deviation to a certain side was more than 5 degrees, allowing the wearer to correct tiny deviation on time to achieve a walking trajectory as straight as possible. The wearer was also carrying a mobile phone with a GPS receiver to record his trajectory for validation. The trajectory was recorded by Strava, which was an application that utilised phone resources (GPS receiver, IMUs) to record user's motion and track in an activity and provided relevant statistics afterward. The test was repeated for three times and the recorded trajectories from Strava together with the track in ideal situation were shown in **Figure 5-29**. The number of times that each buzzer was triggered during each test was summarised in **Table 5-1** below.



Figure 5-29. Ideal straight trajectory (top left, red line) and the recorded trajectory (orange line) from Strava for Test 1 (bottom left), Test 2 (top right) and Test 3 (bottom right)

Table 5-1. Number of times that Buzzer 1 and Buzzer 2 were triggered in each test

	Buzzer 1 (left)	Buzzer 2 (right)
Test 1	16	21
Test 2	12	19
Test 3	15	10

It could be seen from **Figure 5-29** that all three recorded trajectories were very close to a straight line and were also very close to the ideal prediction in the top left corner. This could effectively prove two aspects. One was that the idea of guiding the glasses frame wearer on a stable compass heading using the feedback from HMI components were feasible and reliable, at least in the straight line scenario. Another was that the magnetic meter in the glasses frame was calibrated properly to take measurements and the algorithms of calculating the current bearing and driving the HMI components using the set target and real-time bearing data were fully functional and valid.

The orange lines were not perfectly smooth due to the small deviations in each test and the error of GPS positioning process. It could be seen from **Table 5-1** each buzzer was trigger for 10~20 times in each test, which was a relatively large number considering the length was only 145m. This could also be used as evidence to prove the validity of guidance provided by HMI components since the buzzers were actively responding to small deviations to urge the wearer to correct his moving direction.

5.3.2 Glasses Programming Reflection

5.3.2.1 Potential Improvements of HMI

It had been stated before that the bit-banging driving of LEDs was not efficient. This issue could be fixed by replacing the microcontroller with a model with more hardware resources (peripherals) thus all four LEDs could be dimmable using the built-in PWM drivers. Meanwhile, it was possible to realise a higher frequency (~kHz) PWM signal using the peripherals, which might avoid some negative biological effects [52]. Some research projects [52] had found that the invisible flicker ranging from 50~200 Hz could cause health concerns

such as headache, eye strain and reduced visual performance, while a PWM signal with a higher frequency (~kHz) was likely to reduce such effects [51]. For a long-term safety concern and passing potential regional safety regulations about electronic devices, this issue should be addressed in future generations of the product. Regarding the dimmable feature, adding a photodetector to enable the device to automatically adjust the light intensity of LEDs according to the brightness of surrounding environment would be a good upgrading option. This would achieve a higher level of hands-free operation since the wearer would not need to adjust the light intensity using buttons (not implemented yet) by hands.

The LED indication patterns (such as all blinking slowly to indicate stand-by) used in the current program were not validated based on the intuitiveness of a large group of people. This validation was critical for future commercialisation as LEDs were the main interface for the glasses frame to communicate with the user. A poor indication design would force the user to remember patterns from instruction manual thus it became much less attractive. Also, more functions, such as using a double click to disable the buzzer, could be added to user buttons in future enhancement of the device. This would give the wearers a higher flexibility to customise the user experience based on their own preferences.

5.3.2.2 Algorithm Efficiency and Robustness

It could be seen in the *5.3.1.2 The Derivation of Magnetic North and Current Bearing* section that many assumptions had been made to derive the equation and algorithm to obtain the current bearing based on the raw measurements from the magnetic meter. It was clear that in reality not all assumptions would hold, as the wearer might randomly turn his/her head during the activity and the moving direction might not be in parallel to the ground plane. The projection of B_{earth} vector to the B_yB_z plane would change thus the current algorithm could generate an inaccurate bearing value. The data from accelerometer could be used to analyse the attitude of the wearer thus the rotated B_yB_z plane could be derived, and the updated magnetic coordinates could be used to correct the bearing measurement. This would increase the robustness of the bearing calculation algorithm and also result in a higher accuracy in subsequent trajectory reconstruction.

To reliably achieve the above data fusion algorithm, a good synchronisation of different sensors was necessary. Both the MPU6050 and HMC5883L chip provided an input port for external interrupt signal to achieve a simultaneous sampling process between multiple sensors. Such square-wave interrupt signal could be generated by the microcontroller at the desired frequency to ensure the data from all sensors were sampled at the same time, thus could be used for data fusion and attitude analysis. This synchronisation could also simplify the ISR design in the microcontroller thus the algorithm efficiency could be improved. The efficiency would be even higher if data recording process to the micro SD card was optimised. The data from multiple “frames” could be combined together and written to the SD card in a single process, rather than the current solution of writing the data to SD card at the end of every frame.

5.3.2.3 Battery Life

A simple test was conducted to validate the battery life per charge of the glasses frame. It was set to an orientation where the maximum deviation was detected, i.e., two LEDs and one buzzer were turned on. The microcontroller was also continuously recording the sensor measurements and writing the data into the micro SD card. The test started from a fully charged LiPo battery with a voltage of 4.2 V and ended when the system automatically shut down. The tested duration was one hour and 42 minutes and the terminating voltage level was 3.69 V. This battery life was close to the design specification of 2 hours and the duration could be longer in realistic scenarios as the LEDs and buzzer would not be always on. The process of recording

the data in SD card consumed a large current as shown in **Table 4-1** thus the battery life could be greatly extended if this function was disabled. To further improve the battery life, either the algorithm needed to be optimised or a customised battery pack could be implemented to maximise the exploitation of available space in the glasses frame.

5.4 Post Signal Processing on PC

5.4.1 Post Signal Processing Results and Discussions

5.4.1.1 Flowchart of Three Algorithms

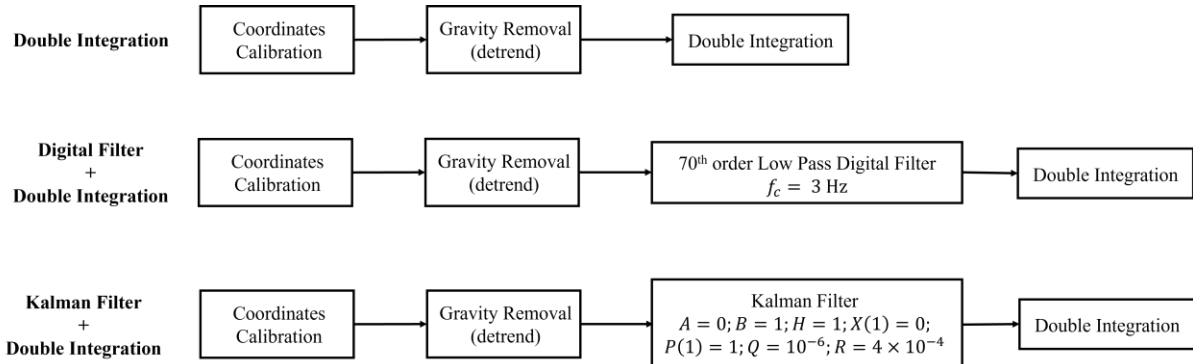


Figure 5-30. Flowchart of three processing algorithms

It had been explained in the *4.6 Post Signal Processing* that the reconstruction of trajectory was based on different filtering techniques and the double integration. The mathematical interpretation of Digital filter, Kalman filter and double integration had also been covered in the *4.6 Post Signal Processing* thus not repeated. Three algorithms consisting of various processing stages were developed and the high-level flowcharts were shown in **Figure 5-30** above. It was the acceleration on the X axis of MPU6050 that would be processed by all the stages to reconstruct the trajectory, calculate the travelled distance and average speed. It could be seen that all algorithms started with “Coordinates Calibration” and “Gravity Removal” stage. In “Coordinates Calibration” stage, a coefficient of “-1” was multiplied to all input data to match the positive direction of acceleration with the actual moving direction of the wearer, as they were originally in reverse directions as shown in **Figure 5-3**. The acceleration was then converted from raw measurement to physical quantity with the unit of m/s^2 . In the “Gravity Removal” stage, the `detrend()` command was executed to the entire dataset to calculate a closest linear regression of the data and subtract it from the raw value. This process would effectively remove the projection of gravitational acceleration and other DC offsets to all axes.

For the basic double integration method, the data (after the removal of gravity) was integrated for the first time to obtain the velocity, and integrated for the second time to obtain the displacement. The trajectory was then constructed using the discrete displacement results and the bearing data. For all trajectory figures in this signal processing section, it was assumed that the player started at the original (0,0) in the virtual cartesian coordinate system.

For the method with digital filter, the data would go through a 70th order low pass digital filter (FIR filter with hamming window) before the double integration process. The order “70” was a recommended value from MATLAB help manual that essentially represented a very high order design, which would result in a very sharp roll-off edge of the frequency response. Because the filter was implemented in the software thus a high order number would not lead to excessive electronic components or similar issues. The cut-off frequency was selected to be 3 Hz, which was selected after a few attempts of other choices. This cut-off frequency could generally preserve the envelop of the acceleration data while not losing too many details. The frequency

response of the designed filter was shown below, where the horizontal axis was substituted by normalised frequency ω_{norm} . The relation between this normalised value and the actual frequency was shown in Eqn.5-3.

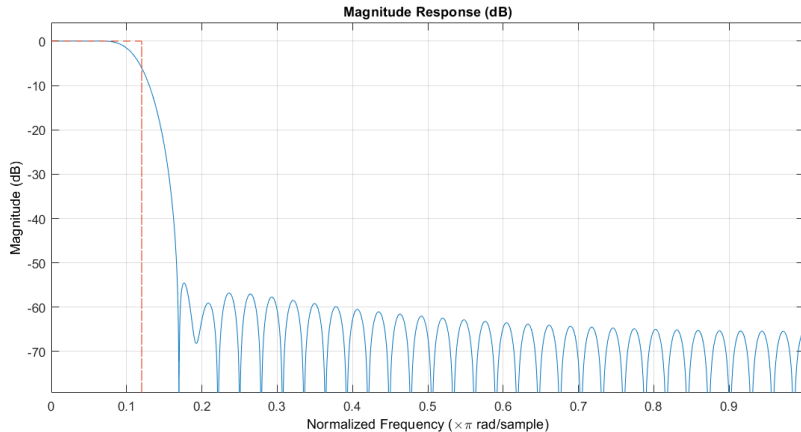


Figure 5-31. Magnitude response of the 70th order low pass filter

$$\omega_{norm} = \frac{\omega}{0.5 \times (2\pi f_s)} = \frac{\omega}{50\pi} \quad \text{Eqn. 5-3}$$

For the method with Kalman filter, the data would be processed by a function developed to perform the Kalman filtering using the equations from *4.6 Post Signal Processing*. The coefficients of Kalman filter were included in the flowchart in **Figure 5-30**. Most coefficients were chosen to be either zero or one to simplify the filter designing process due to limited time. The covariance Q and R (representing the process noise and measurement noise level) were chosen to be relatively large to realise a “strong” filtering process, since the raw data from accelerometer were quite noisy.

5.4.1.2 Basic “Back and Forth (BAF)” Test of Three Algorithms

An initial test of moving back and forth in a straight line was conducted to validate the performance of three algorithms. The test was done in an interior environment at a very small scale (5m) for a quick primary validation. The glasses frame wearer was asked to walk to the other side of the room in a straight line and then return to the starting point following the original track. The theoretical bearing of the first half of the journey was 340° and the value should be 160° for the second half. (The bearing of north was always treated as 0° (360°) and the value increased clockwise, thus east should be 90° and so on) This test only focused on trajectory reconstruction but not travelled distance and average speed since the whole journey was too short to produce reliable results. The waveforms of acceleration (after filtering if applicable), bearing and integrated velocity of three algorithms for a single test were shown in **Figure 5-32**. The actual trajectory and the reconstructed results from three algorithms were shown in **Figure 5-33**.

It could be seen from **Figure 5-33** that none of the algorithms achieved a close reconstruction result to the actual trajectory, and all of them did not return to the start point but produced an extension following the original bearing. This could be explained by the results of integrated velocities in **Figure 5-32**. The velocity did not return to zero at the end of the journey in all three subplots, and the terminating velocity of digital filter and Kalman filter method was larger thus their extensions were longer than the basic method. The integration of velocity was forced to be zero in digital filter and Kalman filter method if the program detected the velocity was becoming negative, as it could be seen from subplot 2 and 3 in **Figure 5-32** that the

velocity was clipped at $v = 0$. This was because realistically the velocity was always positive and the negative velocity generated from the deficiency of the integration algorithm would lead to a reverse moving direction (for example in subplot 2 in **Figure 5-33** where the clipping mechanism was not introduced in basic method), which, strictly speaking should be eliminated by optimising the algorithm, however a simple clipping mechanism was temporarily used due to limited time.

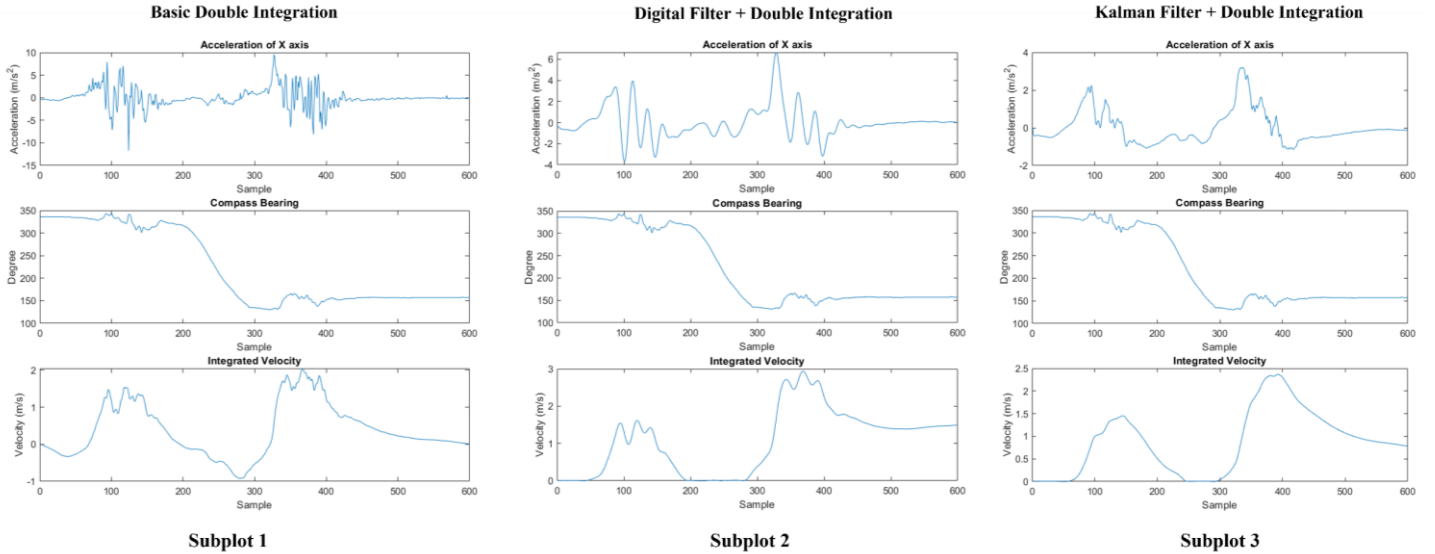


Figure 5-32. Acceleration of X axis, compass bearing and integrated velocity for three processing algorithms in a basic BAF test

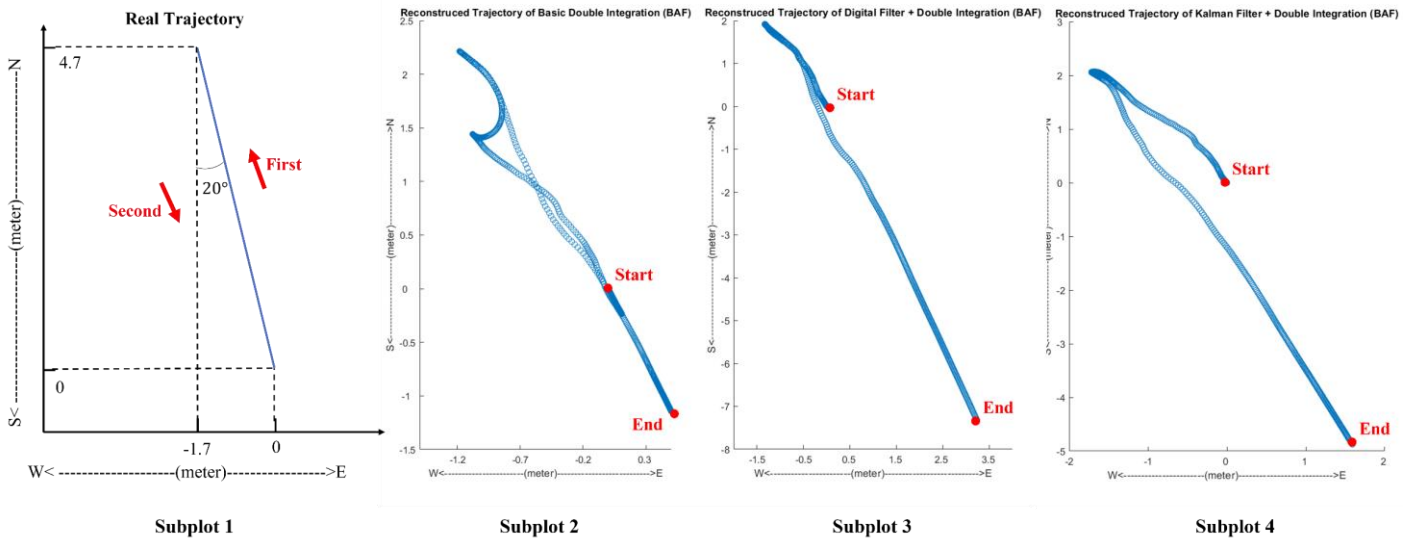


Figure 5-33. The actual trajectory (Subplot 1) and reconstructed trajectories of basic method (Subplot 2), digital filter (Subplot 3) and Kalman filter (Subplot 4)

It could be seen from subplot 2 and subplot 3 in **Figure 5-32** that both the Kalman method's waveforms of acceleration and integrated speed were smoother than the results of digital filter method, and also could reflect the reality better. The envelop of the acceleration after Kalman filter represented the general tendency of walking acceleration with less distortion. This also led to a shorter extension in the reconstruction trajectory of Kalman filter method, indicating it was closer to reality compared with the result of digital filter method, though the results of both methods were not satisfying enough.

5.4.1.3 Field Validation 1: Trajectory around a Building

The second test was done in an exterior environment at a larger scale. The program in the glasses frame and the signal processing algorithms remained unchanged regarding the last interior test. The wearer was asked to travel around a building for a complete cycle, carrying both the glasses frame and a mobile phone as a GPS receiver. The GPS receiver was used to provide a reference to actual trajectory and validate the reconstructed trajectories from inertial navigation. The trajectory together other statistics were still recorded by Strava. The theoretical trajectory and the result from GPS positioning were included in the **Figure 5-34**. The acceleration (after filtering if applicable), compass bearing and integrated velocity of three algorithms were shown in **Figure 5-35**. The reconstructed trajectories of three algorithms were shown in **Figure 5-36**.

It could be seen from **Figure 5-34** that the result from GPS receiver strongly deviated from the theoretical prediction. This was mainly because the test was conducted around a building, which was likely to be consisting of steel and concrete, thus could be treated as a giant metal object. The presence of the building would cause signal blockage and multipath error in GPS navigation and similar problems had also been mentioned in [19] and [53]. The reliability and accuracy of GPS navigation would significantly decrease in such scenarios.

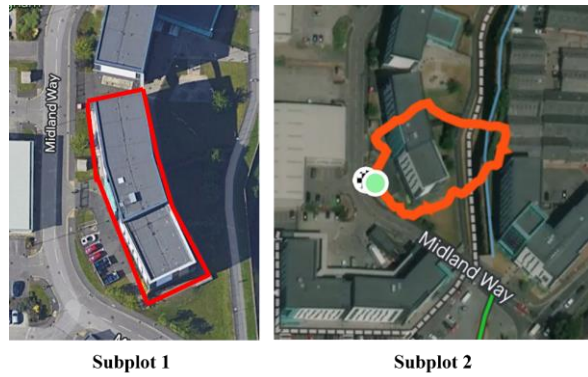


Figure 5-34. Theoretical trajectory (Subplot 1, red line) and result from GPS receiver (Subplot 2, orange line)

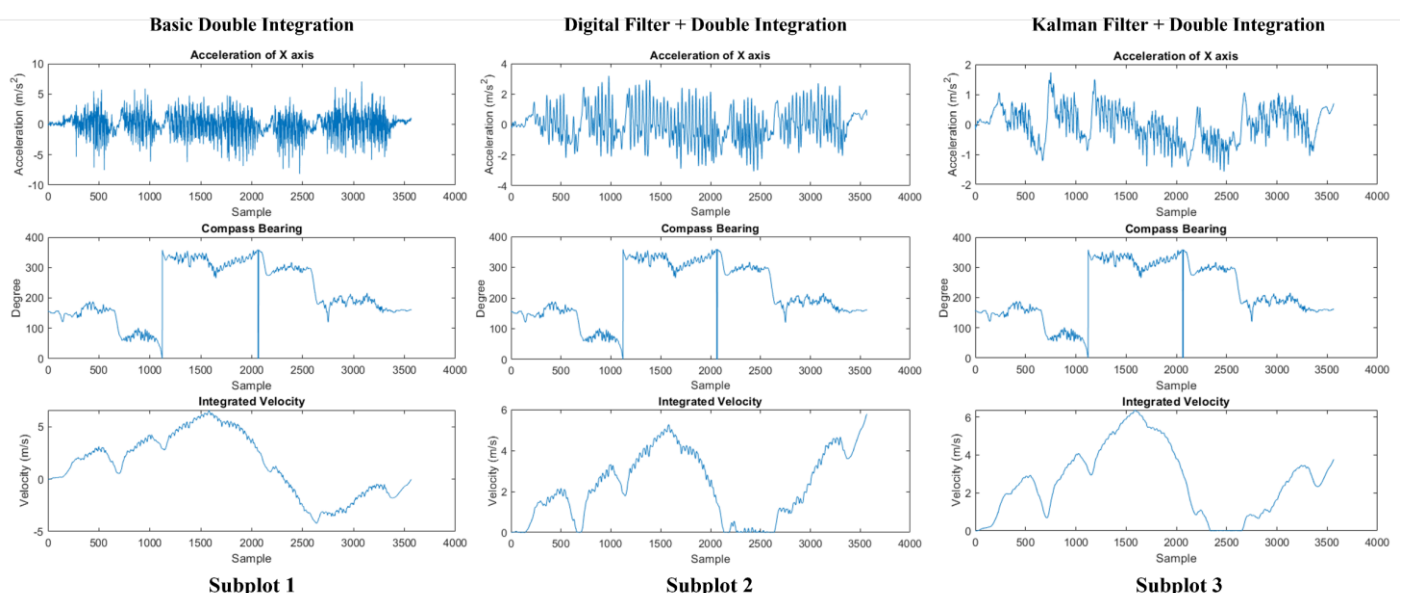


Figure 5-35. Acceleration of X axis, compass bearing and integrated velocity for three processing algorithms in the building test

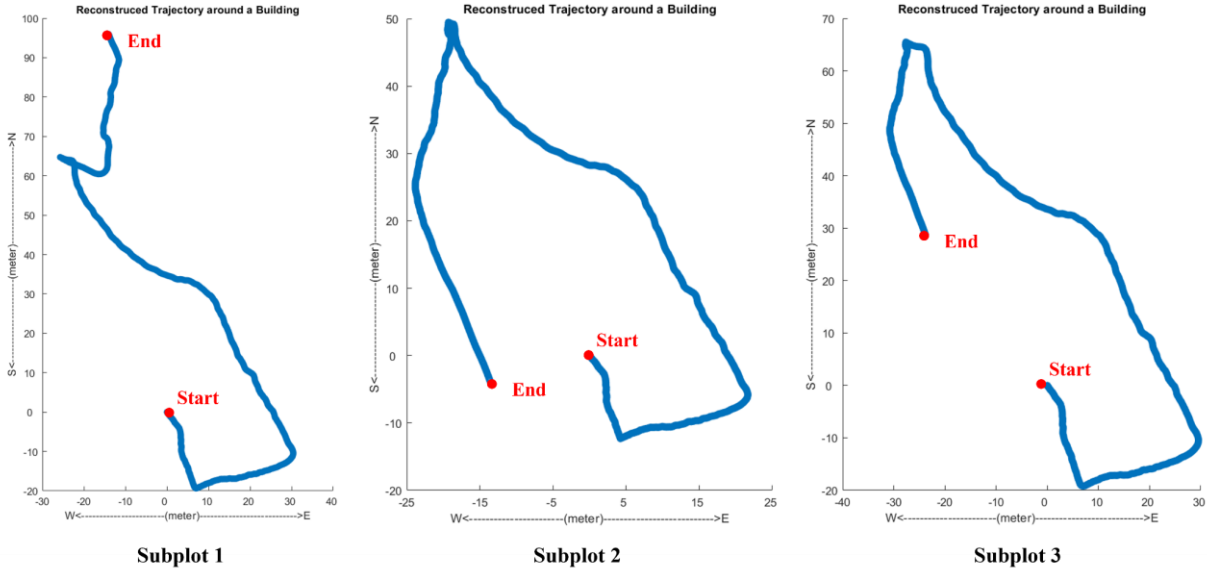


Figure 5-36. The reconstructed trajectories of basic method (Subplot 1), digital filter (Subplot 2) and Kalman filter (Subplot 3) of the building test

Figure 5-36 showed that both the digital filter and Kalman filter method achieved a roughly close replication to the theoretical trajectory, while the deviation of basic double integration method was much higher. The deviation of the basic method mainly resulted from its lack of “zero velocity clipping” mechanism that could stop the velocity being integrated to a negative value, otherwise the bearing could not be properly interpreted thus would lead to wrong travelling direction as the second half of the trajectory in Subplot 1 of **Figure 5-36**.

The trajectory of Kalman filter method (thinner) was closer to the theoretical trajectory than the result of digital filter method (wider). This could be regarded as evidence to support the superiority of Kalman filter in extracting the essential information from the acceleration data and preserving the most important features. The wider shape of digital filter method also indicated that the pure low pass filtering technique might distort the signal and lose information, while the selection of cut off frequency also needed further investigation.

The duration of the journey, travelled distance and average speed calculated from three inertial algorithms and GPS data were summarised in **Table 5-2** below. The percentage in the bracket that was adjacent to each number in **Table 5-2** was its difference regarding the value of GPS test that was treated as a standard reference. The duration of all methods was close to the GPS test, indicating that the 50 Hz sampling frequency was quite accurate. The integrated distance (2.1% error) and derived average speed (6.1% error) of Kalman filter method were closest to the GPS results, further proving the superiority of Kalman filter. (It should be noted that the GPS trajectory was not fully reliable as shown in **Figure 5-34**, thus this conclusion would require further validation.)

Table 5-2. Journey duration (s), distance (m) and average speed(m/s) estimation from GPS data and three inertial algorithms in the building test

	Duration	Distance	Average Speed
GPS	68	190	2.79
Basic method	71 (4.4%)	98.03 (48.4%)	1.38 (50.5%)
Digital Filter	71 (4.4%)	161.39 (15.1%)	2.27 (18.6%)
Kalman Filter	71 (4.4%)	185.94 (2.1%)	2.62 (6.1%)

5.4.1.4 Field Validation 2: Trajectory around a Grassland in Open Field

The second field validation was conducted around a grassland in open field, attempting to remove the potential effect from the building in last test. All parameter settings and algorithms remained unchanged. The wearer was asked to travel around the grassland for a semi-cycle, carrying both the glasses frame and a mobile phone as a GPS receiver. The method to utilise the GPS receiver was same as the last test. The results of this test were shown below.

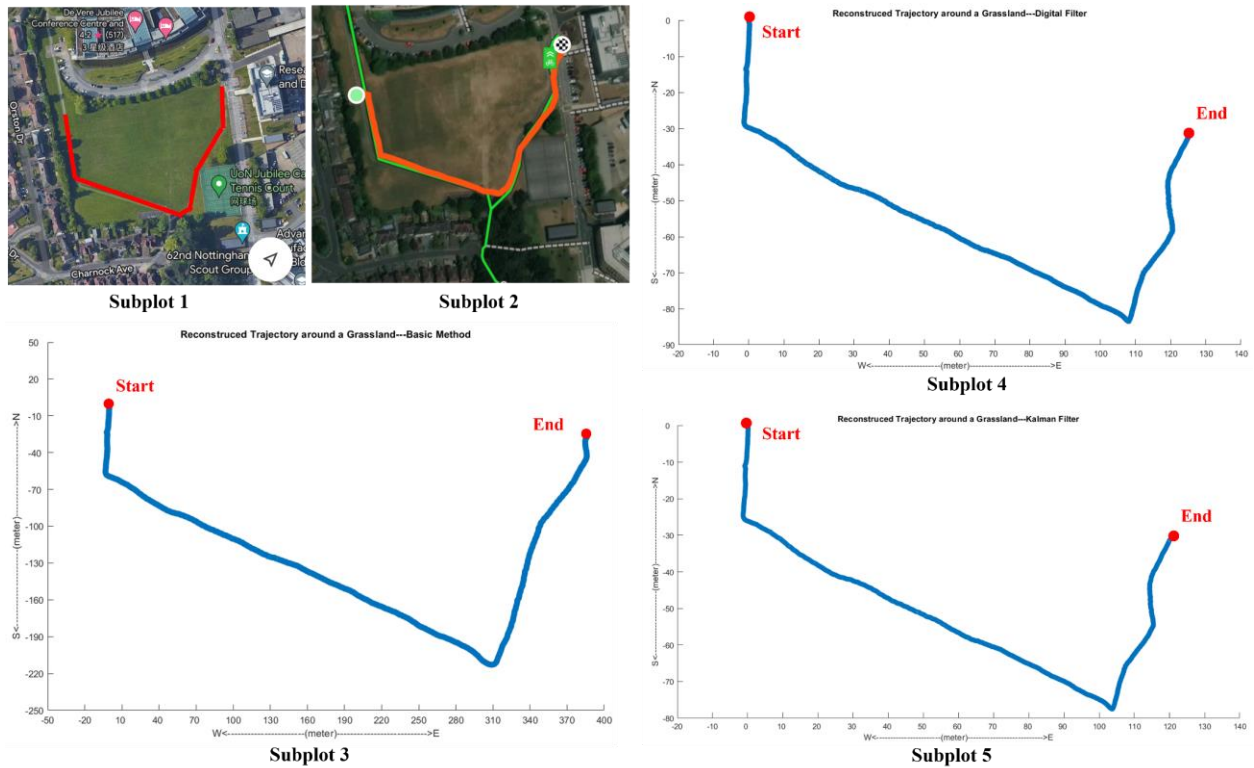


Figure 5-37. Theoretical trajectory (Subplot 1, red line) and result from GPS receiver (Subplot 2, orange line), and reconstructed trajectories of basic method (Subplot 3), digital filter (Subplot 4) and Kalman filter (Subplot 5) of the grassland test

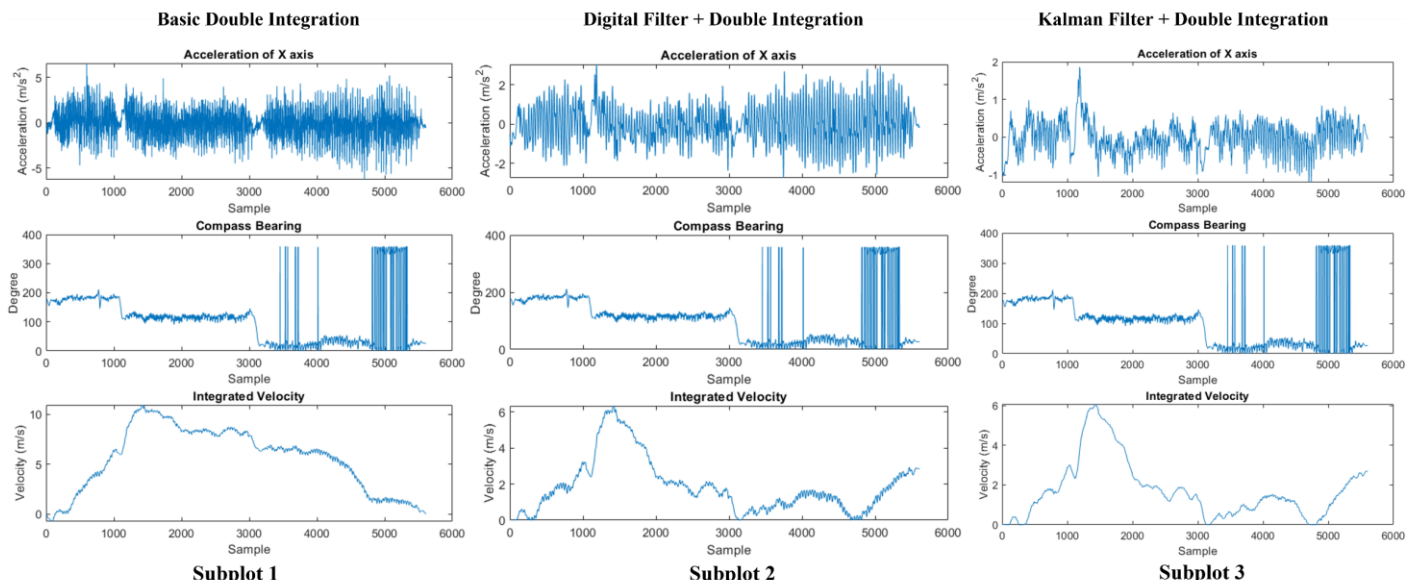


Figure 5-38. Acceleration of X axis, compass bearing and integrated velocity for three processing algorithms in the grassland test

It could be seen from Subplot 1 and 2 in **Figure 5-37** that the recorded trajectory from GPS receiver was now very close to the theoretical trajectory, mainly due to the fact that no metal object (or similar interference) was present in the open field. The trajectories in Subplot 3,4 and 5 all achieved a similar shape to the theoretical prediction, but the track scale and specific statistics of them still deviated from the prediction to some extent, particularly the result of basic method as shown in **Table 5-3** (the percentage in bracket still indicated difference to GPS test). The inferior result from basic method mainly came from the error of the integrated velocity as shown in Subplot 1 in **Figure 5-38**, where the “always positive” velocity did successfully lead to a similar trajectory shape regarding the theoretical prediction, but the velocity seemed to be over-integrated to an excessive value that eventually led to the overestimation of the trajectory distance of 618.82m. The digital filter and Kalman filter method, however, seemed to have suppressed the “over-integration” as shown in Subplot 2 and 3 in **Figure 5-38**, but the eventual accumulative distance was shorter than the value from GPS positioning of 260 m (which was regarded as the actual value as the trajectory was close). Despite the suppression, there were clearly still some problems of the results from digital and Kalman filter method, such as the terminating velocity was increasing rather than dropping to zero and the errors of distance and average speed were relatively large. All these imperfections indicated that the algorithms still needed to be improved.

Table 5-3. Journey duration (s), distance (m) and average speed (m/s) estimation from GPS data and three inertial algorithms in the grassland test

	Duration	Distance	Average Speed
GPS	110	260	2.36
Basic method	112 (1.8%)	618.82 (138%)	5.53 (134%)
Digital Filter	112 (1.8%)	209.98 (19.2%)	1.87 (20.8%)
Kalman Filter	112 (1.8%)	195.46 (24.8%)	1.74 (26.3%)

5.4.2 Post Signal Processing Reflection

5.4.2.1 Legitimacy of Inertial Navigation

Two field validations in the above section had partially proven the effectiveness of inertial navigation. The validations were only “partial” because the reconstructed trajectories and relevant statistics were not close enough to the theoretical predictions. Nevertheless, it was legitimate to claim that the inertial navigation was an appropriate choice for such a glasses frame with very limited battery capacity and space for components. The current results became more convincing if the situation, that the current implementation of inertial navigation was only based on the acceleration of X axis while the other 8 axes were not involved yet, was considered. Some results of inertial navigation had also been proven superior compared to satellite navigation like the test around a building in **Figure 5-34** and **Figure 5-36**. This superiority generally resulted from the independence of inertial navigation, which was also the biggest advantage of it in tackling indoor and lack-of-infrastructure navigation scenarios. These scenarios, such as a dense forest or rural place, were possible to occur in orienteering thus justifying the deployment of inertial navigation in the glasses frame.

Certainly, implementing both navigation methods together would achieve a best result if it could be guaranteed that other product features would not be sacrificed. However, this required a deep customisation of the electronic system to achieve a subtle balance between capability and power consumption, which might involve tailored antenna, GPS and IMU chips. A great number of resources was required to develop such technologies thus it could be more appropriate to consider this path until the 2nd or 3rd generation of the device.

5.4.2.2 Trajectory Reconstruction Algorithms and a Reference to Sailing

The trajectory was reconstructed based on the acceleration on the X axis (same as the moving direction) of accelerometer in current implementation. This was a basic methodology but was not the choice adopted by most modern research papers. As mentioned in *2.1 Wearable Electronic Device and Product Form Choice* and *4.6 Post Signal Processing*, modern reconstruction techniques involved step length estimation and gait analysis using the acceleration data from other axes or the data from gyroscope. For example, the vertical bounce of the user, which corresponded to the acceleration on the Y axis (**Figure 5-3**), could be used to estimate the step length. [19] Other advanced techniques such as Zero Velocity Update could be used to reduce the signal drift based on external constraints [3], and Mode Classification based on machine learning could be used to dynamically adjust algorithm for a better reconstruction [4]. These modern techniques were proper directions for future enhancement.

The sailing scenario had not been discussed in the entire report, mainly due to the lack of proper testing environment and the inherent complexity of the problem. The superposition of the movement from water surface and the wearer would cause many issues that did not exist in land activities, such as the non-negligible water drifting. Developing a device for sailing might require a completely different code structure thus not discussed in this space-limited report.

5.4.2.3 Development of Software Package for Customers

The current post signal processing was completed and visualised in MATLAB, which was acceptable in the prototyping stage for algorithm development and validation, but not appropriate for presenting the results to customers. Ideally a GUI (Graphical User Interface) should be developed to allow the user to drag the recorded txt file into the software and then all results including the trajectory, average speed etc. would be automatically computed and presented to the user in a one-step process. Alternatively, a mobile phone app could be developed to accept the recorded data from the glasses frame via Bluetooth and utilise the computational resources in the phone to visualise the data to user. This would require the hardware enhancement of the glasses frame to equip it with Bluetooth communication chip and potentially a larger battery.

6. Overall Project Reflection

6.1 Attainment of Objectives and Deliverables

The development of the project followed a standard procedure of research, design, implementation and validation. Each stage corresponded to some of the objectives and deliverables stated in *3.2 Objectives* and *3.4 Deliverables*. Generally, most of them were completed to a high extent while certain measures could be taken to further improve some of them. An extensive literature review and background research about the glasses frame were covered in *2 Literature Review and Market Research*, which led to the fulfilment of O1, O2 and D1. A high-level architecture of the glasses frame and the corresponding methodologies for realisation were presented in *4 Methodology* thus the O3 and D2 were finished. The electronic system was designed in PCB forms and the assembly and validation of them indicated the O4, O6, D3, D5 were completed. There was an issue of voltage translator in the PCB but the problem was alleviated by attaching sensor modules to the left leg. It could be fully resolved by a new generation of PCB design. The mechanical structure of the glasses frame was designed and printed with full compatibility with PCBs, hence leading to the accomplishments of O5 and D4. Both the basic guiding function and additional data logging were realised in programming work thus the O7, D6, D7 were reached. The dimensions of the glasses frame were tailored according to a realistic human head model and an intuitive and simplified user interface was designed, to satisfy the requirements in O10 and D9. Recommendations such as ultrasonic

welding and addition of photodetector had also been made to further improve the user experience. A post signal processing script based on MATLAB was developed to reconstruct the trajectory and compute other statistics. All required parameters in O8 could be generated by the developed scripts thus the D9 was fulfilled, but the accuracy of the trajectory still needed to be improved by implementing some advanced techniques. Both the glasses frame and signal processing algorithms had gone through a comprehensive validation process thus O9 and D10 were completed. Eventually the completion of this report would finish O11.

For a company interested in pushing this project forward to a commercial product, there were various technical and marketing details that could be regarded as suggestions for future improvements. Full details could be referred to discussions in previous sections while a summary of these suggestions was covered in *7 Conclusion*.

6.2 Future Hardware Variations and Upgrades

One of the possible upgrades was the Bluetooth connection with mobile phones for data visualisation mentioned in previous sections. Besides this, for example a solar PV (Photovoltaic) panel that matched with the shape of the platform on the frontal frame could be mounted to the device to extend the battery life. Most foot orienteering games were organised in an outdoor environment thus it was reasonable to assume that the device would be exposed to sunlight (if sunny) during the activity and the top of the frontal frame was not likely to be covered. Or, a LED matrix consisting of hundreds of tiny LED units could be implemented to replace the current design of 4 red LEDs (ignoring the problem of power consumption). Stepless light transition could be realised by such a matrix and the interface for displaying the deviation from pre-set target would be much more versatile, which potentially would allow the wearer to better perceive the current heading.

The “LED and buzzer guiding architecture” could also be deployed in other product forms like caps, shoes or a portable module that could be mounted to vehicles like boats or bikes. The product “shell” would need to be redesigned but the electronic system and algorithms would remain unchanged (or at least very similar). Such strategy could broaden the potential market of the device and provide customers an opportunity to select a form that suited their needs best.

6.3 Supply Chain Management (SCM)

SCM was a critical issue for this project as the assembly of the glasses frame involved over 40 different types of components/PCBs/modules shipped from multiple cities within UK and also from locations in other countries like Texas and Hongkong. The current shortage of ICs had made the SCM even more complex, and that was why the components were ordered from multiple sources such as individual sellers on eBay, components distributors or PCB factories. Back-up plans had been made for some components with an uncertain stock number and long lead time, and some of them were indeed implemented to guarantee the regular development timeline of the glasses frame.

The key point for mentioning the SCM issue was to propose relevant suggestions for future large-scale production of the device. Judging merely from the FYP experience, the SCM issue was a determinant in product’s date of delivery, supply stability and unit price, let alone in a mass production. Various suppliers and supplying channels should be established to provide a solid foundation for development and commercialisation. Multiple supplying channels for a single component was preferred to cope with contingencies and irresistible factors.

6.4 Ethical Concerns

The fact that the glasses frame was tracking the wearer’s motional data by a direct body contact caused major ethical concerns of the device. So far, the data was directly stored into the SD

card and the wearer was the only person who had access to it, thus a clear notification of this functionality to user and allowing him/her to freely turn on/off the data storage would be enough. However, future enhancements such as Bluetooth communication with phones would require more measures. A digital agreement containing all data policies must be signed by the user to enable the tracking and storing functions. Data from users must be encrypted in the communication with servers to protect user privacy.

Meanwhile, certain warnings should be noted in the product specifications, such as the device was not appropriate for people with photosensitive epilepsy due to its PWM-driven LEDs. This ensured that customers were notified by the potential biological effects brought by the device.

6.5 Intellectual Property (IP)

IP related issues would be critical when the glasses frame was being pushed from a prototype to a commercial product. The company needed relevant design rights and patents to obtain enough “freedom to operate”. The design rights were related to the appearance and aesthetic factors of the glasses frame and there already existed a great number of similar smart glasses design as shown in [54] and [55]. The patents usually corresponded to the functionalities and features of the device such as the smart glasses with acoustic channel in [56] and the glasses system with LED arrays in [57]. A thorough investigation of such patents should be conducted during the development stage to grasp a complete picture of IP issues of similar products (i.e., competitors, for example the devices mentioned in *2.5 Market Analysis and Available Commercial Products*). Relevant design rights and patents should also be drafted and submitted before commercialisation to protect own IPs and avoid infringements to others.

6.6 Device's Accordance with IOF Foot Orienteering Rules

The IOF (International Orienteering Federation) is a worldwide organisation responsible for holding international-level orienteering events, thus the orienteering rules made by it were regarded as official rules in this section. According to the latest rules published in 2022 [58], the competitors must not wear any communication devices or GPS-enabled devices that could provide any guiding information. The GPS receiver that was only capable of logging data was allowed and such device must be approved by the event organiser before the match started.

Obviously there was no specific regulation for the proposed glasses frame now (since it was a new technology) and it could be inferred from the current rules that such a glasses frame would not be strictly prohibited by the organiser as it could neither communicate with other devices nor provide real-time guiding information other than the information that could be obtained from a normal compass. It was expected that the glasses frame would not be allowed in the matches when it was just launched, but people's acceptance of such device should increase when it became more popular and IOF might update the rules accordingly. If the future generations of the glasses frame were equipped with additional functions that were indeed inappropriate for a formal match, it was possible to sell different models of the device with different enabled/disabled functions that matched with the requirements of the events. Even selling the glasses frame just to amateur players was not a bad option.

6.7 Revision on Time Plan

The original time plan (included in *9.1 Appendix A Time Plan*) was revised according to the actual project progress and was shown in **Figure 6-1**. The original yellow rows (as back-up plans for potential risks) were removed since the relevant risks did not occur during the development. The progress of a task was marked by a green row (same as original) if it remained unchanged in the revised plan and the progress that was different to original plan was marked by a blue row. It should be noted that although there were some changes to the progress of tasks, the original objectives, deliverables and milestones all remained same. A summary

reflection of the measurable outcomes of the project was included in *6.1 Attainment of Objectives and Deliverables*, this section only focused on the progress changes related to time (delayed, extended etc.) and risk mitigation methods.

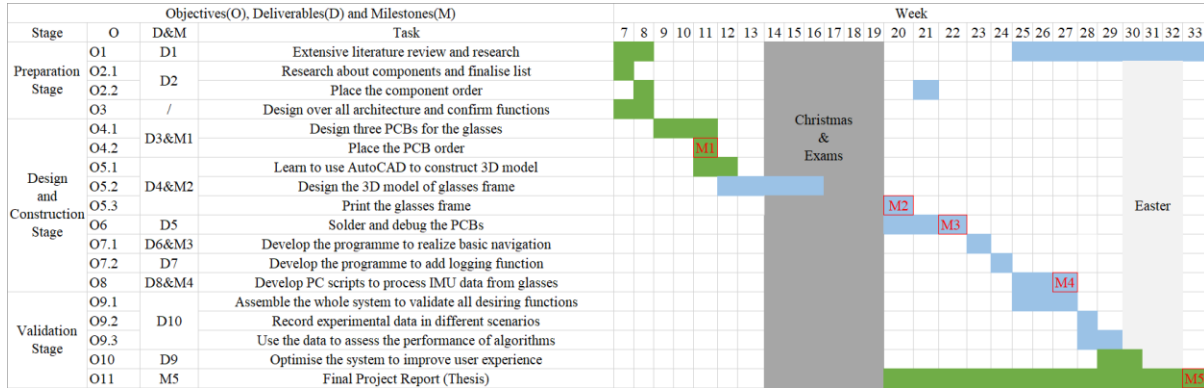


Figure 6-1. Revised time plan based on the actual project development progress

It could be seen from **Figure 6-1** that most progress changes occurred at the end of first semester and in the second semester. The 3D modelling progress (O5.2) of the glasses frame took a longer time than expectation but the Christmas period was used to complete the modelling work before the commencement of the second semester, thus it only had a minimal effect to the overall progress. The soldering and debugging of the PCBs, however, caused a noticeable delay to the overall progress, mainly to the difficulty of soldering tiny leadless chips and the problem of voltage translator mentioned in *5.1.1.1 PCB1: Left Leg*. Although some redundant components had been bought in the first purchase, they were still not enough to complete the soldering process due to chip fragility. A second contingency order was placed in Week 21 immediately after the shortage occurred so that assembly work could continue. The duration of literature view in the second semester was also greatly extended to research more existing inertial navigation algorithms and alleviate the risk of being not able to develop a satisfying trajectory reconstructing algorithm (thus had to discuss the existing ones). Fortunately the developed algorithms had generated fairly good results thus some previous research work was presented as advanced techniques for future improvements in *5.4.2.2 Trajectory Reconstruction Algorithms and a Reference to Sailing*.

7. Conclusion

In conclusion, a glasses frame based on visual and auditory signals, which was capable of guiding the wear on a stable compass bearing, was successfully designed, implemented and validated in this project. A compact electronic system realised by PCBs, a mechanical glasses frame realised by 3D printing and a software program based on Arduino Bootloader constituted the entire glasses frame. MATLAB scripts had also been developed to perform inertial navigation as post signal processing. Generally, fairly satisfying results had been generated in each stage while some aspects could still be improved for a higher accuracy/stability/performance in further development. All original objectives were completed to a high extent and a summary of their completion was covered in *6.1 Attainment of Objectives and Deliverables*.

For the electronic system of the glasses frame, three PCBs located in the left leg (PCB1), frontal frame (PCB2) and right leg (PCB3) were designed and implemented. The implementation of PCB1 successfully provided computational resources (8-bit microprocessor running at 16 MHz), 8GB data storage, magnetic heading measurement with an accuracy of 1°, sensitive inertial measurements of acceleration and rotational speed, one of the buzzers to

the glasses frame. An issue of voltage translator was recognised during validation and a temporarily solution of externally attached modules was used to bypass the problem. The issues could be permanently fixed by another generation of PCB1 design. The responsibilities of PCB2 were providing 6 electrical connections between PCB1 and PCB3, also 4 current paths and mechanical support of all LEDs. These functions were completed fulfilled now but flexible circuits could be introduced in the future to provide a greater freedom to mechanical structure design. The implementation of PCB3 generated required 3.3V and 5V power sources for other boards, and it also provided a user interface through two buttons and a slide switch, together with a battery charging function and a connection of the other buzzer. All objectives of PCB3 were realised while some aspects such as the orientation of the charging port could be improved in the future to make it better.

Regarding the mechanical designs, the entire glasses frame was modelled in a computer CAD software. Totally six components of left/right lid, left/right leg, frontal frame and nose support were successfully designed to constitute the glasses frame. These components could be assembled using only two screws as hinges and they were perfectly compatible with three PCBs. Methods such as ultrasonic welding and potting material could be implemented in future to improve waterproof and shock-resistant features of the glasses frame if commercialised.

The program of the glasses frame was based on various ISRs under different frequencies. The program started with a 1 Hz low frequency ISR as a stand-by mode to save power and wait for instructions. It was driven by a 250 Hz ISR when operating in working mode, meanwhile providing a 50 Hz clock signal as a PWM driving waveform for LEDs and a constant sampling frequency for sensors. It had been validated that this mechanism could allow the wearer to intuitively press a button to start a journey, reset target or terminate the journey, meanwhile the data from sensors was securely stored into a SD card at 50 Hz. The LEDs and buzzers were turned on/off accordingly in the journey for guidance based on the calculated bearing and pre-set target. An optimised displaying logic and more robust bearing calculation algorithm could be developed in future for enhancements.

Three different algorithms (methods) were developed to perform the inertial navigation to compute and visualise statistics to user. All methods were based on the double integration of the acceleration along the moving direction of the glasses frame wearer. A 70th order low pass FIR filter and a Kalman filter were implemented to remove noise and distortion in the raw data before the integration process. Generally, the method involving Kalman filter had achieved a reconstructed trajectory shape that was close to theoretical prediction in most validation tests, and it also achieved a minimum distance error of 2.1% and a minimum average speed error of 6.1% in the building test, mainly due to its superiority in motion tracking. Other advanced techniques such as step length estimation and mode classification could be investigated in future development to improve the accuracy of inertial navigation.

Many lessons in this project were valuable for a company interested in pushing this prototype to a commercial product. The idea of guiding the wearer based on the visual and auditory feedback from LEDs and buzzers was indeed feasible and effective. The implementation of chip-based magnetic and inertial sensors could achieve a very lightweight and compact device at a low cost, especially with the introduction of modern component package and assembly methodology. Such characteristics of the device differentiated itself from other powerful though expensive smart glasses, which consolidated the competitiveness of the proposed glasses frame. Inertial navigation was a promising direction for future development if the cost and compactness were the main focuses, while its fusion with satellite navigation would further boost the accuracy and versatility in different scenarios if the problem of power consumption could be solved.

8. Reference

- [1] C. Ferguson and R. Turbyfill, Orienteering USA, Ed. *Discovering Orienteering: Skills, Techniques, and Activities*. IL: Versa Press, 2013.
- [2] Columbia River Orienteering. "Learning Orienteering." <https://www.croc.org/new-to-o> (accessed 8 Apr., 2022).
- [3] S. Qiu, Z. Wang, H. Zhao, K. Qin, Z. Li, and H. Hu, "Inertial/magnetic sensors based pedestrian dead reckoning by means of multi-sensor fusion," *Information Fusion*, vol. 39, pp. 108-119, 1 Jan. 2018, doi: <https://doi.org/10.1016/j.inffus.2017.04.006>.
- [4] F. Inderst, F. Pascucci, and M. Santoni, "3D pedestrian dead reckoning and activity classification using waist-mounted inertial measurement unit," in *2015 International Conference on Indoor Positioning and Indoor Navigation (IPIN)*, 13-16 Oct. 2015, pp. 1-9, doi: <http://doi.org/10.1109/IPIN.2015.7346953>.
- [5] M. Ortiz, M. De Sousa, and V. Renaudin, "A New PDR Navigation Device for Challenging Urban Environments," *Journal of Sensors*, vol. 2017, pp. 479-480, 12 Nov. 2017, doi: <http://doi.org/10.1155/2017/4080479>.
- [6] X. Xiong, "Designing turn-by-turn navigation system for customized wearable user interface," Master's thesis, Department of Information Processing Science, University of Oulu, 2016. [Online]. Available: <http://urn.fi/URN:NBN:fi:oulu-201609132773>
- [7] A. Grzybowski and K. Kupidura-Majewski, "What is color and how it is perceived?," *Clinics in Dermatology*, vol. 37, no. 5, pp. 392-401, 1 Sept. 2019, doi: <https://doi.org/10.1016/j.clindermatol.2019.07.008>.
- [8] D. Cao, "Chapter 10 - Color Vision and Night Vision," in *Retina (Fifth Edition)*, S. J. Ryan *et al.* Eds. London: W.B. Saunders, 2013, pp. 285-299.
- [9] A. K. R. Choudhury, "4 - Principles of colour perception," in *Principles of Colour and Appearance Measurement*, A. K. R. Choudhury Ed.: Woodhead Publishing, 2014, pp. 144-184.
- [10] M. Sliwinska-kowalska, "Chapter 19 - Hearing," in *Handbook of Clinical Neurology*, vol. 131, M. Lotti and M. L. Bleecker Eds.: Elsevier, 2015, pp. 341-363.
- [11] Y.-Y. Juo *et al.*, "17 - Center for Advanced Surgical and Interventional Technology Multimodal Haptic Feedback for Robotic Surgery," in *Handbook of Robotic and Image-Guided Surgery*, M. H. Abedin-Nasab Ed.: Elsevier, 2020, pp. 285-301.
- [12] Y. Huang *et al.*, "Recent advances in multi-mode haptic feedback technologies towards wearable interfaces," *Materials Today Physics*, vol. 22, p. 100602, 1 Jan. 2022, doi: <https://doi.org/10.1016/j.mtphys.2021.100602>.
- [13] N. K. Dim and X. Ren, "Investigation of suitable body parts for wearable vibration feedback in walking navigation," *International Journal of Human-Computer Studies*, vol. 97, pp. 34-44, 1 Jan. 2017, doi: <https://doi.org/10.1016/j.ijhcs.2016.08.002>.
- [14] Y. Hsu, J. Wang, and C. Chang, "A Wearable Inertial Pedestrian Navigation System With Quaternion-Based Extended Kalman Filter for Pedestrian Localization," *IEEE Sensors Journal*, vol. 17, no. 10, pp. 3193-3206, 2017, doi: <http://doi.org/10.1109/JSEN.2017.2679138>.
- [15] A. A. D. Toro, S. E. C. Bastidas, and E. F. C. Bravo, "Methodology to Build a Wearable System for Assisting Blind People in Purposeful Navigation," in *2020 3rd International Conference on Information and Computer Technologies (ICICT)*, 9-12 Mar. 2020, pp. 205-212, doi: <http://doi.org/10.1109/ICICT50521.2020.00039>.
- [16] H. Kim *et al.*, "Design of a Low-Power BLE5-Based Wearable Device for Tracking Movements of Football Players," in *2019 International SoC Design Conference (ISOCC)*, 6-9 Oct. 2019, pp. 11-12, doi: <http://doi.org/10.1109/ISOCC47750.2019.9027630>.
- [17] J. Galos, A. A. Khatibi, and A. P. Mouritz, "Vibration and acoustic properties of composites with embedded lithium-ion polymer batteries," *Composite Structures*, vol. 220, pp. 677-686, 15 July 2019, doi: <https://doi.org/10.1016/j.compstruct.2019.04.013>.
- [18] P. Pattanaik and M. Ojha, "Review on challenges in MEMS technology," *Materials Today: Proceedings*, 3 May 2021, doi: <https://doi.org/10.1016/j.matpr.2021.03.142>.
- [19] X. Hou and J. Bergmann, "Pedestrian Dead Reckoning With Wearable Sensors: A Systematic Review," *IEEE Sensors Journal*, vol. 21, no. 1, pp. 143-152, 2021, doi: <http://doi.org/10.1109/JSEN.2020.3014955>.

- [20] British Orienteering Federation. "Annual Report & Review of 2020." <https://www.britishorienteering.org.uk/home> (accessed 22 Apr., 2022).
- [21] International Orienteering Federation. "History and archives." <https://orienteering.sport/ioc/history-and-archives/> (accessed 22 Apr., 2022).
- [22] Google. "Discover Glass Enterprise Edition." <https://www.google.com/glass/start/> (accessed 22 Apr., 2022).
- [23] A. Klein, C. Sørensen, A. S. d. Freitas, C. D. Pedron, and S. Elaluf-Calderwood, "Understanding controversies in digital platform innovation processes: The Google Glass case," *Technological Forecasting and Social Change*, vol. 152, p. 119883, 1 Mar. 2020, doi: <https://doi.org/10.1016/j.techfore.2019.119883>.
- [24] VR Expert. "Google Glass Enterprise Edition 2." <https://vr-expert.com/ar-headsets/buy-google-glass-enterprise-edition-2/> (accessed 22 Apr., 2022).
- [25] Ray-Ban. "RAY-BAN STORIES SMART GLASSES." <https://www.ray-ban.com/uk/ray-ban-stories> (accessed 22 Apr., 2022).
- [26] Amazon. "Echo Frames (2nd Gen) | Smart audio glasses with Alexa | Classic Black with prescription ready frames." <https://www.amazon.com/All-new-Echo-Frames/dp/B083C58VDP> (accessed 22 Apr., 2022).
- [27] Atmel, "8-bit AVR Microcontroller with 32K Bytes In-System Programmable Flash," *ATmega328P Datasheet*, 2015.
- [28] InvenSense, "MPU-6000/MPU-6050 Product Specification," *MPU6050 Datasheet*, 2013.
- [29] Honeywell, "3-Axis Digital Compass IC," *HMC5883L Datasheet*, 2010.
- [30] VISHAY, "High Efficiency LED in Ø 5 mm Tinted Diffused Package," *Red LED Datasheet*, 2019.
- [31] CUI DEVICES, "PIEZ0 BUZZER TRANSDUCER," *Buzzer Datasheet*, 2021.
- [32] Würth Elektronik, "WS-SLSU SMT Mini Slide Switch," *Slide Swtich Datasheet*, 2019.
- [33] Panasonic, "3.5 mm×2.9 mm Side-operational SMD Light Touch Switches," *Push Button Datasheet*, 2013.
- [34] Nexpria, "Dual supply translating transceiver," *Voltage Translator Datasheet*, 2020.
- [35] maxim integrated, "400mV to 5.5V Input, nanoPower Synchronous Boost Converters with True Shutdown," *Boost chip Dataheet*, 2021.
- [36] MICREL, "150mA µCap Ultra-Low Dropout LDO Regulator" *LDO Datasheet*, 2007.
- [37] MICROCHIP, "Single-Cell Li-Ion/Li-Polymer Battery Charge Management Controllers in 2x2 TDFN," *Battery Charging IC Datasheet*, 2019.
- [38] molex, "FFC Cable Jumpers, Premo-Flex Flat-Flexible Cable Jumpers," *FFC Datasheet*, 2021.
- [39] R. S. Bridger, *Introduction to Ergonomics*. London: Taylor & Francis e-Library, 2003.
- [40] J.-H. Lee, S.-J. Shin, and C. Istook, "Analysis of Human Head Shapes in the United States," *International journal of human ecology*, vol. 7, 1 Jan. 2006.
- [41] N. Shahrubudin, T. C. Lee, and R. Ramlan, "An Overview on 3D Printing Technology: Technological, Materials, and Applications," *Procedia Manufacturing*, vol. 35, pp. 1286-1296, 1 Jan. 2019, doi: <https://doi.org/10.1016/j.promfg.2019.06.089>.
- [42] B. Zabala *et al.*, "Mechanism-based wear models for plastic injection moulds," *Wear*, vol. 440-441, p. 203105, 15 Dec. 2019, doi: <https://doi.org/10.1016/j.wear.2019.203105>.
- [43] N. Mary Jasmin *et al.*, "An overview on characteristics and performance of ultrasonic welding process on different materials," *Materials Today: Proceedings*, vol. 50, pp. 1508-1510, 2022/01/01/ 2022, doi: <https://doi.org/10.1016/j.matpr.2021.09.096>.
- [44] SparkFun, "Interface Development Tools SparkFun USB to Serial Breakout - FT232RL," *Debugger Datasheet*, 2021.
- [45] MIT. "MIT License." <https://www.mit.edu/~amini/LICENSE.md> (accessed 24 Apr., 2022).
- [46] A. G. Constantinides, "DIGITAL FILTERS," in *Encyclopedia of Vibration*, S. Braun Ed. Oxford: Elsevier, 2001, pp. 380-395.
- [47] S. Krishnan, "3 - Biomedical signals and systems," in *Biomedical Signal Analysis for Connected Healthcare*, S. Krishnan Ed.: Academic Press, 2021, pp. 85-127.
- [48] B. Alsadik, "Chapter 10 - Kalman Filter," in *Adjustment Models in 3D Geomatics and Computational Geophysics*, vol. 4, B. Alsadik Ed.: Elsevier, 2019, pp. 299-326.

- [49] E. Ashely. "Flexible Printed Circuit Board, Introduction and importance." <https://www.rs-online.com/designspark/flexible-printed-circuit-board-introduction-and-importance> (accessed 26 Apr., 2022).
- [50] M. Schwerter, M. Lester-Schädel, and A. Dietzel, "Waterproof sensor system for simultaneous pressure and hot-film flow measurements," *Sensors and Actuators A: Physical*, vol. 257, pp. 208-215, 15 Apr. 2017, doi: <https://doi.org/10.1016/j.sna.2017.02.010>.
- [51] A. V. Kudryashov, E. S. Galishheva, and G. N. Yagovkin, "Experimental PWM Controlled Device," in *2019 International Conference on Industrial Engineering, Applications and Manufacturing (ICIEAM)*, 25-29 Mar. 2019, pp. 1-5, doi: <http://doi.org/10.1109/ICIEAM.2019.8742952>.
- [52] A. Wilkins, J. Veitch, and B. Lehman, "LED lighting flicker and potential health concerns: IEEE standard PAR1789 update," in *2010 IEEE Energy Conversion Congress and Exposition*, 12-16 Sept. 2010, pp. 171-178, doi: <http://doi.org/10.1109/ECCE.2010.5618050>.
- [53] D. Loh, S. Zihajehzadeh, R. Hoskinson, H. Abdollahi, and E. J. Park, "Pedestrian Dead Reckoning With Smartglasses and Smartwatch," *IEEE Sensors Journal*, vol. 16, no. 22, pp. 8132-8141, 15 Nov. 2016, doi: <http://doi.org/10.1109/JSEN.2016.2606539>.
- [54] T. W. Porter, M. Tappeiner, and F. Strauss, "SMART GLASSES," US Patent USD949956 (S) Patent Appl. US201929696293F, 26 Jun., 2019. [Online]. Available: https://worldwide.espacenet.com/publicationDetails/biblio?CC=US&NR=D949956S&KC=S&FT=D&ND=3&date=20220426&DB=EPODOC&locale=en_EP
- [55] A. William, A. Yu, G. Jaren, and W. Chee, "Smart Glasses," US Patent US2021088810 (A1) Patent Appl. US202016777256, 25 Mar., 2020. [Online]. Available: https://worldwide.espacenet.com/publicationDetails/originalDocument?CC=US&NR=2021088810A1&KC=A1&FT=D&ND=3&date=20210325&DB=EPODOC&locale=en_EP
- [56] T. Porter and C. O'Conner, "Smart Glasses with Acoustic Channel," US Patent WO2022051426 (A1) Patent Appl. WO2021US48752, 01 Sept., 2021. [Online]. Available: https://worldwide.espacenet.com/publicationDetails/biblio?CC=WO&NR=2022051426A1&KC=A1&FT=D&ND=3&date=20220310&DB=EPODOC&locale=en_EP
- [57] R. Schultz, "Smart Glasses with LED Projector Arrays," US Patent WO2022051407 (A1) Patent Appl. WO2021US48728, 01 Sept., 2021. [Online]. Available: https://worldwide.espacenet.com/publicationDetails/biblio?CC=WO&NR=2022051407A1&KC=A1&FT=D&ND=3&date=20220310&DB=EPODOC&locale=en_EP
- [58] International Orienteering Federation. "COMPETITION RULES FOR INTERNATIONAL ORIENTEERING FEDERATION (IOF) FOOT ORIENTEERING EVENTS." <https://orienteering.sport/orienteering/competition-rules/> (accessed 1 May, 2022).

9. Appendices

9.1 Appendix A Time Plan

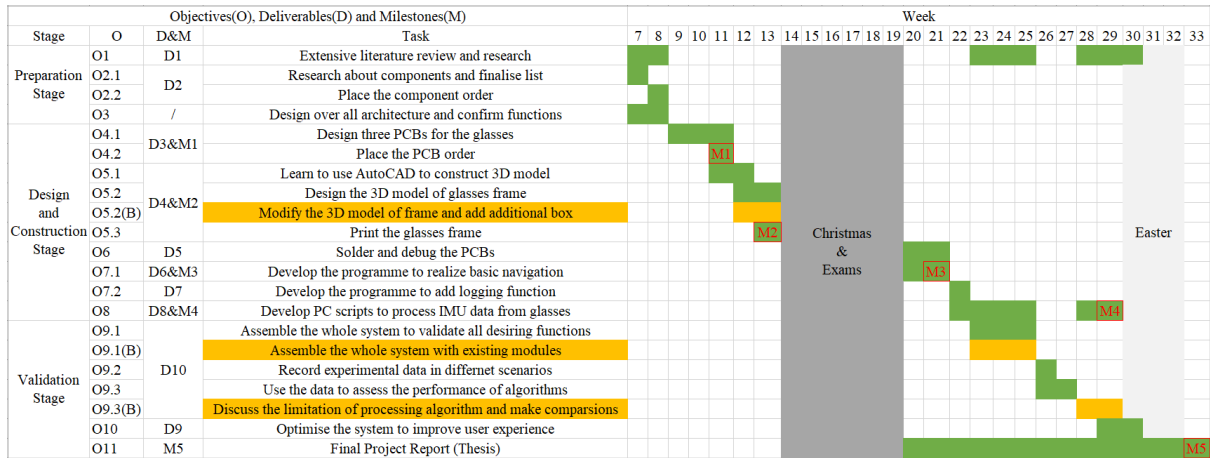


Figure 9-1. Original project time plan

The time plan started from the first week after proposal submission and ended at the deadline of final thesis. The first semester focused on hardware development, including selecting components, PCB design and frame 3D printing that cover O1-O5. The second semester focuses on programming, system validation and final thesis that were related with the rest O6-O11. The green rows indicated the normal project progress while the yellow rows reflected the progress of Plan B that been specified in risk management in *3.6 Risk Management & Elaboration for Deliverable and Milestones*. If these risks did occur, the yellow rows would be conducted instead. Milestones M1-M5 were marked as red boxes at the end of each relevant objectives. Most tasks would be accomplished before the deadline of thesis draft (Week 28), the rest time before final deadline was devoted to system optimisation and polish of thesis.

It should be noted that some tasks such as “literature review and research” occurred discretely for multiple times. This was because O1 was generalised to represent all potential research workload. O8 was re-started at Week 28 because it considered the optimisation of algorithms on PC after conducting tests and evaluation of the previous method in Week 26 and 27.

(The above was the interpretation of the original time plan. The revised time plan and its discussion were included in *6.7 Revision on Time Plan*)

9.2 Appendix B PCB Schematics and 2D Layout Designs

9.2.1 PCB1 in Left Leg

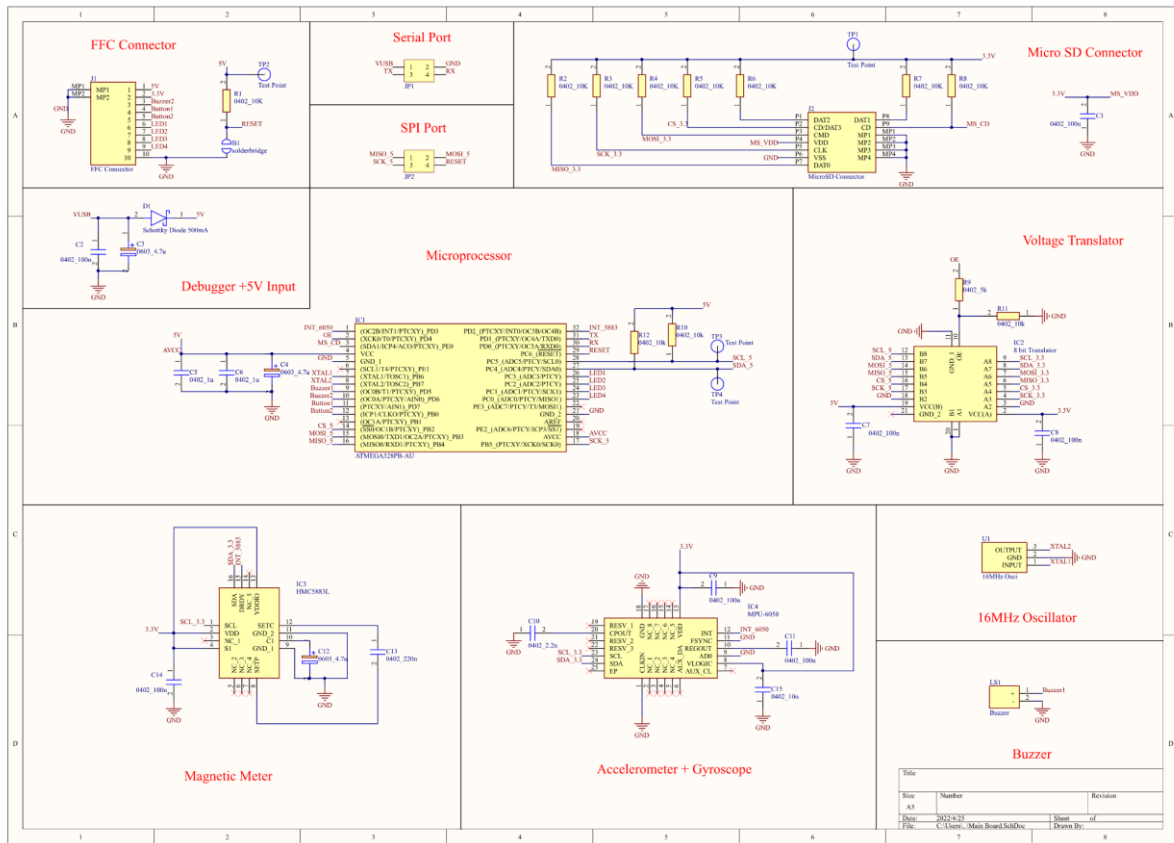


Figure 9-2. Schematic of PCB1 in the left leg of the glasses frame

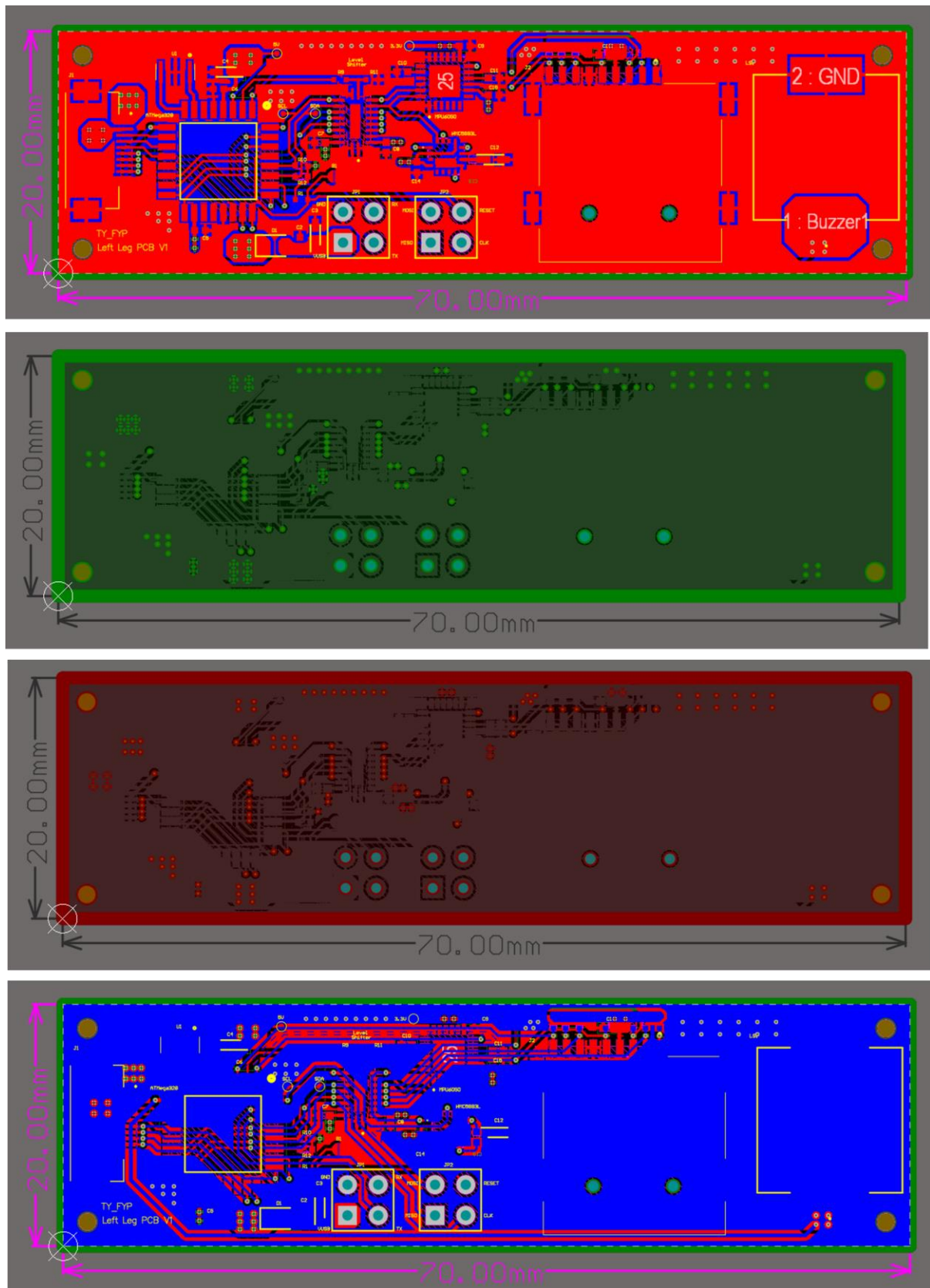


Figure 9-3. Top layer (top), middle layer of 5V (second top), middle layer of 3.3V (second bottom), bottom layer (bottom) of 2D PCB layout design of PCB1

9.2.2 PCB2 in Frontal Frame

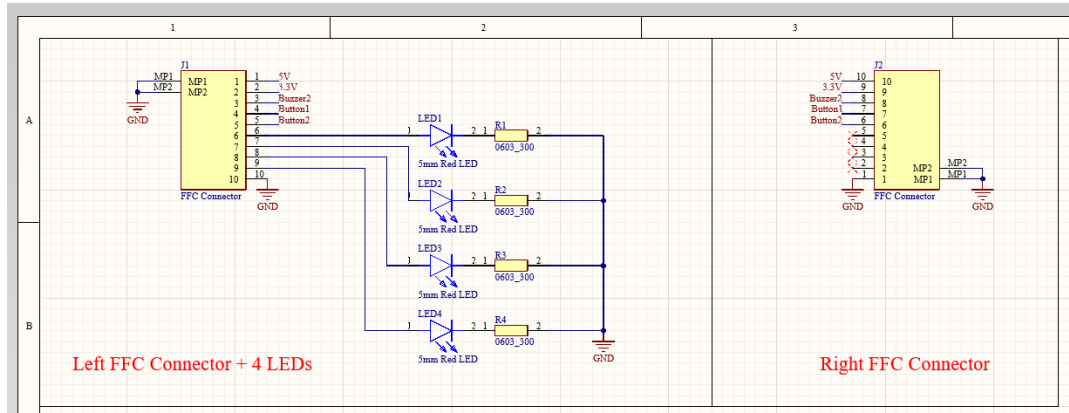


Figure 9-4. Schematic of PCB2 in the frontal frame

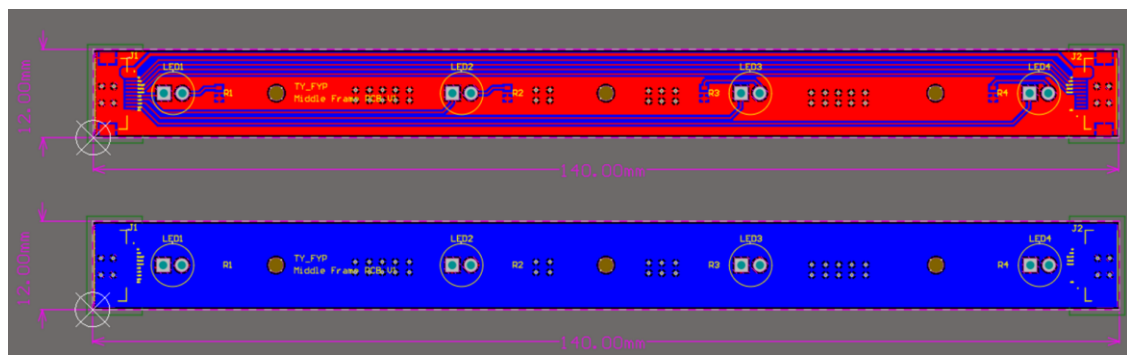


Figure 9-5. Top layer (top) and bottom layer (bottom) of 2D PCB layout design of PCB2

9.2.3 PCB3 in Right Leg

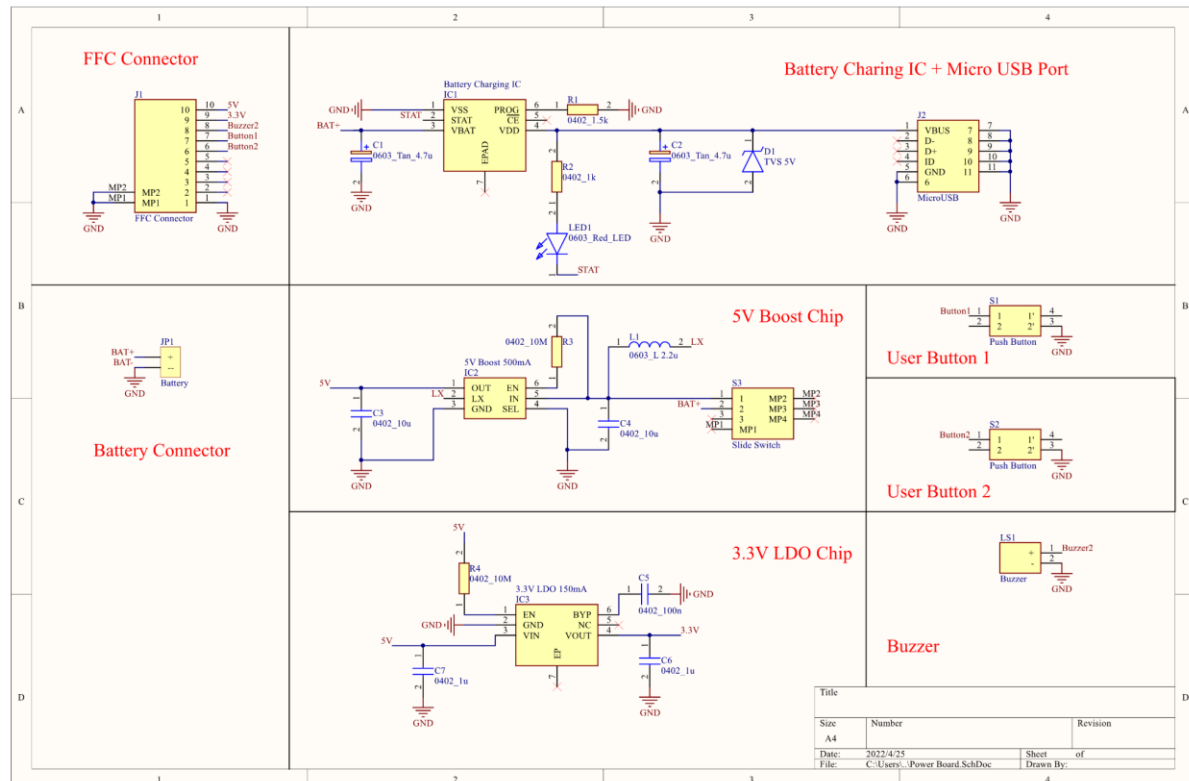


Figure 9-6. Schematic of PCB3 in the right leg

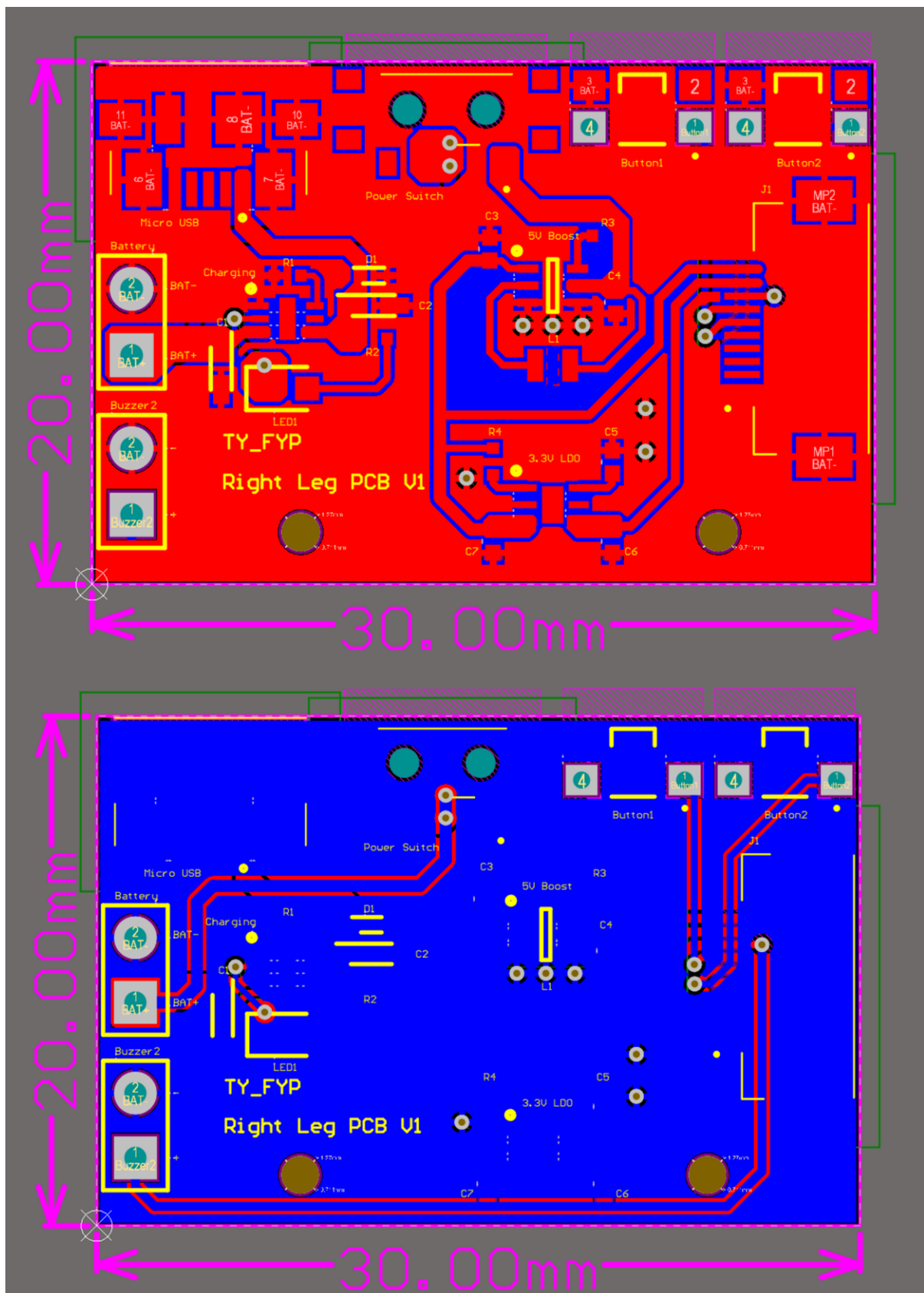


Figure 9-7. Top layer (top) and bottom layer (bottom) of 2D PCB layout design of PCB3

9.3 Appendix C PCB BOM List

Table 9-1. BOM List of three PCBs of the glasses frame

Comment	Description	Designator	Footprint	LibRef	Quantity
0603_Tan_4.7u	Capacitor Polarised	C1, C2	CAPPM168X90N	0603_Tan_4.7u	5
0402_100n	Capacitor	C1, C2, C7, C8, C9, C11, C14	CAPC1005X55N	0603_C	8
0402_10u	Capacitor	C3, C4	CAPC1005X55N	0402_C	2
0402_1u	Capacitor	C5, C6, C7	CAPC1005X55N	0603_C, 0402_C	4
0402_2.2n	Capacitor	C10	CAPC1005X55N	0603_C	1
0402_220n	Capacitor	C13	CAPC1005X55N	0603_C	1
0402_10n	Capacitor	C15	CAPC1005X55N	0603_C	1
Schottky Diode 500mA	Schottky Diode	D1	DIOC1709X85N	Schottky Diode 500mA	1
TVS 5V	TVS Diode (Uni-directional)	D1	SODFL1006X40N	TVS 5V	1
ATMEGA328PB-AU	Integrated Circuit	IC1	QFP80P900X900X120-32N	ATMEGA328PB-AU	1
Battery Charging IC	Integrated Circuit	IC1	SON50P200X200X80-7N-D	Battery Charging IC	1
5V Boost 500mA	Integrated Circuit	IC2	SON65P200X200X80-6N	5V Boost 500mA	1
8 bit Translator	Integrated Circuit	IC2	NXB0108BQX	8 bit Translator	1
3.3V LDO 150mA	Integrated Circuit	IC3	SON65P200X200X90-7N-D	3.3V LDO 150mA	1
HMC5883L	Integrated Circuit	IC3	HMC5883L	HMC5883L	1
MPU-6050	Integrated Circuit	IC4	MPU_6050	MPU-6050	1
FFC Connector	Connector	J1, J2	528921033	FFC Connector	4
MicroSD Connector	Connector	J2	MEM20750014001A	MEM2075-00-140-01-A	1
MicroUSB	Connector	J2	473461001	MicroUSB	1
Battery	HDR-1X2	JP1	Buzzer & Battery	Battery	1
Header2X2	Header 2X2	JP1, JP2	HDR2.54-LI-2x2P	Header 2X2	2
0603_L 2.2u	Inductor	L1	Inductor	0603_L 2.2u	1
0603_Red_LED	LED	LED1	LEDC1608X80N	0603_Red_LED	1
5mm Red LED	LED	LED1, LED2, LED3, LED4	TLHR_6400	TLHR6400	4
Buzzer	Loudspeaker or Buzzer	LS1	Buzzer & Battery	Buzzer	2
0402_1.5k	Resistor	R1	0402_R	0402_R	1
0603_300	Resistor	R1, R2, R3, R4	ERA3KV_(0603)	0603_R	4
0402_10K	Resistor	R1, R2, R3, R4, R5, R6, R7, R8, R10, R11, R12	0402_R	0402_R	11
0402_1k	Resistor	R2	0402_R	0402_R	1
0402_10M	Resistor	R3, R4	0402_R	0402_R	2
0402_5k	Resistor	R9	0402_R	0402_R	1
Push Button	Switch	S1, S2	Push_Button	Push Button	2
Slide Switch	Switch	S3	4.50404E+11	Slide Switch	1
16MHz Osci	Undefined or Miscellaneous	U1	CSTNE16M0V530000R0	16MHz Osci	1

9.4 Appendix D Public Human Head Model Dataset

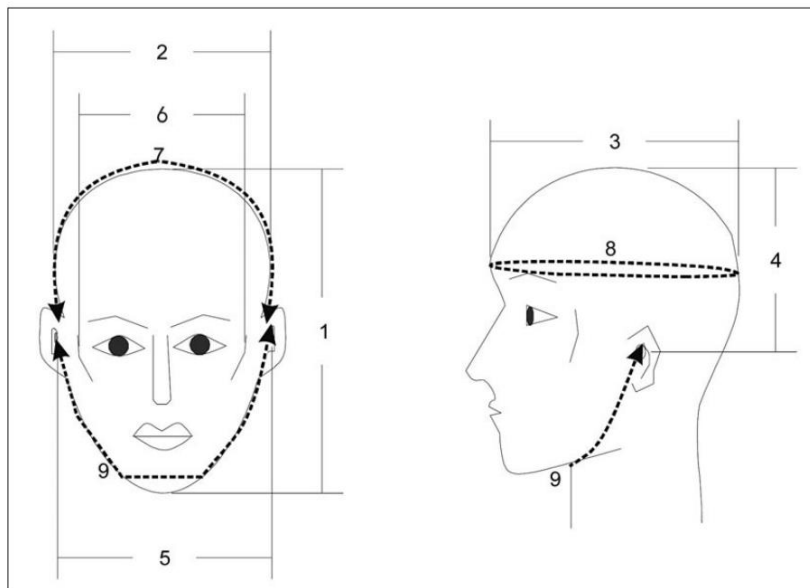


Figure 9-8. Head dimensions marked by numbers [40]

Table 9-2. Explanations of head dimensions and relevant measurement methods [40]

No.	Dimensions	Measurement methods
1	Menton-top of head	The vertical distance between the menton landmark at the bottom of the chin and the horizontal plane tangent to the top of the head is measured.
2	Head breadth	The maximum horizontal breadth of the head above the attachment of the ears is measured with a spreading caliper.
3	Head thickness	The distance from the glabella landmark between the grow ridges to the posterior point on the back of the head is measured with a spreading caliper.
4	Tragion-top of head	The vertical distance between the tragion landmark on the cartilaginous flap in front of the ear hole and the horizontal plane tangent to the top of the head is measured.
5	Bitragion breadth	The straight line distance between the right and left tragion landmark on the cartilaginous flaps in front of each ear hole is measured.
6	Bizygomatic breadth	The maximum horizontal breadth of the face (between the zygomatic arches) is measured with a spreading caliper.
7	Bitragion Coronal Arc	The surface distance between the right and left tragion landmarks across the top of the head is measured with a tape.
8	Head circumference	The maximum circumference of the head above the attachment of the ears to the head is measured with a tape passing just above the ridges of the eyebrows and around the back of the head.
9	Bitragion submandibular arc	The surface distance between the right and left tragion landmarks across the submandibular landmark at the juncture of the jaw and the neck is measured with a tape.
10	Head breadth & thickness Ratio	$\text{Head breadth} / \text{Head length} \times 100$
11	Menton top of head & bizygomatic breadth Ratio	$\text{Menton-top of head} / \text{Bizygomatic breadth} \times 100$

Table 9-3. Statistics of head dimensions [40]

Scale: cm, kg

Dimensions	Mean	St. Dv	Min.	Max.
Height	176.2	9.7	152.4	198.1
Weight	80.6	15.0	54.4	136.1
Menton-top of head	24.1	2.5	19	29.1
Head breadth	14.5	1.3	10.2	17.4
Head thickness	19.4	2.5	13.8	23.9
Tragion-top of head	14.2	1.5	11	16.9
Bitragion breadth	13.2	1.7	9.4	16.8
Bizygomatic breadth	13.9	1.2	11.1	16.8
Bitragion Coronal Arc	38.0	2.3	34	43.5
Head circumference	57.4	2.1	53.4	61.6
Bitragion submandibular arc	29.9	2.9	25	35.8
Head breadth & thickness Ratio	76.4	13.4	48.5	110
Menton top of head & bizygomatic breadth Ratio	174.5	22.3	129.2	231.5